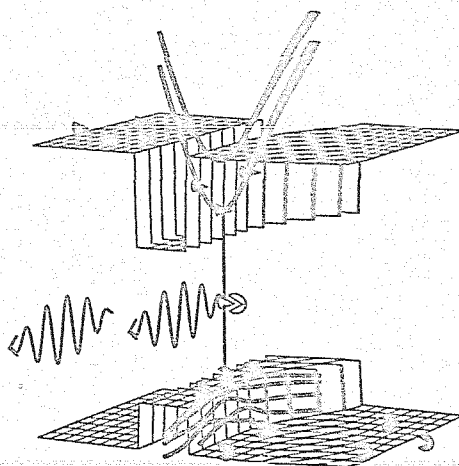


The Electronic and Optical Properties of GaAs/AlGaAs Quantum Wells

Rob Eppenga



TR diss
1655

627 220
317 052
TR diss 1655

The Electronic and Optical Properties of GaAs/AlGaAs Quantum Wells

Proefschrift ter verkrijging van de graad van doctor
aan de Technische Universiteit Delft, op gezag van de
Rector Magnificus, Prof. Drs. P.A. Schenck, in het
openbaar te verdedigen ten overstaan van een commissie
door het college van Dekanen daartoe aangewezen, op

donderdag 15 september 1988 te 14.00 uur

door

Robert Eppenga,

geboren te Weesp,
doctorandus in de natuurkunde.



TR diss
1655

Dit proefschrift is goedgekeurd door de promotor Prof. Dr. Ir. M.F.H. Schuurmans.

**aan mijn ouders
aan Marjolein**

Dankwoord

Het schrijven van dit proefschrift is voor mij een leerproces geweest waar ik met plezier op terugkijk. Daartoe heeft de prettige samenwerking met vele anderen, die ik op deze pagina wil bedanken, in belangrijke mate bijgedragen.

Ik wil mijn promotor, Martin Schuurmans, bedanken voor de uiterst plezierige manier van samenwerken. Enkele aspecten daarvan die ik met name wil noemen zijn: de deur van je kamer die altijd open (te krijgen) bleek, jouw voorlezen van mijn zinsformuleringen en de inspirerende discussies aan de Nat. Lab. vijver.

Sel Colak, I thank you for our good collaboration which has resulted in your laser program accepting the output of my k,p program as input, and for initiating me in the subject of laser modeling.

Peter Blood and Alicia Kucharska, I thank you for the enlightening discussions about lasers and laser modeling.

I thank Geoff Duggan and Hugh Ralph for the many valuable discussions and their critical testing of my implementation of the k,p model.

Siegfried Hagen, jij hebt mij als theoretic een meer praktische kijk op GaAs/AlGaAs quantumputlasers gegeven.

Gert 't Hooft en Laurens Molenkamp, jullie enthousiaste gebruik van het k,p -model bij de interpretatie van jullie fotoluminescentie-excitatiemetingen aan GaAs/AlGaAs-quantumputten heeft mij van het nut van het ontwikkelen van ingewikkelde k,p -modellen overtuigd.

Pap en mam, jullie wil ik bedanken voor de mogelijk die jullie mij geboden hebben om een leuke studietijd te kunnen hebben.

Tenslotte wil ik jou, Marjolein, bedanken voor het aangenaam helpen invullen van de niet-quantumwell kant van het leven.

Contents

	page
Introduction	1
<i>Chapter 1</i> A new k,p theory for GaAs/GaAlAs-type quantum wells	13
<i>Chapter 2</i> Effects of band mixing on the radiative properties of a quantum well	41
<i>Chapter 3</i> Band mixing effects on quantum well gain	53
<i>Chapter 4</i> The art of quantum well laser modeling	77
<i>Chapter 5</i> The effect of bulk inversion asymmetry on [001], [110] and [111] GaAs/AlAs quantum wells	97
<i>Chapter 6</i> Thin [001] and [110] GaAs/AlAs superlattices: direct or indirect?	107
Summary	117
Samenvatting	119
Curriculum vitae	121

Apart from some minor modifications, the material in this thesis is contained in the following publications:

- Chapter 1* R. Eppenga, M.F.H. Schuurmans and S. Colak, Phys. Rev. B36, pp. 1554-1564 (1987).
- Chapter 2* R. Eppenga, S. Colak and M.F.H. Schuurmans, Proceedings SPIE Vol. 800 Novel Electronic Devices, pp. 38-42 (1987); also in Fiber and Integrated Optics 7, pp. 57-67 (1987).
- Chapter 3* S. Colak, R. Eppenga and M.F.H. Schuurmans, IEEE J. of Quantum Electron. QE-23, pp. 960-968, June 1987
(the expressions for the TE optical matrix elements of the conventional model as presented in appendix A of the IEEE publication contain a minor error; the correct expressions are used in Chapter 3. Most results for the conventional model, as presented in Chapter 3, differ therefore slightly from those presented in the IEEE publication).
- Chapter 5* R. Eppenga and M.F.H. Schuurmans, accepted for publication in Phys. Rev. B as a Rapid Communication (scheduled for the 15th of June 1988 issue)
- Chapter 6* R. Eppenga and M.F.H. Schuurmans, accepted for publication in Phys. Rev. B as a Brief Report.

Introduction

The art of semiconductor technology lies in obtaining absolute control over the fabrication process on the atomic length scale. Nowadays, the smallest in-plane details realized in semiconductor devices are in the micron ($1 \mu\text{m} = 10^{-6} \text{ m}$) range, still large compared to the size of atoms ($1 \text{ \AA} = 10^{-10} \text{ m}$). However, in the last decade it has become possible to deposit single monolayers (a few \AA thick) of a specific semiconductor material on a macroscopic semiconductor surface ($\sim \text{cm}^2$) in a controlled manner. Layered crystalline semiconductors thus grown, the so-called semiconductor heterostructures, find important applications in, for example, fast transistors (HEMT) and efficient and powerful semiconductor lasers. They exhibit interesting physical effects /1/ of which the Quantum Hall Effect /2/ may be the most famous (Nobel prize 1985).

Molecular Beam Epitaxy (MBE), Metal Organic Vapor Phase Epitaxy (MOVPE) and Liquid Phase Epitaxy (LPE) are some of the techniques used to grow semiconductor heterostructures. In the high-vacuum chamber of a MBE apparatus, beams consisting of semiconductor atoms are deposited on a heated semiconductor substrate; in MOVPE and LPE quartz reactors, vapors and liquids of compounds containing the semiconductor elements react chemically at the heated substrate to form a semiconductor layer. Shutters control the flows of the various atomic, vapor or liquid "beams" and thereby the composition of the successively deposited layers.

The choice of the constituent elements of the semiconductor heterostructure is determined by the desired application. GaAs/ $\text{Al}_x\text{Ga}_{1-x}\text{As}$ structures are being used for fast transistors (HEMT) /3/ and near-infrared lasers ($\lambda = 650\text{-}800 \text{ nm}$) /4/, $\text{Ga}_x\text{In}_{1-x}\text{P}_{1-y}\text{As}_y/\text{InP}$ structures for infrared lasers ($\lambda = 1.3\text{-}1.5 \mu\text{m}$) /4/ and HgTe/CdTe structures for infrared detectors /5/. In pure scientific research, these and many other combinations of semiconductors (SiGe /6/, GaSb/AlSb /7/, $\text{ZnS}_{1-x}\text{Se}_x/\text{ZnS}$ /8/, *nipi* structures /9/), semimagnetic semiconductors ($\text{Hg}_x\text{Mn}_{1-x}\text{Te}$) /10/ and metals (Fe/Cu,Co/Pd,Ni/Co) /11/ are being employed.

Optimum-quality structures have been obtained in the GaAs/ $\text{Al}_x\text{Ga}_{1-x}\text{As}$ system by MBE growth. The principal reason is the almost perfect lattice matching of GaAs and AlAs (and thereby $\text{Al}_x\text{Ga}_{1-x}\text{As}$): the relative difference $\Delta a/a$ of their lattice constants a ($a = 5.655 \text{ \AA}$ for GaAs) is 0.1% at room temperature. The interfaces between the different layers can be sharp on the level of a single monolayer and are perfect i.e. the atoms in the different layers sit exactly 'on top of each other'. The composition is constant within each individual layer, and, important for the electrical properties of the structure, the material can be very pure, having less than 10^{14} cm^{-3} electrically active impurities (cf. GaAs contains $4.4 \cdot 10^{22} \text{ atoms/cm}^3$).

Introduction

Basic building blocks of most semiconductor heterostructures are the heterojunction, the quantum well and the superlattice (see Figure 1). The heterojunction consists of two different semiconductors on top of each other. The quantum well consists of a thin semiconductor slab (typically $\sim 10\text{-}100$ Å), the well, in between two thick other semiconductor layers, the barriers. Finally, the superlattice consists of a periodically repeated sequence of thin slabs of two different semiconductors. Modulation-doped heterojunctions form the basis of fast transistors (HEMT). Single and multiple quantum wells are being used as the active region of a semiconductor laser and superlattices have prospects for use as barrier material in a quantum well leading to superior laser performance.

The physical properties of these systems reflect their layered structure. Free carriers, i.e. conduction-band electrons and/or valence-band holes, are typically confined to a few energetically favorable layers. This confinement expresses itself in quantum size effects if the de Broglie wavelength of the carriers becomes equal to or smaller than the thickness of those layers. The carriers can only occupy a discrete set of energy states. The motion of the carriers becomes effectively 2-dimensional for large enough level splittings.

This thesis focuses on the theoretical description of conduction-band states and valence-band states in GaAs/Al_xGa_{1-x}As quantum wells. This structure offers several

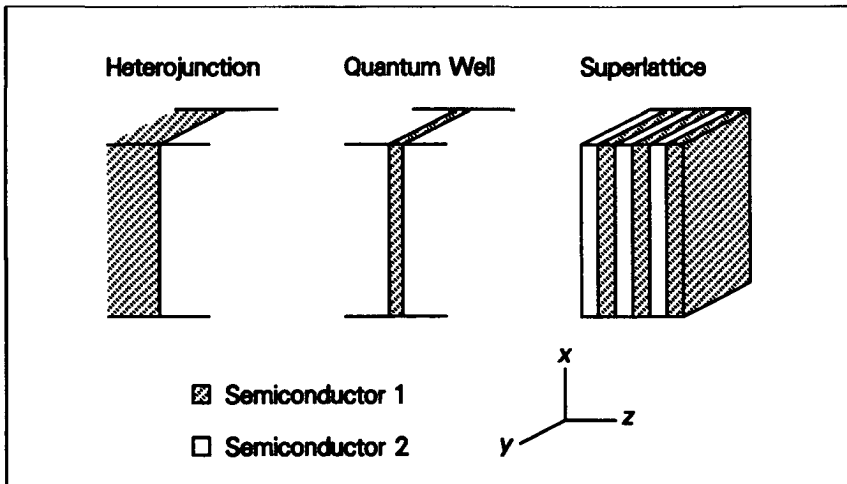


Figure 1 The three basic building blocks of layered semiconductors.

advantages when a theoretical description is intended. Firstly, the properties of both constituent semiconductors, and in particular GaAs, are relatively well-known. Secondly, the growth process is best understood and controlled in the GaAs/Al_xGa_{1-x}As system resulting in well-defined quantum wells. The combination enables a quantitative comparison of theoretical and experimental results. Moreover, a GaAs/Al_xGa_{1-x}As (multiple) quantum well finds an important application in its use as the active region of a quantum-well laser (Figure 2). Much of the work is therefore focused on a better understanding of the optical properties of a quantum well.

The outline of this thesis is as follows. The theoretical model is described in Chapter 1. The optical properties of the GaAs/Al_xGa_{1-x}As quantum well are described in Chapters 2-4 with an emphasis on the laser application. Chapter 5 describes an interesting detail of the quantum well, the spinsplitting of the conduction-bands due to inversion asymmetry. Chapter 6 describes the optical properties of GaAs/AlAs superlattices where the unit cell consists of only a few monolayers of GaAs and AlAs.

Before turning to a more detailed description of the contents of the individual chapters, first the general characteristics of the model, to be used in Chapters 1-5, will be briefly reviewed. The theoretical model for the GaAs/Al_xGa_{1-x}As quantum well is a semi-empirical one based on the bulk properties of the constituents GaAs and Al_xGa_{1-x}As. This model is designed for the calculation of the one-electron quantum-

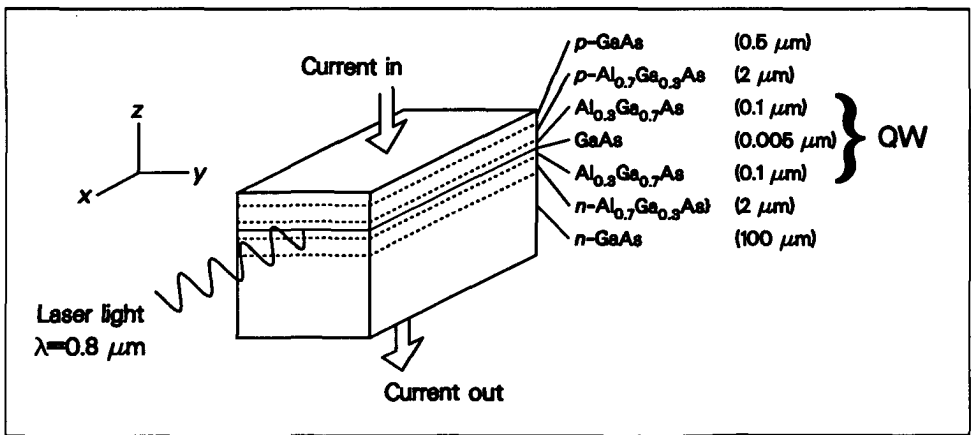


Figure 2 The GaAs/AlGaAs quantum-well laser containing a single GaAs quantum well (QW) in the active region. Typical numbers for the thickness of the successive layers are indicated between parentheses.

Introduction

well confinement conduction-band and valence-band eigenstates and eigenenergies that are energywise close to the bulk GaAs states at the center Γ of the Brillouin zone. Only the so-called quantum-well envelope function, i.e. the slowly (on the scale of the lattice constant a) varying part of the quantum-well wavefunction, and the corresponding slowly varying macroscopic potential are considered. The detailed behavior of the quantum-well wavefunction and the microscopic potential on the scale of the lattice constant a need not be considered. The appropriate elimination of the microscopic potential from the Schrödinger equation leads, for each band and approximatively, to a piecewise constant macroscopic potential in a Schrödinger-like equation. The bare electron mass is replaced by a piecewise constant effective mass. The macroscopic potential of the conduction-bands and the valence-bands in a thin layer of GaAs in between thick layers of $\text{Al}_x\text{Ga}_{1-x}\text{As}$ has the form of rectangular well in which *quantum* size effects are important: the GaAs/ $\text{Al}_x\text{Ga}_{1-x}\text{As}$ quantum well (see Figure 3).

The quantum-well envelope function can be expressed conveniently in the envelope functions of the bulk constituents of the quantum well. A Schrödinger-like equation, derived on the basis of *k.p* theory [12], describes the envelope function of each bulk constituent. Finally, the envelope functions of the bulk constituents must be joined

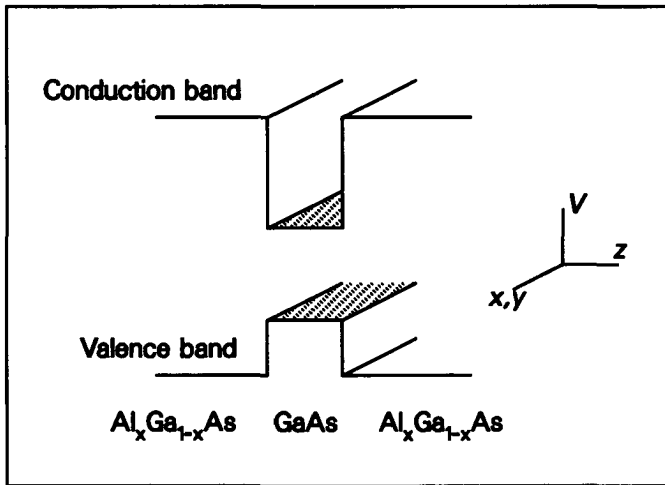


Figure 3 The macroscopic potential V that is seen by the electrons in the conduction band and the holes in the valence band in a GaAs/ $\text{Al}_x\text{Ga}_{1-x}\text{As}$ quantum well.

across the well-barrier interfaces by suitable boundary conditions. This determines the allowed quantum-well eigenstates and eigenenergies and corresponding quantum-well envelope functions (Figure 4).

The contents of the thesis will now be discussed in somewhat more detail. In Chapter 1 the eight-band $k \cdot p$ model is presented which incorporates the electron, the heavy-hole, the light-hole and the spin-orbit split-off band (see Figure 5), their mutual coupling and, perturbatively, their coupling to all other bands. Conduction-band non-parabolicity and valence-band mixing are naturally accounted for by treating the conduction and valence-bands in a unified way. On the basis of this model the envelope function formalism for the quantum well is developed.

The inclusion of the spin-orbit split-off band in the model is new. The unphysical behavior of the light-hole band for energies close to the spin-orbit splitting Δ (~ 0.3 eV) found in like models which do not incorporate this band, is removed. Moreover, the calculated first ($n = 1$) light-hole confinement energy is affected at the level of a few meV /13/. This is significant for the interpretation of state-of-the-art excitation photoluminescence measurements /14/.

The results of the model are compared with those of the sophisticated tight-binding model of Chang and Schulman /15/, which employs exact boundary conditions. By

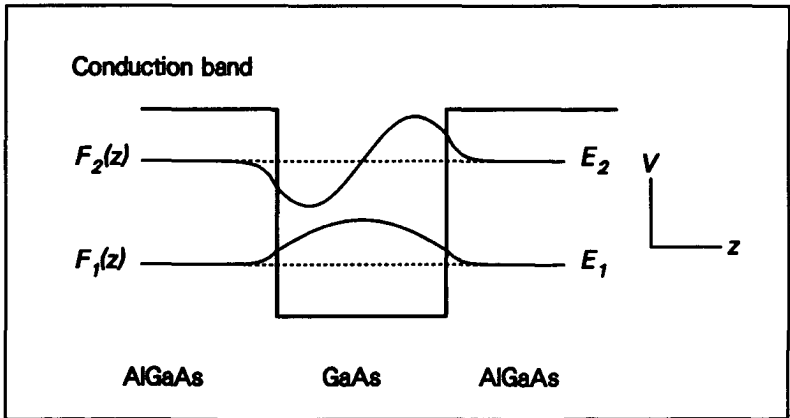


Figure 4 The quantum-well envelope functions of the first, $F_1(z)$, and second, $F_2(z)$, conduction-band confinement states in a GaAs/AlGaAs quantum well. E_1 and E_2 are the corresponding confinement energies.

Introduction

comparing the matrix elements for optical transitions between confinement conduction-band states and valence-band states it will be specifically shown that the quantum-well envelope functions and the tight-binding wavefunctions contain essentially the same information. This agreement, which is new, constitutes an important justification for the choice of the boundary conditions that are employed at the well-barrier interfaces.

In Chapters 2-4, the model is applied to describe the optical properties of GaAs/Al_xGa_{1-x}As quantum wells. This is important from an application point of view since quantum wells constitute the active region in quantum-well lasers. Chapter 2 may be viewed as a brief introduction to this field. Chapter 3 is more elaborate in that a discussion of the significance of the theoretical results for the interpretation of experimentally obtained spectra on quantum-well lasers is included. Furthermore, gain and spontaneous emission spectra calculated with the eight-band $k \cdot p$ model are compared with those obtained from simpler envelope function approaches which disregard conduction-band non-parabolicity and valence-band mixing. It will be shown that the peak gain of a quantum-well laser as obtained from the $k \cdot p$ model is lowered significantly as that obtained from the simpler model. A more complete description of a

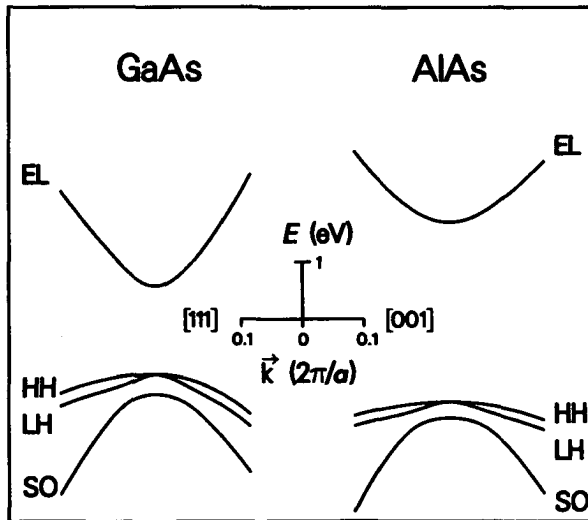


Figure 5 The bandstructure of GaAs and AlAs at the center of the Brillouin zone. The electron (EL), heavy-hole (HH), light-hole (LH) and spin-orbit split-off (SO) band are indicated. a is the lattice constant.

GaAs/Al_xGa_{1-x}As quantum-well laser is presented in Chapter 4. It incorporates the effects of e.g. carrier-carrier scattering, well-width fluctuations and current spreading on calculated gain and spontaneous emission spectra.

Chapter 5 focuses on a detail of the bandstructure of the bulk constituents of the quantum well that has been disregarded so far. The inversion asymmetry of the microscopic crystalpotential leads to a spinsplitting of the bands of the bulk materials. This splitting is zero for k along [001] and [111] and reaches a maximum value of ~ 75 meV (for GaAs) and ~ 60 meV (for AlAs) for k along [110] (Figure 6). The spinsplitting is therefore expected to be very different for GaAs/AlAs quantum wells grown along the [001] and [111] the crystallographic direction and those grown along the [110] the crystallographic direction. In Chapter 5 analytical expressions for the in-plane spinsplitting for GaAs/AlAs quantum wells grown along different crystallographic directions ([001], [110] and [111]) are derived. The most remarkable result found is the *linear* dependence of this splitting on the parallel wavenumber k_{\parallel} , whereas in the bulk the spinsplitting is *cubic* in k .

Chapter 6 deals with the very thin $n \times n$ GaAs/AlAs superlattices consisting of a periodic sequence of n monolayers of GaAs and n monolayers of AlAs. For small n ($n = 1, 2$) these superlattices constitute a new class of materials. They differ from the corresponding alloy Al_{0.5}Ga_{0.5}As. Their (optical) properties depend on n and on the crystallographic growth direction.

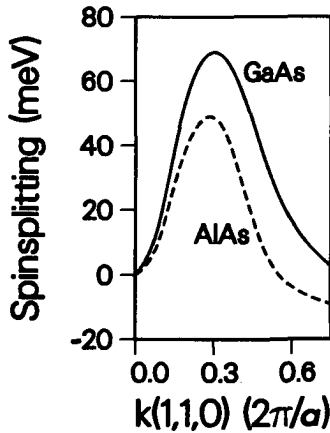


Figure 6 Calculated results for the spinsplitting of the conduction bands in GaAs (drawn) and AlAs (dotted) along $\Gamma - K$ ($= [110]$ direction) using the augmented spherical wave (ASW) bandstructure method.

Introduction

In principle, these superlattices can be described by the envelope function formalism and a suitable adaptation of the boundary conditions. However, for superlattices with a periodicity of a few monolayers the macroscopic potential, and therefore the envelope function, will vary on the scale of the lattice constant a . For these very thin superlattices the microscopic potential and the wavefunctions must be calculated from first principles (*ab-initio*) i.e. without resorting to measured (bulk) parameters. *Ab-initio* approaches in solid-state physics are based on the density functional theory introduced by Hohenberg and Kohn /16/. They proved the existence of a universal functional of the electron density. It is minimized by the electron density corresponding to the ground state of the many-electron system considered. The minimum value of the density functional corresponds to the ground-state energy of the true many-electron system. Kohn and Sham /17/ have shown that the minimization leads to a set of Schrödinger-like one-electron equations valid for slowly varying or high electron density. The hard part of the non-local potential appearing in those equations, the exchange-correlation potential, is treated in the local density approximation (LDA) /18/. The eigenenergies appearing in the Kohn and Sham Schrödinger-like equation are usually interpreted as the one-electron excitation spectrum (bandstructure) and the corresponding eigenfunctions as the one-electron wavefunctions.

A technical implementation of such an *ab-initio* bandstructure method, the augmented spherical wave (ASW) method /19/, is employed in Chapter 6 to calculate the bandstructure and the optical properties of very thin ($n = 1,2$) $n \times n$ GaAs/AlAs superlattices. The strength of the direct across-gap transitions will be calculated and compared to that of the indirect transition. The optical properties will be shown to depend strongly on n and the crystallographic growth direction.

The larger part of this work has been published in the form of regular articles in the scientific literature. The chapters are therefore self contained. The work was done in the group of M.F.H. Schuurmans at the Philips Research Laboratories (PRL) in Eindhoven. The k,p model was developed as an extension of an earlier model by M.F.H. Schuurmans and G.W. 't Hooft /13/ to explain all the features in the photoluminescence excitation spectra of GaAs/Al_xGa_{1-x}As quantum wells obtained by P. Dawson and K.J. Moore /20/ from PRL Redhill. Furthermore, H.I. Ralph and G. Duggan from PRL Redhill have used the k,p model to obtain the effective in-plane hole masses for use in their exciton model /21/. Recently, the k,p model has been used by L.W. Molenkamp and G.W. 't Hooft to interpret the photoluminescence excitation spectra of GaAs/Al_xGa_{1-x}As quantum wells grown along the [001], [310] and the [111] crystallographic direction /14/. The theoretical work on quantum-well laser

modeling was initiated by S. Colak during his one-year stay at PRL Eindhoven. In collaboration with P. Blood, A. Kucharska and S.W. Hagen, Colak's model has been refined and extended. The work on the very thin GaAs/AlAs superlattices was started to facilitate the interpretation of the photoluminescence and photoluminescence excitation spectra of these systems as obtained by P. Dawson and K.J. Moore /22/. It is finally worth noting that the availability of the high-quality GaAs/Al_xGa_{1-x}As quantum wells and quantum-well lasers that are grown at the PRL in Redhill by C.T. Foxon using MBE and in Eindhoven by H.F. 't Blik using MOVPE, has been crucial in achieving our model for the GaAs/Al_xGa_{1-x}As quantum well.

References.

1. V. Narayanamurti, "Semiconductor Heterostructures and Superlattices at the Frontier of Solid State Electronics and Photonics", in 'Proceedings of the 18th International Conference on the Physics of Semiconductors', Stockholm 1987, ed. by O. Engström, Vol. 1, pp. 3-10, World Scientific Publishing Co. (Singapore);
L. Esaki, "A Bird's-Eye View on the Evolution of Semiconductor Superlattices and Quantum wells", IEEE J. Quantum Electron., Vol. QE-22, pp. 1611-1624, Sept. 1986.
2. H. Aoki, "Quantised Hall effect", Reports on Progress in Physics 50, pp. 655-730 (1987).
3. M. Abe, T. Mimura, K. Nishiuchi, A. Shibatomi and M. Kobayashi, "Recent Advances in Ultra-High-Speed HEMT Technology", IEEE J. Quantum Electron., Vol. QE-22, pp. 1870-1879, Sept. 1986.
4. See e.g. H.C. Casey and M.B. Panish, "Heterostructure Lasers" Part A and B, Academic Press (New York, 1978);
G.H.B. Thompson, "Physics of Semiconductor Laser Devices", New York: Wiley, 1980; Special Issue on Semiconductor Lasers, IEEE J. Quantum Electron., Vol. QE-23, June 1987.
5. J.P. Faurie, "Growth and Properties of HgTe-CdTe and other Hg-Based Superlattices", IEEE J. Quantum Electron., Vol. QE-22, pp. 1656-1665, Sept. 1986;
J.M. Berroir, Y. Guldner and M. Voos, "HgTe-CdTe Superlattices: Magneto-optics and Bandstructure", *ibid.*, pp. 1793-1798.
6. R. People, "Physics and Applications of GeSi/Si Strained-Layer Heterostructures", IEEE J. Quantum Electron., Vol. QE-22, pp. 1696-1710, Sept. 1986.
7. A. Forchel, U Cebulla, G. Tränkle, E. Lach, T.L. Reinecke and H. Kroemer, S. Subbanna and G. Griffiths, " $2E_g$ Transitions in GaSb-AlSb Quantum-Well Structures", Phys. Rev. Lett. 57, pp. 3217-3220 (1986).
8. R.N. Bhargava, "Materials Growth and its Impact on Devices from Wide Band Gap II-VI Compounds", J. of Crystal Growth 86, pp. 873-879 (1988).

Introduction

9. G.H. Döhler, "Doping Superlattices (n-i-p-i Crystals)", *IEEE J. Quantum Electron.*, Vol. QE-22, pp. 1682-1695, Sept. 1986.
10. A.V. Nurmikko, R.L. Gunshor and L.A. Kolodziejski, "Optical Properties of CdTe/(Cd,Mn)Te Multiple Quantum Wells", *IEEE J. Quantum Electron.*, Vol. QE-22, pp. 1785-1792, Sept. 1986;
Chapter on "Semimagnetic and II-IV Semiconductor Heterostructures", in 'Proceedings of 7th International Conference on Electronic Properties of Two-Dimensional Systems', ed. J.M. Worlock, *Surface Science* 196, pp. 632-670 (1988).
11. H.J.G. Draaisma, H.M. van Noort and F.J.A. den Broeder, "Magnetic, Microstructural and Mössbauer Studies of Cu/Fe Composition-Modulated Thin Films", *Thin Solid Films* 126, pp. 117-121 (1985);
T. Katayama, Y. Suzuki, H. Awano, Y. Nishihara and N. Koshizuka, "Enhancement of the Magneto-Optical Kerr Rotation in Fe/Cu Bilayered Films", *Phys. Rev. Lett.* 60, pp.1426-1429 (1988).
12. E.O. Kane, "Energy Band Theory", in 'Handbook on Semiconductors', (North-Holland, New York, 1982), Vol. I, pp. 193-217.
13. M.F.H. Schuurmans and G.W. 't Hooft, "Simple calculations of confinement states in a quantum well", *Phys. Rev.* B31, pp. 8041-8048 (1985).
14. L.W. Molenkamp, R. Eppenga, G.W. 't Hooft, P. Dawson, C.T. Foxon and K.J. Moore, "Determination of valence-band effective-mass anisotropy in GaAs quantum wells by optical spectroscopy", in print *Phys. Rev. B*;
L.W. Molenkamp, G.E.W. Bauer, R. Eppenga and C.T. Foxon, "Exciton binding energy in (Al,Ga)As quantum wells: effects of crystal orientation and envelope function symmetry", submitted to *Phys. Rev. B*.
15. Y.C. Chang and J.N. Schulman, "Interband optical transitions in GaAs-GaAlAs and InAs-GaSb superlattices", *Phys. Rev.* B31, pp. 2069-2079 (1985).
16. P. Hohenberg and W. Kohn, "Inhomogeneous Electron Gas", *Phys. Rev.* 136B, pp. 864-871 (1964).
17. W. Kohn and L.J. Sham, "Self-Consistent Equations Including Exchange and Correlation", *Phys. Rev.* 140A, pp. 1133-1138 (1965)
18. L. Hedin and B.I. Lundqvist, "Explicit local exchange-correlation potentials", *J. Phys.* C4, pp. 2064-2083 (1971).
19. A.R. Williams, J. Kubler, C.D. Gelatt, "Cohesive Properties of metallic compounds: Augmented-spherical-wave calculations", *Phys. Rev.* B19, pp. 6094-6118 (1979)
20. P. Dawson, K.J. Moore, G. Duggan, H.I. Ralph and C.T. Foxon, "Unambiguous observation of the 2s state of the light- and heavy-hole excitons in GaAs-(AlGa)As multiple-quantum-well structures", *Phys. Rev.* B34, pp. 6007-6010 (1986);
K.J. Moore, P. Dawson and C.T. Foxon, "Observation of luminescence from the 2s heavy-hole exciton in GaAs-(AlGa)As quantum-well structures at low temperatures", *Phys. Rev.* B34, pp. 6022-6025 (1986).

21. G. Duggan and H.I. Ralph, "Exciton binding energy in type-II GaAs-(Al,Ga)As quantum-well heterostructures", Phys. Rev. B35, pp. 4152-4154 (1987).
22. K.J. Moore, G. Duggan, P. Dawson and C.T. Foxon, "Short period GaAs-AlAs superlattices: Optical properties and electronic structure", submitted to Phys. Rev. B.

Chapter 1

A new $k.p$ theory for GaAs/Ga_{1-x}Al_xAs-type quantum wells

A new $k.p$ theory for the description of GaAs/Ga_{1-x}Al_xAs-type quantum wells is presented. The theory combines a unified description of electron and hole states with only five adjustable parameters for each material constituting the quantum well. Unlike earlier $k.p$ work it fully accounts for the coupling between the lowest electron, the light-hole, the heavy-hole and the spin-orbit split-off hole bands and the coupling to all other bands is taken into account perturbatively. The theory thereby also applies to quantum wells where the spin-orbit splitting is comparable to the hole confinement potential energies. The full inclusion of the k_{\parallel} dependence of confinement energies and electron-hole transition strengths allows for accurate predictions of excitation spectra of quantum wells. In this respect the results of our simple $k.p$ theory stand comparison to the results of the more complicated tight-binding theory of Chang and Schulman. Our theory can thus explain the recently observed $\Delta n \neq 0$ transitions. As a final application we have calculated gain spectra of quantum-well lasers.

I. Introduction

GaAs/Ga_{1-x}Al_xAs quantum wells have been studied in great detail using excitation and luminescence spectroscopy /1/. The pioneering theoretical work on quantum wells such as that of Dingle /2/, Bastard /3/, White and Sham /4/ and Altarelli /5/ has described the *gross* features of quantum wells very well. This work did not intend to describe *all* detailed features currently being observed in excitation spectroscopy. An interesting example in this respect is Miller's /6,7/ observation of "forbidden" transitions from $n = 1$ electron to $n = 2$ and $n = 3$ hole states. To explain such features the k_{\parallel} dependence of confinement energies *and* transition strengths must be taken into account; k_{\parallel} is the crystal-momentum-like quantum number associated with the translational invariance in the stacking planes of the quantum well. Accounting for the k_{\parallel} dependence was beautifully done in the recent theoretical work of Chang and Schulman /8/. Unfortunately their theory, being based on many parameter tight-

binding descriptions and transition matrix techniques, is complicated and does not lend itself easily to interpretation.

In this paper we present a new and simple k,p theory for the description of GaAs/Ga_{1-x}Al_xAs-type quantum wells. It withstands comparison with the more complicated but admittedly more complete Chang-Schulman approach in the description of quantum wells. Apart from the gap and the spin-orbit splitting, our theory contains only five adjustable parameters for each material constituting the quantum well. Moreover these parameters are easily interpretable in terms of Γ -point effective masses. Unlike earlier k,p work /2-5/ on quantum wells it takes full account of the coupling between the lowest electron band, the heavy-, the light- and the spin-orbit split-off hole band and, perturbatively, of the coupling to all other bands. The complete account of the coupling to the spin-orbit split-off band is particularly relevant since the recent revision of the band-edge-discontinuity ratio of GaAs/Ga_{1-x}Al_xAs quantum wells from 85/15 to 67/33 /9/ implies that the hole confinement energy and the spin-orbit splitting energy already become of comparable magnitude for Al contents of 50%.

After the introduction of the new k,p model in section II we apply the model to the calculation of the k_{\parallel} dependence of the confinement energies and the optical transition strengths in section III. Particular emphasis will be given to the comparison with results from the Chang-Schulman theory. The excellent agreement of our results with their tight-binding results is particularly gratifying since their model employs exact boundary conditions. In section IV, the results for the k_{\parallel} dependence of the confinement energies and the transition strengths are then combined for the evaluation of excitation or absorption spectra. It is shown that unless exciton effects are included, the so-called $\Delta n \neq 0$ transitions, although allowed for $k_{\parallel} \neq 0$ hardly show up in the excitation spectra. In section V we consider a GaAs/AlAs quantum well with a band-edge-discontinuity ratio of 67/33. The excitation spectrum of such a quantum well may be dramatically affected by the inclusion of the hitherto /4-5/ disregarded spin-orbit split-off states. Section VI gives a brief account of the application of our theory to the calculation of gain spectra of quantum-well lasers. Strong deviations from results obtained earlier /10/ from "particle-in-the-box" effective mass type treatments of hole and electron confinement are indicated. A detailed account of these results will be published elsewhere /11/. Section VII briefly summarizes the paper.

II. The $k.p$ approach to quantum wells

This theory is based upon earlier work of 't Hooft and one of the authors for the case $k_{\parallel} = 0$ /12/. Their paper will henceforth be referred to as I. Each constituent material of the quantum well is described with an eight-band Kane model. The set of basis states includes the s -like spin-up and spin-down conduction-band states, the fourfold p -like $j = 3/2$ valence-band states and the twofold $j = 1/2$ spin-orbit split-off valence-band states. All the other bands are taken into account perturbatively /13/. The quantization axis of the angular momenta is taken to be perpendicular to the quantum-well interfaces and it is called the z axis. Parallel "motion" will be described by the position vector $r_{\parallel} = (x, y)$ and the crystal momentum vector $\hbar k_{\parallel} = \hbar(k_x, k_y)$ in the x - y plane. We disregard the k -dependent part of the spin-orbit coupling, since the corresponding term linear in k is extremely small /13/. The eight Γ -point basis states are chosen to be

$$u_1 = |s\uparrow\rangle, \quad (1a)$$

$$u_2 = \sqrt{1/6} |(x + iy)\downarrow\rangle - \sqrt{2/3} |z\uparrow\rangle, \quad (1b)$$

$$u_3 = \sqrt{1/3} |(x + iy)\downarrow\rangle + \sqrt{1/3} |z\uparrow\rangle, \quad (1c)$$

$$u_4 = \sqrt{1/2} |(x + iy)\uparrow\rangle, \quad (1d)$$

$$u_5 = -|s\downarrow\rangle, \quad (1e)$$

$$u_6 = -\sqrt{1/6} |(x - iy)\uparrow\rangle - \sqrt{2/3} |z\downarrow\rangle, \quad (1f)$$

$$u_7 = -\sqrt{1/3} |(x - iy)\uparrow\rangle + \sqrt{1/3} |z\downarrow\rangle, \quad (1g)$$

$$u_8 = \sqrt{1/2} |(x - iy)\downarrow\rangle. \quad (1h)$$

The designations s , x , y and z refer to the corresponding symmetry properties under operations of the tetrahedral group; \uparrow and \downarrow refer to spin up and down. The states u_1 - u_4 refer to the Γ -point electron (EL), light-hole (LH), spin-orbit split-off (SO) and heavy-hole (HH) states. The states u_5 - u_8 are the Kramers counterparts of u_1 - u_4 respectively. In each material we expand the wave function according to

$$\psi^j(\mathbf{r}) = \sum_{j=1}^8 F_j^j(z) e^{ik_{\parallel} r_{\parallel}} u_j^j(\mathbf{r}). \quad (2)$$

The designation l refers to the well material ($l = 1$) or the barrier material ($l = 2$). The label j runs over the states specified by Eq.(1) and all other Γ -point states. When the effect of the latter is included in the Schrödinger equation by Löwdin renormalization /14/ we obtain

$$\{ \underline{H}^l - [(l-1)\delta E_v + E] \underline{I} \} \underline{F}^l = 0, \quad (3)$$

where \underline{F} is the column vector with elements $F_1^l - F_8^l$, \underline{I} the 8x8 unit matrix, E is the energy corresponding to state ψ with the zero of energy at the valence-band edge in the well, δE_v is the valence-band discontinuity and \underline{H}^l is the matrix operator

$$\underline{H} = \begin{pmatrix} E_{EL} & -\sqrt{2} P_z & P_z & \sqrt{3} P_+ & 0 & -P_- & -\sqrt{2} P_- & 0 \\ & E_{LH} & G_1 & \sqrt{2} G_+ & -P_+^* & 0 & -\sqrt{3} G_- & G_2 \\ & & E_{SO} & -G_+ & -\sqrt{2} P_+^* & \sqrt{3} G_- & 0 & \sqrt{2} G_2 \\ & & & E_{HH} & 0 & -G_2 & -\sqrt{2} G_2 & 0 \\ & & & & E_{EL} & \sqrt{2} P_z & -P_z & -\sqrt{3} P_- \\ & & & & & E_{LH} & G_1 & \sqrt{2} G_- \\ & & & & & & E_{SO} & -G_- \\ & & & & & & & E_{HH} \end{pmatrix}. \quad (4)$$

Here, and in the following, we will omit the superscript l when confusion is unlikely. Only the upper triangle of the Hermitean matrix is indicated. The diagonal matrix elements of \underline{H} are given by

$$E_{EL} = E_g + s \tilde{e}, \quad (5a)$$

$$E_{LH} = -\gamma_1 \tilde{e} - \gamma_2 \tilde{e}_1, \quad (5b)$$

$$E_{SO} = -\Delta - \gamma_1 \tilde{e}, \quad (5c)$$

$$E_{HH} = -\gamma_1 \tilde{e} + \gamma_2 \tilde{e}_1, \quad (5d)$$

where E_g is the gap, Δ the spin orbit splitting and the dimensionless parameters s , γ_1 and γ_2 describe the effect of the free-electron term in the Kane approach and the coupling of the s states (s) and x, y, z states (γ_1 and γ_2) to the other bands. The

Chapter 1

“energies” \tilde{e} and \tilde{e}_1 , satisfy $\tilde{e} = (\hbar^2/2m)(k_x^2 + k_y^2 + \tilde{k}_z^2)$ and $\tilde{e}_1 = (\hbar^2/2m)(2\tilde{k}_z^2 - k_x^2 - k_y^2)$, where $\tilde{k}_z = i \frac{\partial}{\partial z}$. The off-diagonal matrix elements of \underline{H} are given by

$$P_z = \sqrt{1/3} [iP\tilde{k}_z + Bk_xk_y], \quad (6a)$$

$$P_{\pm} = \sqrt{1/6} [iP(k_x \pm ik_y) + B\tilde{k}_z(k_y \pm ik_x)], \quad (6b)$$

$$G_1 = \sqrt{2} \gamma_2 \tilde{e}_1, \quad (6c)$$

$$G_2 = -\sqrt{3} \gamma_2 e_2 + i2\sqrt{3} \gamma_3 k_x k_y, \quad (6d)$$

$$G_{\pm} = \sqrt{6} \gamma_3 \tilde{k}_z (k_x \pm ik_y), \quad (6e)$$

where

$$P = -\frac{\hbar^2}{m} \int_{\text{unit cell}} d\vec{r} \phi_s^* \frac{\partial}{\partial z} \phi_z \quad (7)$$

describes the coupling between the Γ conduction-band-edge s state and the Γ valence-band edge z state, the dimensionless parameter γ_3 describes the anisotropy of the energy bandstructure around the Γ -point when $\gamma_2 \neq \gamma_3$, the “energy” $e_2 = (\hbar^2/2m)(k_x^2 - k_y^2)$ and the Kane B parameter describes the inversion asymmetry.

The parameters s , γ_1 , γ_2 , γ_3 and P can be determined from effective masses at the Γ -point of the bulk materials. The wave functions and energy bandstructure of the bulk materials are obtained from the ansatz $F \propto \exp(ik_z z)$, where k_z labels the wave functions in accordance with translational symmetry along the z direction.

Combining k_z and k_{\parallel} in $k = (k_{\parallel}, k_z) = (k_x, k_y, k_z)$ the energy-dispersion $E(\mathbf{k})$ of the bulk material l is obtained from the secular equation

$$\| H^l(\tilde{k}_z = k_z) - [(l-1)\delta E_v + E] I \| = 0. \quad (8)$$

For $k_{\parallel} = 0$, i.e. for k along $[001]$, the matrix \underline{H} decouples into two 4x4 blocks as described in Eq.(4) of I. Moreover the HH band is then completely decoupled from the other bands and its dispersion is purely parabolic with an effective mass satisfying

$$m/m_{\text{HH}(001)} = \gamma_1 - 2\gamma_2. \quad (9)$$

From the earlier work in I we also obtain

$$m/m_{\text{EL}}(001) = s + \lambda(1 + \frac{1}{2} r), \quad (10)$$

$$m/m_{\text{LH}}(001) = \gamma_1 + 2\gamma_2 + \lambda, \quad (11)$$

$$m/m_{\text{SO}}(001) = \gamma_1 + \frac{1}{2} \lambda r, \quad (12)$$

where the dimensionless parameters λ and r are given by

$$\lambda = 4mP^2/(3\hbar^2 E_g), \quad (13)$$

$$r = E_g/(E_g + \Delta). \quad (14)$$

Equations (9)-(12) for the effective masses along [001] determine the parameters s , λ , γ_1 and γ_2 . The parameter γ_3 is determined from the HH mass at Γ along [111]:

$$m/m_{\text{HH}}(111) = \gamma_1 - 2\gamma_3. \quad (15)$$

It is interesting to note that analytical expressions for the HH and LH mass in a general direction \hat{k} can be derived from our model as

$$m/m^*(\hat{k}) = \gamma_{1,L} \mp \left\{ \gamma_{2,L}^2 (\varepsilon_1^2 + 3\varepsilon_2^2) + 12 \gamma_{3,L}^2 (k_x^2 k_y^2 + k_y^2 k_z^2 + k_z^2 k_x^2) \right\}^{\frac{1}{2}}. \quad (16)$$

In this expression \hat{k} has unit length, $\varepsilon_1 = 2k_z^2 - k_x^2 - k_y^2$, $\varepsilon_2 = k_x^2 - k_y^2$, the Luttinger /15/ parameters $\gamma_{1,L}$, $\gamma_{2,L}$ and $\gamma_{3,L}$ satisfy

$$\gamma_{1,L} = \gamma_1 + \lambda/2, \quad (17a)$$

$$\gamma_{2,L} = \gamma_2 + \lambda/4, \quad (17b)$$

$$\gamma_{3,L} = \gamma_3 + \lambda/4, \quad (17c)$$

and the - and + sign refer to the HH and LH effective mass, respectively. The heavy- and light-hole mass are isotropic for $\gamma_2 = \gamma_3$. The electron and spin-orbit split-off masses are always isotropic. The effective masses along [001] and [111] to be used for the determination of s , γ_1 , γ_2 , γ_3 and λ are independent of the value of B . The inversion asymmetry leads to a splitting of the bands except along [001] and [111] where the splitting is prevented by symmetry elements of the group of k . The parameter B can be determined by comparison with results for the spin-splitting along [110] from *ab-initio* LMTO bandstructure calculations as done by Christensen and Cardona /16/;

the splitting has recently been used to produce spin-polarized photo-electrons /17/. In our model the splitting of the lower conduction band along [110] is evaluated to be given by

$$\Delta E = \frac{2PB\Delta}{3E_g(E_g + \Delta)} k^3, \quad (18)$$

where $k = |\mathbf{k}|$. According to Christensen and Cardona /16/ the splitting is 60 meV for $k = 3\pi/8a$, with a the lattice constant. This may lead to observable effects in thin quantum wells (30 Å). Results will be published elsewhere /18/. Henceforth we take $B = 0$ in this paper.

We stress at this point that knowledge of $m_{EL}(001)$, $m_{HH}(001)$, $m_{LH}(001)$, $m_{SO}(001)$ and $m_{HH}(111)$ at the center of the Brillouin zone precisely determines the five parameters s , γ_1 , γ_2 , γ_3 and λ of our $\mathbf{k}\cdot\mathbf{p}$ model and thus leads to a unified description of electron and hole bands. Accurate experimental knowledge of these masses is thus called for. Unfortunately the spin-orbit split-off band mass $m_{SO}(001)$ is not at present experimentally known. As additional information we can use the value of P , i.e. λ , as determined from conduction electron spin resonance by Hermann and Weisbuch /19/. Note, however, that, especially for $\text{Ga}_{1-x}\text{Al}_x\text{As}$, the values of the effective masses are still subject to discussion /20/.

Having established the $\mathbf{k}\cdot\mathbf{p}$ model for the bulk bandstructure we now turn to the quantum-well problem. We proceed along the lines of the work in I; details are therefore omitted. The envelope functions $F^{(1)}$ and $F^{(2)}$ must be joined across the interfaces by suitable boundary conditions. Since we deal with $\text{GaAs}/\text{Ga}_{1-x}\text{Al}_x\text{As}$ -type quantum wells (type I) we will work in the "flat-band" approximation /21/. From the structural similarity of the isoelectronic materials in the quantum well, the approximation is invoked in which the basis functions u_{EL} , u_{HH} , u_{LH} and u_{SO} are the same in the materials 1 and 2. This troublesome approximation will be checked *a fortiori* in section 3 when we come to the comparison with the results of the Chang/Schulman approach not containing this approximation. Continuity of the wave functions (2) now implies

$$F^{(1)} = F^{(2)} \quad (19)$$

at the two interfaces in the quantum well. To discuss the other boundary conditions at the interfaces we write the matrix operator \underline{H} in the form

$$\underline{H}^I = \underline{A}^I \frac{\partial^2}{\partial z^2} + \underline{B}^I \frac{\partial}{\partial z} + \underline{C}^I, \quad (20)$$

where the 8x8 matrices \underline{A}^l , \underline{B}^l and \underline{C}^l depend on k_{\parallel} and on the parameters s , γ_1 , γ_2 , γ_3 and λ , but not on the coordinate z . The superscript l can be omitted when we formally adopt \underline{A} , \underline{B} and \underline{C} as slowly varying functions of z across the quantum-well interfaces. The resulting "effective-mass-type" matrix functions must be considered to vary slowly on the scale of the lattice parameter but rapidly on the scale of the envelope changes. The resulting $\underline{H}(z)$ must be modified to ensure its hermiticity /22/. We use

$$\underline{A}(z) \frac{\partial^2}{\partial z^2} \rightarrow \frac{\partial}{\partial z} \underline{A}(z) \frac{\partial}{\partial z}, \quad (21a)$$

$$\underline{B}(z) \frac{\partial}{\partial z} \rightarrow \frac{1}{2} \left[\underline{B}(z) \frac{\partial}{\partial z} + \frac{\partial}{\partial z} \underline{B}(z) \right]. \quad (21b)$$

Integration of the resulting equations across the interfaces then yields

$$\left[\underline{A}^{(1)} \frac{\partial}{\partial z} + \frac{1}{2} \underline{B}^{(1)} \right] \underline{F}^{(1)} = \left[\underline{A}^{(2)} \frac{\partial}{\partial z} + \frac{1}{2} \underline{B}^{(2)} \right] \underline{F}^{(2)} \quad (22)$$

at the interfaces. Hermiticity of $\underline{H}(z)$ can also be assured by other choices than (21) /22/. However, requiring $\partial\psi/\partial z$ to be continuous across the interfaces with ψ given by Eq.(2), keeping in mind that other bands than the eight ones explicitly considered also contribute to $\partial\psi/\partial z$, we also obtain precisely Eq.(22). The boundary conditions are completed by giving the ones at $z = \pm \infty$. We only consider confined states and so for $|z| \rightarrow \infty$

$$\underline{F} \rightarrow \underline{0}. \quad (23)$$

Obtaining the confinement wave functions and energies is now in principle simple. At a given sought confinement energy E the dispersion relation (8) is a polynomial of degree 8 in k_z^2 ($\underline{B} = 0$) and so it yields 16 solutions $k_{z\alpha}^l(E)$, $\alpha = 1, 2, \dots, 16$. The corresponding eigensolutions are $\underline{F}_\alpha^l(E)$. A confinement state is then formed out of a linear combination of 16 well and 16 barrier solutions and involves 3x16 adjustable coefficients. The boundary conditions (19), (22) and (23) furnish 48 conditions for the determination of 48 coefficients and the solution of the corresponding secular equation yields the confinement energies and states. Unfortunately, the problem is not all that simple. Note that, whereas in the complex bandstructure of GaAs and AlAs for $k_{\parallel} = 0$ only real and purely imaginary k_z values appear (see I), truly complex k_z values for $k_{\parallel} \neq 0$ are found /23/. For a given energy E we count only 6 spin degenerate ($\underline{B} = 0$) k_z^2 solutions. Indeed the remaining 2 spin degenerate k_z^2 solutions of the polynomial

Chapter 1

secular equation (8) of degree 8 in k_z^2 are unphysical and thereby spurious solutions. Basically the spurious solutions have their origin in the incompleteness of the set of basis functions in the $k.p$ approach, which makes it impossible for $E(\mathbf{k})$ to be a periodic function of \mathbf{k} when \mathbf{k} moves through the various Brillouin zones. A spurious solution corresponds to a solution outside the first Brillouin zone which is not, but should actually be, a periodic continuation of the solution inside that zone.

In earlier more simple $k.p$ models of quantum wells spurious solutions did not arise or were considered to be harmless. For example, in Bastard's work /3/ the omission from $k.p$ theory of the free electron contributions and the coupling to other bands than the principal one except for the HH band, leads to a polynomial of degree 2 in k_z^2 and no spurious solutions. However, this approach is inappropriate for the hole states, since for $k_x = 0$ one of the resulting k_z^2 solutions diverges when E approaches $-(2/3)\Delta$. In Altarelli's work /5/ the principal bands are the EL, HH and LH bands and the coupling to the spin-orbit split-off band is treated perturbatively. The secular equation for the determination of the energy-dispersion is then of degree 6 in k_z^2 . Two spurious solutions appear, which are rapidly decaying in nature and are therefore considered to be harmless. Our spurious solutions are oscillatory in nature and are not harmless when taken seriously in the construction of the wave functions. However, the LH-SO and HH-SO coupling is relevant for confinement energies close to the spin-orbit split-off energy in the well and may then not be ignored. Finally, in the work of White and Sham /4/ spurious solutions do also appear. They are called wing-band solutions and are, like in Altarelli's work /5/, rapidly decaying in nature and harmless. We note that the Hamiltonian proposed by White and Sham /4/ is not consistent with the Kane matrix for GaAs. White and Sham have actually modified /4/ their matrix to get rid of the oscillating solutions and replace them by harmless wing-band solutions. This procedure is justified since they were only interested in vanishingly small diagonal k^2 terms i.e. $A \rightarrow 0$ in Ref. 4.

It seems to us that an adequate treatment of the coupling of both electrons, heavy-hole, light-holes and spin-orbit split-off holes by $k.p$ theory inevitably leads to the appearance of spurious solutions. Fortunately, it is quite easy to get rid of these solutions. We separate the approach into one for the electrons and one for the holes by proceeding as follows. Put $\tilde{k}_z = k_z$ in the Kane operator matrix H , i.e. consider a particular bulk solution $F = f \exp(ik_z z)$ where f is a constant vector. Eliminate analytically either the hole or the electron states from the matrix equation resulting from (3). We find

$$\left\{ \underline{H}_Q - [(l-1)\delta E_v + E] \underline{I}_Q \right\} f_Q = 0, \quad (24)$$

where $Q = el$ or $hole$ refers to the electron or hole problem. The vector $f_{el} = (f_1, f_2)$ and \underline{H}_{el} and \underline{I}_{el} are 2×2 matrices. Similarly, $f_{hole} = (f_2, f_3, f_4, f_6, f_7, f_8)$ and \underline{H}_{hole} and \underline{I}_{hole} are 6×6 matrices. The matrix \underline{H}_Q has a complicated dependence on k_z , k_{\parallel} and E . It is such that both \underline{H}_{el} and \underline{H}_{hole} describe exactly the eight $k_{za}^2(E)$ solutions discussed before, i.e. inclusive the 2 spurious $k_{za}^2(E)$ solutions. The 6×6 hole matrix \underline{H}_{hole} follows from the corresponding part of the 8×8 matrix H by the replacements

$$\gamma_1 \rightarrow \tilde{\gamma}_1 = \gamma_1 + \Lambda/2, \quad (25a)$$

$$\gamma_2 \rightarrow \tilde{\gamma}_2 = \gamma_2 + \Lambda/4, \quad (25b)$$

$$\gamma_3 \rightarrow \tilde{\gamma}_3 = \gamma_3 + \Lambda/4, \quad (25c)$$

where

$$\Lambda = \lambda E_g / (E_g + s e - E), \quad (26)$$

with $e = (\hbar^2/2m)(k_x^2 + k_y^2 + k_z^2)$. Note the similarity of $\tilde{\gamma}_1$, $\tilde{\gamma}_2$ and $\tilde{\gamma}_3$ with the Luttinger parameters $\gamma_{1,L}$, $\gamma_{2,L}$ and $\gamma_{3,L}$ as given by Eq.(17). The origin of the spurious solutions lies in the k_z^2 dependence of Λ . A possibility to ignore the spurious solutions is therefore to ignore $s e$ as compared to $E_g - E$. This will not be too bad an approximation for confinement energies of the holes ($E < 0$). The 6×6 hole matrix \underline{H}_{hole} then gives rise to a polynomial of degree 6 in k_z^2 and therefore to 6 physical $k_z^2(E)$ solutions. The 6×6 hole matrix operator is obtained from $k_z = \tilde{k}_z = i\partial/\partial z$. From the hole part of Eqs.(19), (22) and (23) but with the replacement (25) for γ_1 , γ_2 and γ_3 , we obtain the boundary conditions following the procedure already outlined above. We thus obtain 36 boundary conditions for the evaluation of $3 \times 12 = 36$ expansion coefficients involved in the linear combination of the 12 well and 12 barrier wave function. The problem of the determination of the hole confinement energies can thus be solved without resort to the spurious solutions.

For the electron confinement states the deletion of the spurious solutions is even more simple. We find that \underline{H}_{el} can be written in the form

$$\underline{H}_{el} = \left[\frac{\hbar^2 \tilde{k}_z^2}{2m(E, k_{\parallel})} + E_o(k_{\parallel}) \right] \underline{I}, \quad (27)$$

Chapter 1

where $E_o(\mathbf{k}_\parallel) \equiv E(k_z = 0, \mathbf{k}_\parallel)$ and the E and \mathbf{k}_\parallel dependent effective mass is chosen in such a way that for given \mathbf{k}_\parallel and E the wave number k_z is on the electron branch according to Eq.(8). For given \mathbf{k}_\parallel the problem of the determination of the electron confinement states is then completely similar to a "particle-in-the-box" problem with an energy (and \mathbf{k}_\parallel) dependent effective mass as described in I.

Finally, it should be noted that, for the B parameter equal to zero, the inversion symmetry is effectively restored in the sense that two degenerate hole solutions f_1 and f_2 exist with components even (e_i) or odd (o_i) in z : $f_1 = (e_1, e_2, o_3, o_4, o_5, e_6)$ and $f_2 = (o_4, o_5, e_6, -e_1, -e_2, -o_3)$. The use of this functional form of the envelope function reduces the number of expansion coefficients by a factor of two. This completes the description of our new $\mathbf{k}\cdot\mathbf{p}$ approach to quantum wells. Admittedly the approach is more complex than the earlier /5/ $\mathbf{k}\cdot\mathbf{p}$ approaches but its merits will become clear in the next sections.

III. $\mathbf{k}\cdot\mathbf{p}$ versus tight-binding

Earlier and detailed considerations of quantum wells and superlattices by Chang and Schulman (CS)/8/ have been based upon the nearest neighbor tight-binding approach and a s, p and s^* basis set. The wave functions were "exactly" continued across the interfaces between dissimilar materials in the superlattice using transfer matrix techniques /24/. An approximation still lies in the choice of the tight-binding matrix elements at or near these interfaces. However, for electronically similar materials such as, for example, GaAs and AlAs, results for quantum wells will not depend sensitively on this choice. Boundary conditions for wave functions are in this sense exactly met in the Chang and Schulman approach.

On the contrary, the boundary conditions in the $\mathbf{k}\cdot\mathbf{p}$ approach are not exactly met as we have discussed in the previous section. The problem of the boundary conditions in the $\mathbf{k}\cdot\mathbf{p}$ approach to quantum wells has been considered from various points of view /22/ but there is still no consensus on the usefulness of the *ad hoc* assumption of u -continuity across the interface.

In this section we compare results from our extensive $\mathbf{k}\cdot\mathbf{p}$ approach with results from the CS approach. The comparison is made for a [001] GaAs/Ga_{0.75}Al_{0.25}As quantum well consisting of 68 layers of GaAs in the well, i.e. a well width of 192 Å For such a quantum well, or rather a (68/71) GaAs/Ga_{0.75}Al_{0.25}As superlattice, valence-band confinement energies as a function of \mathbf{k}_\parallel (Fig. 1 of CS) and squared optical matrix elements (Figs. 3 and 4 of CS) have been published. The difference in results for the

Table I All effective masses refer to the center of the Brillouin zone. The unprimed ones are taken along [001], the primed one along [111].

	E_g (eV)	Δ (eV)	m_{EL}	m_{HH}	m_{LH}	m_{SO}	m'_{HH}
GaAs	1.430	.343	.0670	.4537	.0700	.1434	.8526
Ga _{0.75} Al _{0.25} As	1.823	.327	.0942	.5100	.0900	.1720	.9815

superlattice and the quantum well can be ignored in view of the large barrier thickness of the superlattice; it is effectively a multi quantum well. Chang and Schulman have optimized /8/ their tight-binding parameters, not only with respect to certain energies in the bandstructure but also with respect to a certain given set of Γ -point EL, HH, LH and SO effective masses in GaAs and Ga_{0.75}Al_{0.25}As. The CS Γ -point effective masses m_{EL} , m_{HH} , m_{LH} and m_{SO} along [001] and m_{HH} along [111] are given in Table I. In our $k.p$ approach we have used these masses to calculate the parameters s , γ_1 , γ_2 , γ_3 and P for the two materials involved. They are given in Table II. Note that in line with our assumption in the previous section the parameter P is approximately the same in the well (5.310) and the barrier (5.095). To become fully in line with that assumption, we have also done the calculations with P equal in the well and barrier. We have chosen the well value for P , i.e. $P = 5.310$. The EL, LH and HH masses in the barrier have not been allowed to change. The SO mass in the barrier changes from .172 for the earlier P value (5.095) to .174 for the new P value. We have verified that all results that follow are virtually the same for the two cases studied. More precisely, the differences in the results are not visible to the eye in the pictures that we are going to show! All further results in this section can thus be considered to be obtained by either of the two approaches.

We have verified that the bulk bandstructures of GaAs and Ga_{0.75}Al_{0.25}As as obtained from the CS and our $k.p$ approach are in excellent agreement over the range of energies of interest for the confinement energy calculation. Consistent with CS we choose the band-edge-discontinuity ratio to be 85/15. Fig. 1 shows the hole confinement energies as a function of $k_{||}$ along [100] and [110] as calculated from our $k.p$ approach. A comparison with the corresponding CS result (their Fig. 1) shows no visible difference. For the confinement energies at $k_{||} = 0$ this nearly perfect agreement between the CS tight-binding results and our $k.p$ results was expected from our earlier work /12/. The agreement for $k_{||} \neq 0$ is new and opens the possibility for further detailed comparisons. To this end we have considered the strengths of transitions between confined hole and electron states. Depending on the light polarization e , the strength is proportional to

Chapter 1

Table II k_p parameters corresponding to the data in Table I.

	$(2m/\hbar^2)P^2$ (eV)	s	γ_1	γ_2	γ_3
GaAs	28.196	-3.519	1.673	-0.266	0.250
Ga _{0.75} Al _{0.25} As	25.959	-2.903	1.789	-0.086	0.385

$$Q_{ij}(k_{\parallel}) = \left| \langle \psi_{ik_{\parallel}} | e \cdot \frac{\hbar}{i} \nabla | \psi_{jk_{\parallel}} \rangle \right|^2 \quad (28)$$

for a transition between the electron confinement state $\psi_{ik_{\parallel}}$ and the hole confinement state $\psi_{jk_{\parallel}}$. Using expansion (2) for these states and the definition of the basis functions one can straightforwardly express $Q_{ij}(k_{\parallel})$ in terms of the matrix elements P , (Eq. (7)), of the well and the barrier material. Results for linear light polarization in the well (in x - y plane) and perpendicular to the well (along the z -axis) are presented in Figs. 2a

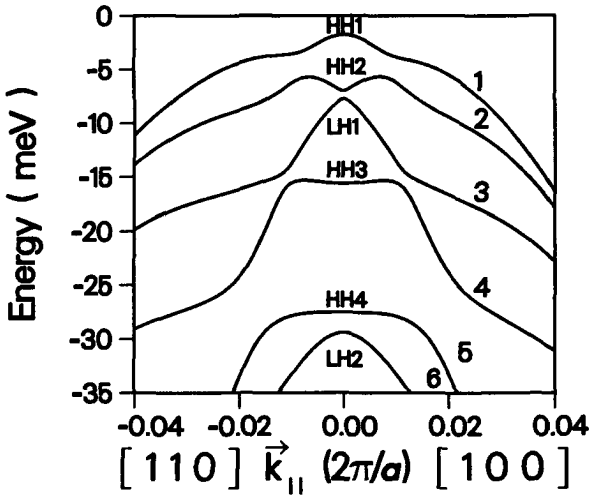


Figure 1 Hole confinement energy spectrum for a GaAs/Ga_{0.75}Al_{0.25}As quantum well of width 192 Å; a is the lattice constant. Energies are measured relative to the top of the valence band of the well material. The labels HH and LH pertain to the prevailing character of the confinement states at $k_{\parallel} = 0$.

and 2c, respectively. States have been labelled according to their order of appearance in the electron and hole confinement spectrum; cf. Fig. 1. For example, the transitions $1 \rightarrow 1$, $1 \rightarrow 2$, $1 \rightarrow 3$ and $1 \rightarrow 4$ correspond in a more common notation to $EL1 \rightarrow HH1$, $EL1 \rightarrow HH2$, $EL1 \rightarrow LH1$ and $EL1 \rightarrow HH3$, respectively. The strong admixture of LH, HH and SO components in the wavefunctions makes the latter designation less useful. The transitions $1 \rightarrow 1$, $1 \rightarrow 3$ and $1 \rightarrow 4$ are allowed even for $k_{\parallel} = 0$. The $1 \rightarrow 4$ ($EL1 \rightarrow HH3$) transition is very weak; $Q_{14} = 10^{-3}$. For $k_{\parallel} \neq 0$, the transitions $1 \rightarrow 2$ and $1 \rightarrow 4$ borrow strength from the $1 \rightarrow 1$ and $1 \rightarrow 3$ transitions because of light hole-heavy hole admixture. Figs. 2b and 2d display the corresponding results from the CS tight-binding approach. The resemblance between the corresponding figures is remarkable good. An interesting difference occurs for Q_{12} at $k_{\parallel} = 0$, i.e. the so-called $EL1 \rightarrow HH2$ transition. In the CS approach the HH and LH bands admix even at $k_{\parallel} = 0$ in the quantum-well wave functions. This effect is absent

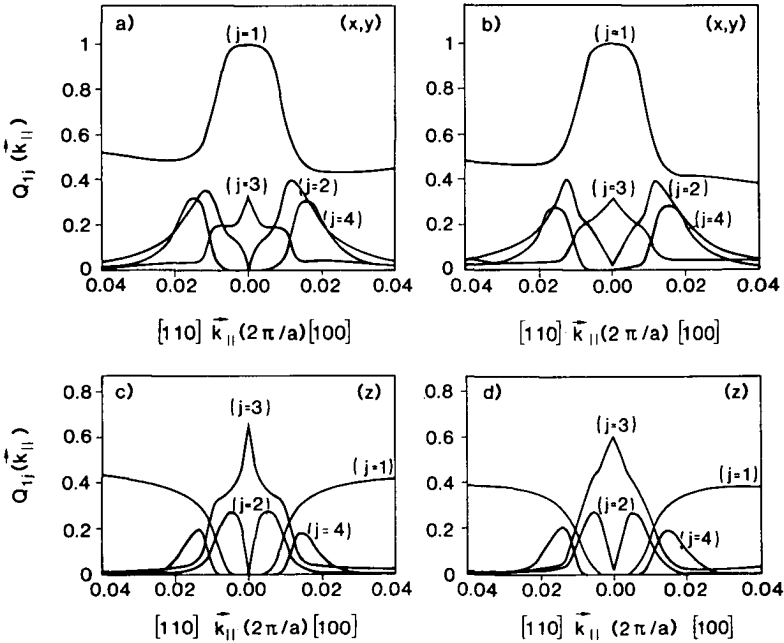


Figure 2 Squared optical matrix elements for (x,y) and z light-polarization between the conduction band 1 and the valence band j in units of $(2m/\hbar^2)P^2$ for a GaAs/Ga_{0.75}Al_{0.25}As quantum well of width 192 Å. a) and c) refer to our $k \cdot p$ results, b) and d) to Chang and Schulman's tight-binding results /8/.

Chapter 1

in our $k.p$ approach. However, the CS matrix element $Q_{12}(k_{\parallel}) = 2.10^{-2}$, i.e. it is rather small.

The above comparisons, in combination with our earlier work, clearly show the ability of our $k.p$ approach to fully produce the band admixture effects as first obtained by Chang and Schulman /8/ using tight-binding. Band admixture effects as have been clearly demonstrated by the observation of EL1 \rightarrow HH2 and EL1 \rightarrow HH3 transitions by Miller et. al. /6,7/ can thus be explained equally well by the CS tight-binding and our $k.p$ approach.

The present results yield an *a fortiori* demonstration of the usefulness of the boundary conditions based upon the u -continuity in the $k.p$ approach, at least for [001] GaAs/Ga_{1-x}Al_xAs quantum wells. The tight-binding approach is more complex in that it contains 15 adjustable parameters, whereas the $k.p$ approach contains only 7 (s , γ_1 , γ_2 , γ_3 , P , E_g and Δ). However, the tight-binding approach is more flexible in that it can, in principle, also deal with, for example, X - and L -derived confinement states. The definite advantage of the $k.p$ approach is that it lends itself to a more direct interpretation of results.

IV. Absorption spectra

With the information on confinement energies and transition strengths as a function of k_{\parallel} available, absorption spectra can be calculated. The absorption coefficient α for light of frequency ω and polarization e is given by

$$\alpha(\hbar\omega) = \frac{\alpha_o}{\omega} \sum_{ij} \alpha_{ij}(\hbar\omega), \quad (29)$$

where the proportionality constant α_o is given by

$$\alpha_o = 4\pi^2 e^2 / (nm^2 cw) \quad (\text{cgs units}), \quad (30)$$

with n the effective refractive index of the quantum well and w the well width. The partial absorption α_{ij} on the transition between the electron confinement state ψ_{ik_1} and the hole confinement state ψ_{jk_1} is given by

$$\alpha_{ij}(\hbar\omega) = 2 \int_{2D \text{ B.Z.}} \frac{dk_{\parallel}}{(2\pi)^2} Q_{ij}(k_{\parallel}) \delta(E_i(k_{\parallel}) - E_j(k_{\parallel}) - \hbar\omega), \quad (31)$$

where the prefactor 2 accounts for the spin degeneracy of the confinement states, the δ -function accounts for energy conservation and $Q_{ij}(\mathbf{k}_\parallel)$ is defined in Eq. (28). Henceforth, the light polarization will be in the plane of the quantum well, i.e. in the x - y plane. When the \mathbf{k}_\parallel dependence of $Q_{ij}(\mathbf{k}_\parallel)$ is ignored we can write

$$\alpha_{ij}(\hbar\omega) = \overline{Q}_{ij} J_{ij}(\hbar\omega), \quad (32)$$

where $J_{ij}(\hbar\omega)$ is the partial joint density of states

$$J_{ij}(\hbar\omega) = 2 \int_{2D \text{ B.Z.}} \frac{d\mathbf{k}_\parallel}{(2\pi)^2} \delta(E_i(\mathbf{k}_\parallel) - E_j(\mathbf{k}_\parallel) - \hbar\omega). \quad (33)$$

However, Eq.(32) is not a valid approximation. For example, if we take $\overline{Q}_{ij} = Q_{ij}(\mathbf{k}_\parallel = \mathbf{0})$, then Eq.(32) implies that we ignore contributions from transitions that are not allowed at $\mathbf{k}_\parallel = \mathbf{0}$. However, from the previous section, in particular Fig. 2, it is clear that such transitions do contribute, for $\mathbf{k}_\parallel \neq \mathbf{0}$, significantly to the absorption coefficient. So we will not use the unjustified simplification (32) but instead we will directly evaluate Eq. (31). The only further approximation will be the neglect of the small anisotropy of $E_i(\mathbf{k}_\parallel)$, $E_j(\mathbf{k}_\parallel)$ and $Q_{ij}(\mathbf{k}_\parallel)$, i.e. their dependence on the direction of \mathbf{k}_\parallel . Figs. 1 and 2 indicate that this is not too bad an approximation. The integration with respect to \mathbf{k}_\parallel in Eq. (31) can now be performed. Let $k_\parallel(E)$ satisfy $E_i(k_\parallel) - E_j(k_\parallel) = E$. Then we find

$$\alpha_{ij}(\hbar\omega) = Q_{ij}(k_\parallel(\hbar\omega)) J_{ij}(\hbar\omega), \quad (34)$$

where the ‘‘isotropic’’ joint density of states is given by

$$J_{ij}(\hbar\omega) = \frac{k_\parallel(\hbar\omega)}{\pi} \left(\frac{dk_\parallel}{dE} \right) \Big|_{E = \hbar\omega} \quad (35)$$

When $E_i(k_\parallel) - E_j(k_\parallel) = E$ has more than one solution $k_\parallel(E)$, Eqs. (34) and (35) must correspondingly be adjusted.

Before turning to the results for the optical absorption it is interesting to consider results for the density of states of electrons and holes and for their joint density of states. The density of confined electron states is given by

$$D_e(E) = 2 \sum_i \int_{2D \text{ B.Z.}} \frac{d\mathbf{k}_\parallel}{(2\pi)^2} \delta(E_i(\mathbf{k}_\parallel) - E), \quad (36)$$

or disregarding the anisotropy of $E_i(\mathbf{k}_\parallel)$, by

$$D_e(E) = \sum_i \frac{\tilde{k}_\parallel^i(E)}{\pi} \left(\frac{d\tilde{k}_\parallel^i}{dE} \right), \quad (37)$$

where $\tilde{k}_\parallel^i(E)$ satisfies $E_i(\tilde{k}_\parallel^i) = E$. For the density of confined hole states we find similar results.

Our calculations pertain to the example quantum well of the previous section, i.e. [001] GaAs/Ga_{0.75}Al_{0.25}As with parameters according to Tables I and II and a band-edge-discontinuity ratio of 85/15. Fig. 3 displays the density of confined electron states as a function of energy, evaluated using the energy dispersion in the [100] and the [110] direction. It clearly shows that the anisotropy of $E_i(\mathbf{k}_\parallel)$ is small and the use of Eq. (37) is validated. We find considerable deviations from step-like behavior. This is due to the non-parabolic behavior of the confined electron energies $E_i(\mathbf{k}_\parallel)$. However, parabolicity is still recognizable in the sense that the results can be interpreted from

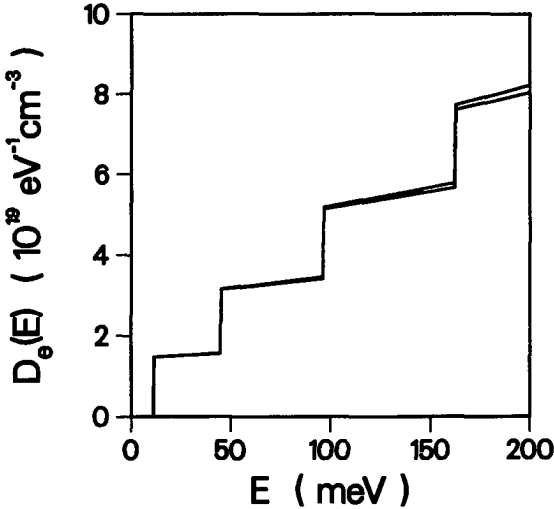


Figure 3 Electron density of states for a GaAs/Ga_{0.75}Al_{0.25}As quantum well of width 192 Å. Energies are measured relative to the bottom of the conduction band of the well material. The two curves were calculated using the energy dispersion in the [100] and the [110] direction, respectively.

“particle-in-the-box” calculations using energy dependent effective electron masses in well and barrier. Fig. 4 displays the density of confined hole states. The anisotropy of $E_j(k_{\parallel})$ is not small in this case and the use of the equivalence of Eq. (37) is not validated. The deviations from step-like behavior are even larger in this case and a description in terms of “particle-in-the-box” behavior with energy dependent masses is clearly useless. Moreover the overall step-like behavior as recognizable in Fig. 4 cannot be simply described in terms of light- and heavy-hole masses due to strong HH-LH admixture. For example the hole confinement states 2 (HH2) and 3 (LH1) in Fig. 1 have parallel masses at $k_{\parallel} = 0$ which deviate strongly from the HH and LH masses appearing at $k = 0$ in the bulk bandstructures. The upward curvature of various hole bands in Fig. 1 leads to singularities in the density of confined hole states in Fig. 4. It is interesting to note that the strong deviations from step- and “particle-in-the-box” like behavior of the holes must manifest itself in the transport properties of these holes in heterojunctions. This issue has to the best of our knowledge not been studied experimentally so far. For example the peak in the density of confined

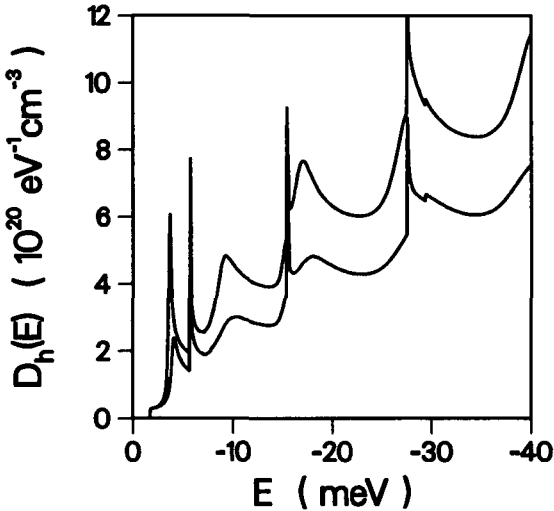


Figure 4 Hole density of states for a GaAs/Ga_{0.75}Al_{0.25}As quantum well of width 192 Å. Energies are measured relative to the top of the valence band of the well material. The two curves were calculated using the energy dispersion in the [100] and the [110] direction, respectively.

states around 4 meV is due to an avoided crossing of the confinement states 1 and 2 and may be observable in transport measurements.

Fig. 5 displays the joint density of states of confined electron i to hole j transitions. The spectrum shows strong deviations from step-like behavior and singularities due to the upward curvature of certain hole-confinement bands. The wiggles arising from avoided crossings in the density of confinement hole states are almost absent in the joint density of states. The latter spectrum is to a large extent dominated by the density of confined electron states because of the light effective mass of the electron. This also explains the small anisotropy in $E_i(k_{\parallel}) - E_j(k_{\parallel})$.

Next, we turn to the absorption spectrum as calculated from Eqs. (34) and (35), evaluated for the energy dispersion in the [100] and the [110] direction. The arithmetic mean of the two resulting absorption spectra is shown in Fig. 6. We have verified that it differs at most 1% from the absorption spectrum which would result from the evaluation of Eqs. (29) and (31). Again strong deviations from step-like behavior and singularities due to the upward curvature of hole states occur. From the previous

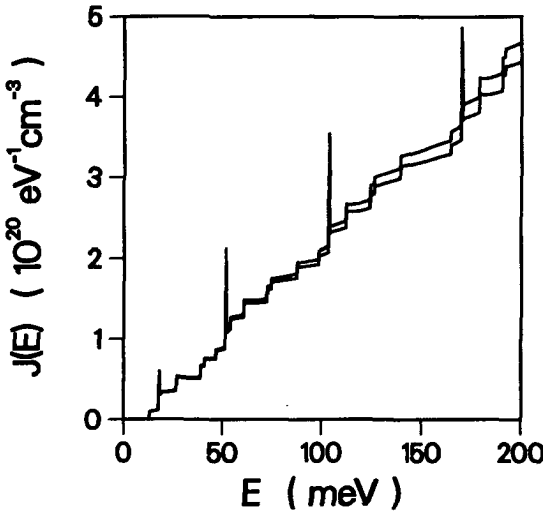


Figure 5 Joint density of states for a GaAs/Ga_{0.75}Al_{0.25}As quantum well of width 192 Å. The two curves were calculated using the energy dispersion in the [100] and the [110] direction, respectively. The labels ij identify the onset of the conduction band i to valence band j transition.

consideration it will be clear that an interpretation in terms of a step-like spectrum as calculated from “particle-in-the-box” considerations for electrons, light-holes and heavy-holes with their bulk effective masses at $k = 0$ is useless. The forbidden or almost forbidden transition at $k_{\parallel} = 0$ which become allowed for $k_{\parallel} \neq 0$ do not appear as visible structures in the spectrum although they do appear as such in the corresponding separate $\alpha_j(\hbar\omega)$ contributions. This result is understandable since the sum of the strengths for transitions from the various strongly admixed hole confinement states to an electron confinement state is to some extent constant. This can clearly be seen from Fig. 2. We note that the forbidden transitions will appear in the spectrum as measured because of exciton formation. The exciton radius will be typically such that the larger part of the k_{\parallel} space shown in Fig. 2 for the transition strength will participate in the exciton. The recent observation of EL1 to HH2 and HH3 excitons by Miller et. al. [25] is an example of this kind of behavior. We will not pursue this subject here any further since it has been dealt with meanwhile in considerable detail by Sanders and Chang [26].

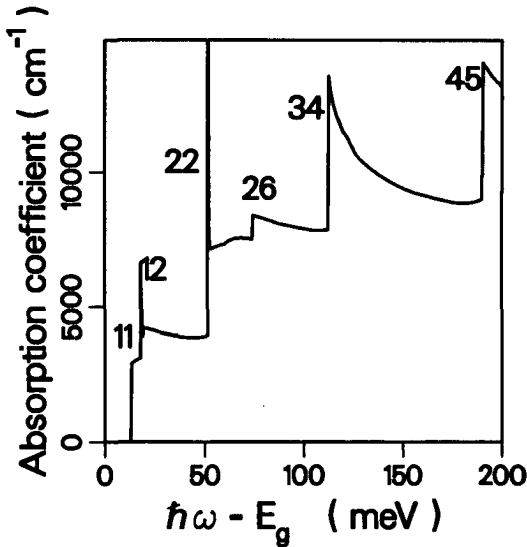


Figure 6 Absorption spectrum for (x,y) -polarization for a GaAs/Ga_{0.75}Al_{0.25}As quantum well of width 192 Å; the refractive index was taken to be 3.6. The labels ij identify the onset of the conduction band i to valence band j transition.

Table III All effective masses refer to the center of the Brillouin zone. The unprimed ones are taken along [001], the primed one along [111].

	E_g (eV)	Δ (eV)	m_{EL}	m_{HH}	m_{LH}	m_{SO}	m'_{HH}
GaAs	1.430	0.343	0.0667	0.3800	0.0870	0.1735	0.9524
AlAs	3.002	0.279	0.1500	0.4785	0.2079	0.3147	1.1490

V. The role of the spin-orbit split-off band

In view of the presently /9/ accepted 67/33 value for the band-edge-discontinuity ratio of GaAs/Ga_{1-x}Al_xAs quantum wells, as opposed to the earlier considered 85/15 value /2/, the consideration of the role of the spin-orbit split-off band in such quantum wells deserves interest. We have studied a [001] GaAs/AlAs quantum well of width 62.21 Å corresponding to 22 GaAs layers. In this case the depth of the potential well

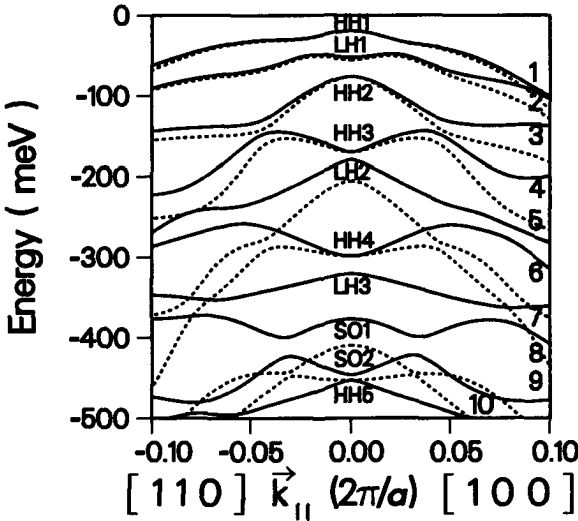


Figure 7 Hole confinement energy spectrum for a GaAs/AlAs quantum well of width 62.21 Å. The solid and dashed lines represent the data with and without ($\Delta = 8$ eV) the inclusion of the spin-orbit band, respectively. The labels HH,LH and SO pertain to the prevailing character of the confinement states at $k_{\parallel} = 0$ for the spin-orbit included data.

Table IV $k.p$ parameters corresponding to the data in Table IV.

	$(2m/\hbar^2)P^2$ (eV)	s	γ_1	γ_2	γ_3
GaAs	28.8	-3.849	0.350	-1.141	-0.350
AlAs	28.8	-2.655	0.252	-0.919	-0.309

for the holes is 519 meV and therefore considerably larger than the spin-orbit splitting of 343 meV in GaAs. We then expect transitions between spin-orbit derived hole confinement states and electron confinement states to appear in the absorption spectrum. The ordering and strength of transitions between HH, LH and SO-derived hole confinement states and electron confinement states depends on the admixture of HH, LH and SO character in the hole confinement states. Such information cannot be obtained from earlier $k.p$ approaches to quantum wells /5/ since they apply to the $\Delta \rightarrow \infty$ limit.

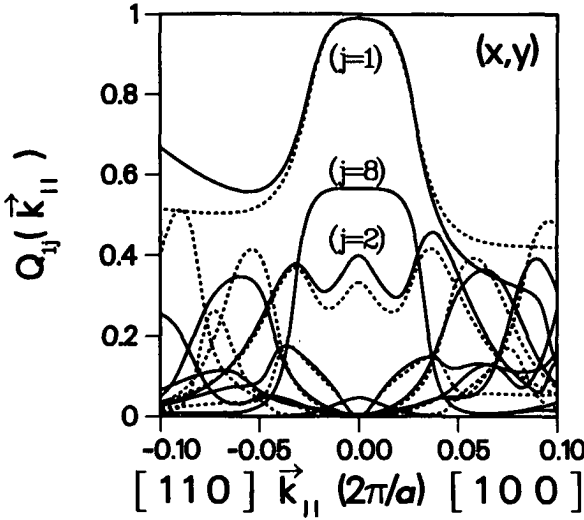


Figure 8 Squared optical matrix elements for the transition between the conduction band 1 and the valence band j in units of $(2m/\hbar^2)P^2$ for a GaAs/AlAs quantum well of width 62.21 Å. The light polarization is in the xy plane. The solid and dashed lines represent the data with and without ($\Delta = 8$ eV) the inclusion of the spin-orbit band, respectively. The labels refer to the solid lines.

The SO bands are then simply not present in the theory. We note that this also implies that the strength of transitions to HH and LH “derived” confinement states lying close in energy to the omitted SO-derived confinement states will not be calculated properly.

Figs. 7, 8 and 9 show results for the [001] GaAs/AlAs quantum well of width 62.21 Å. In line with the recent 67/33 value for the band-edge-discontinuity ratio we have adjusted the effective mass parameters for GaAs to be in better agreement with recent experimental knowledge /20/ on these parameters. Effective masses and corresponding k,p parameters are given in Tables III and IV. Note that we have chosen equal P values in the well and the barrier. Fig. 7 presents hole confinement energies as a function of k_{\parallel} . The labels HH, LH and SO pertain to the prevailing character of the confinement states at $k_{\parallel} = 0$; note that only the HH states are decoupled at $k_{\parallel} = 0$. Close to the spin-orbit splitting of 343-meV of GaAs we observe the appearance of two SO-derived states (8 and 9). Moreover all the other bands are modified due to interaction with these SO-derived bands.

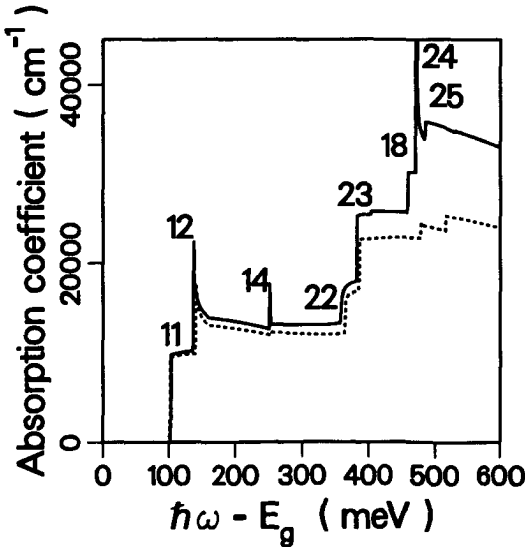


Figure 9 Absorption spectrum for (x,y) -polarization for a GaAs/AlAs quantum well of width 62.21 Å. The solid and dashed lines represent the data with and without the inclusion of the spin-orbit band, respectively. The labels ij identify the onset of the conduction band i to valence band j transition for the spin-orbit included data.

The admixture of HH, LH and SO states is evidently very strong. This is even more pronounced in Fig. 8 for the squared optical matrix elements between the EL1 and hole confinement states. The $1 \rightarrow 8$ (EL1 \rightarrow SO1) transition strength squared is large; it is 0.5 of the $1 \rightarrow 1$ strength squared.

Fig. 9 displays the absorption spectrum. It contains one additional step due to the $1 \rightarrow 8$ (EL1 \rightarrow SO1) transition. When exciton effects are taken into account we expect in addition to the EL-HH and EL-LH peaks two additional EL1-SO1 and EL1-SO2 exciton peaks. A warning is appropriate here. The additional exciton peaks will lie in the midst of various other exciton peaks and ignoring the spin-orbit split-off states may thus easily lead to a misinterpretation of experimental spectra.

The very observation by excitation, Raman or Brillouin spectroscopy of transitions involving the spin-orbit split-off states yields the unique opportunity to gain information on the value of m_{so} , the spin-orbit split-off band mass along [001]. The position of the corresponding exciton peaks will depend sensitively on the value of m_{so} in GaAs and, to a lesser extent, on the value of m_{so} in AlAs.

VI. Gain in quantum-well lasers

Recently the gain in quantum-well lasers was studied using "particle-in-the-box" models for the confinement of electrons and holes and constant optical matrix elements for the transitions between electron and hole states /10/. The $k.p$ approach presented in this paper provides a unique opportunity to improve on this situation, i.e. to take into account fully the effects of admixture of light-, heavy- and spin-orbit split-off holes.

We have calculated the gain of a [001] GaAs/Ga_{1-x}Al_xAs quantum well of width 192 Å as studied in sections 3 and 4. Parameters are from Tables I and II and the band-edge-discontinuity ratio was taken to be 85/15. We have assumed a pumped (electrically or optically) carrier density of $3 \cdot 10^{18} \text{ cm}^{-3}$. Of course this carrier density must not be confused with a density arising from doping the quantum well. The present analysis would not pertain to such a quantum well since we have assumed flat-band conditions. Using charge neutrality $n = p$, we can obtain the quasi Fermi levels for the electrons, E_n , and the holes, E_p , using the earlier density of states results. The gain as a function of photon energy $\hbar\omega$ can then be evaluated from

$$g(\hbar\omega) = \frac{\alpha_0}{\omega} \sum_{ij} g_{ij}(\hbar\omega), \quad (38)$$

Chapter 1

where the partial gain g_{ij} on the transition between electron confinement state $\psi_{e\mathbf{k}_\parallel}$ and hole confinement state $\psi_{h\mathbf{k}_\parallel}$ is given by

$$g_{ij}(\hbar\omega) = 2 \int_{2D \text{ B.Z.}} \frac{dk_{\parallel}}{(2\pi)^2} Q_{ij}(\mathbf{k}_{\parallel}) \delta(E_i(\mathbf{k}_{\parallel}) - E_j(\mathbf{k}_{\parallel}) - \hbar\omega) [f_n(E_i(\mathbf{k}_{\parallel})) - f_p(E_j(\mathbf{k}_{\parallel}))] \quad (39)$$

and $f_n(E_i(\mathbf{k}_{\parallel}))$ and $f_p(E_j(\mathbf{k}_{\parallel}))$ are the probabilities that the electron (i) and hole (j) states are occupied i.e.

$$f_n(E_i(\mathbf{k}_{\parallel})) = 1 / \{ 1 + \exp[(E_i(\mathbf{k}_{\parallel}) - E_n)/k_B T] \} . \quad (40)$$

and

$$f_p(E_j(\mathbf{k}_{\parallel})) = 1 / \{ 1 + \exp[(E_j(\mathbf{k}_{\parallel}) - E_p)/k_B T] \} . \quad (41)$$

Ignoring again the dependence of $E_i(\mathbf{k}_{\parallel})$, $E_j(\mathbf{k}_{\parallel})$ and $Q_{ij}(\mathbf{k}_{\parallel})$ on the direction of \mathbf{k}_{\parallel} , Eq. (39) can be easily evaluated. We have verified that the gain curves, calculated using the energy dispersion along [100] and [110] differ at most 2%.

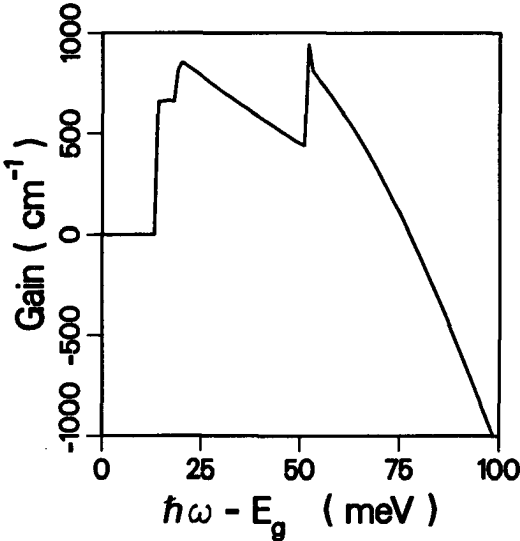


Figure 10 Gain spectrum for (x,y) -polarization for a GaAs/Ga_{0.75}Al_{0.25}As quantum well of width 192 Å. The carrier density was taken to be $3.10^{18} \text{ cm}^{-3}$ and the temperature is 300 K.

Fig. 10 shows the gain (in cm^{-1}) as a function of photon energy for light polarization in the plane of the quantum well, i.e. the TE mode. We have verified that the peak gain with and without hole admixture effects differs by a factor of 2 typically, the former being smaller. Moreover the structure in the gain spectra appears at different photon energies. We have also calculated radiative lifetimes of carriers in quantum wells and gain-current relationships. The results will be published elsewhere [11]. Here we note that when the gain in a quantum-well laser is dominated by single-particle band to band transitions with k -conservation (as was assumed in Eq. (39)), the gain spectrum is seriously affected by band admixture.

VII. Conclusions

We have presented a very advanced k,p envelope function formalism for GaAs/Ga_{1-x}Al_xAs and alike quantum wells. The Kane-type, unified description of the conduction and valence bands of the well and the barrier material results in a small set of adjustable parameters. Apart from the gap and the spin-orbit splitting they may be taken to be the EL,HH,LH and SO Γ -point effective masses along [001] and the HH Γ -point effective mass along [111] in each material.

Our calculated confinement energies and optical matrix elements as a function of k_{\parallel} are in excellent agreement with those obtained by the Chang and Schulman 20-band tight-binding approach. It demonstrates the usefulness of the chosen boundary conditions in the k,p envelope function formalism. Typical accuracies have been described in section 3.

The main virtues of the model are that it contains only a small set of adjustable and experimentally measurable parameters and that it can, with these parameters, explain the main features in experimentally observed absorption spectra like the so-called forbidden $\Delta n \neq 0$ transitions.

As expected, the inclusion of the spin-orbit split-off band changes the calculated absorption spectra for GaAs/AlAs quantum wells dramatically at higher photon energies. This is particularly relevant since the newly accepted value for the valence-band discontinuity ratio of approximately 67/33 brings the spin-orbit split-off band well within the hole well. As a result spin-orbit split-off confined states arise.

Finally, we have applied our model to the calculation of gain spectra of GaAs/Ga_{1-x}Al_xAs quantum wells. The valence-band admixture has a large effect on both the magnitude of the gain spectrum and the energy position of the gain peaks.

Chapter 1

References

1. R. Dingle, W. Wiegmann and C.H. Henry, *Phys. Rev. Lett.* 14, 827 (1974); R. Dingle, A.C. Gossard and W. Wiegmann, *Phys. Rev. Lett.* 21, 1327 (1975); P. Dawson, G. Duggan, H.I. Ralph and K. Woodbridge, *Superlattices and Microstructures* 1, 231 (1985).
2. R. Dingle, *Festkörperprobleme*, ed. by J. Treusch, *Advances in Solid State Physics*, Pergamon, New York (1975), Vol. 15, p. 15
3. G. Bastard, *Phys. Rev. B* 24, 5693 (1981); G. Bastard, *Phys. Rev. B* 25, 7584 (1982).
4. S.R. White and L.J. Sham, *Phys. Rev. Lett.* 47, 879 (1981).
5. M. Altarelli, *Physica* 117B/118B, 747 (1983) and *J. Lumin.* 30, 472 (1985); M. Altarelli, U. Ekenberg and A. Fasolino, *Phys. Rev.* B32, 5138 (1985).
6. R.C. Miller, D.A. Kleinman, W.A. Nordland, Jr., and A.C. Gossard, *Phys. Rev.* B22, 863 (1980).
7. C. Weisbuch, R.C. Miller, R. Dingle, A.C. Gossard and W. Wiegman, *Solid State Commun.* 37, 219 (1980).
8. Y.C. Chang and J.N. Schulman, *Phys. Rev.* B31, 2069 (1985).
9. R.C. Miller, A.C. Gossard and D.A. Kleinman, *Phys. Rev.* B32, 5443 (1985); J. Menendez, A. Pinczuk, D.J. Werder, A.C. Gossard and J.H. English, *Phys. Rev.* B33, 8863 (1986); H. Kroemer in *Molecular Beam Epitaxy and Heterostructures*, ed. by L.L. Chang and K. Ploog Nijhoff, Dordrecht, 1985).
10. Y. Masamichi and I. Suemune, *Jap. Journ. of Appl. Phys.* 23, L35 (1984). M. Asada, A. Kameyama and Y. Suematsu, *IEEE Journ. of Quant. Elec.* QE-20, 745 (1984).
11. S. Colak, R. Eppenga and M.F.H. Schuurmans, to be published.
12. M.F.H. Schuurmans and G.W. 't Hooft, *Phys. Rev.* B31, 8041 (1985).
13. E.O. Kane, in *Handbook on Semiconductors* (North-Holland, New York, 1982), Vol. I, p. 193.
14. P.O. Löwdin, *J. Chem. Phys.* 19, 1396 (1951).
15. J.M. Luttinger, *Phys. Rev.* 102, 1030 (1956).
16. N.E. Christensen and M. Cardona, *Solid State Commun.* 51, 491 (1984).
17. S.F. Alvarado, H. Riechert and N.E. Christensen, *Phys. Rev. Lett.* 55, 2716 (1985).
18. R. Eppenga and M.F.H. Schuurmans, in print *Phys. Rev. B*.
19. C. Hermann and C. Weisbuch, in *Optical orientation*, ed. F. Meier and B.P. Zakharchenya (Elsevier Science Publishers B.V., Amsterdam 1984).
20. W.P. Dumke, M.R. Lorenz and G.D. Pettit, *Phys. Rev.* B5, 2978 (1972). P. Lawaetz, *Phys. Rev.* B4, 3460 (1971). G. Duggan, *J. Vac. Sci. Technol.* B 3(4), 1224 (1985).

A new $k.p$ theory for GaAs/GaAlAs-type quantum wells

21. L.J. Sham and M. Nakayama, Phys. Rev. B20, 734 (1979).
22. R.A. Morrow and K.R. Brownstein, Phys. Rev. B30, 678 (1984).
23. D.L. Smith and C. Mailhot, Phys. Rev. B33, 8345 (1986).
24. J.N. Schulman and Y.C. Chang, Phys. Rev. B27, 2346 (1983).
25. R.C. Miller, A.C. Gossard, G.D. Sanders, Y.C. Chang, J.N. Schulman, Phys. Rev. B32, 8452 (1985).
26. G.D. Sanders and Y.C. Chang, Phys. Rev. B32, 5517 (1985); G.D. Sanders and Y.C. Chang, Phys. Rev. B31,6982, (1985)

Effects of band mixing on the radiative properties of a quantum well

The effect of band mixing and non-parabolicity on quantum well gain and spontaneous emission is studied using $k \cdot p$ theory. Spectra of gain and spontaneous emission are strongly modified but the relation of maximum gain versus nominal current density is not strongly affected.

Introduction

In recent years several theoretical studies on the gain of quantum-well lasers have appeared /1-6/. All of these studies were incomplete to the extent that they have ignored the band mixing and the non-parabolicity of the electron and the hole bands. In the context of the study of light absorption, band mixing and non-parabolicity have been dealt with by Chang and Schulman using a very involved and complete tight binding approach /7/ and by the present authors using a more simple $k \cdot p$ approach /8/. The results for absorption spectra of the two approaches were the same.

The purpose of this paper is the study of gain and spontaneous-emission spectra of quantum wells using our $k \cdot p$ approach and the comparison of the results with those from earlier conventional approaches /1-6/.

Our results pertain specifically to GaAs/AlGaAs [001] quantum wells but the results are expected to be indicative for all type 1 quantum wells.

Model

Our $k \cdot p$ envelope function approach for the calculation of electron and hole confinement states in a GaAs/AlGaAs [001] quantum well has been described elsewhere /8/. We briefly summarize. In the Γ -point basis set we treat the electron (EL), light hole (LH), heavy hole (HH) and the spin-orbit split-off (SO) bands exactly and all other bands perturbatively. Apart from the gap and the spin orbit splitting the resulting

model contains 6 parameters for each material. They may be taken to be the EL, LH, HH and SO effective mass m_{EL} , m_{LH} , m_{HH} , m_{SO} at the center Γ of the Brillouin zone along $[001]$, the HH effective mass m'_{HH} at Γ along $[111]$ and a parameter B which describes the inversion asymmetry of each material. We take $B=0$.

Note that our $k.p$ model extends on that of Altarelli /9/ in that we do take into account the non-parabolic behavior of the SO band and the mixing of the LH and SO band, even at $k_{\parallel} = 0$. The vector k_{\parallel} describes the translational symmetry in the parallel plane of the quantum well.

Since the conventional approaches vary a bit from paper to paper /1-6/, we will define the conventional model to be the one based on independent parabolic bands with the effective masses equal to the bulk masses at Γ in the various directions, Dingle's /10/ approach for each such band but with the envelope function connection rule that does take into account the difference in effective masses in the two materials constituting the quantum well and with optical matrix elements being constant and equal to their values at the center of the quantum-well Brillouin zone.

Band structure and optical matrix elements

In this section we present the calculated confinement energies and optical matrix elements between hole and electron confinement states as a function of k_{\parallel} for a GaAs/ $Al_{.35}Ga_{.65}As$ quantum well of width 62.2 Å. The parameters used are listed in Table 1 and are chosen to accurately reproduce the bulk bandstructures of GaAs and $Al_{.35}Ga_{.65}As$ /11/. The ratio of conduction to valence-band discontinuity is taken to be 67/33 /12/. For a transition between the electron confinement state $\psi_{ik_{\parallel}}$ and the hole confinement state $\psi_{jk_{\parallel}}$ the optical matrix element is defined as follows

$$Q_{ij}(k_{\parallel}) = \left| \langle \psi_{ik_{\parallel}} | e \cdot \frac{\hbar}{i} \nabla | \psi_{jk_{\parallel}} \rangle \right|^2, \quad (1)$$

where e is the light polarization.

Earlier /8/, we have shown that the results of our model are in excellent agreement with the results of the more complicated tight binding calculations by Chang and Schulman /7/. This is particularly gratifying since their model employs exact boundary conditions. In a $k.p$ envelope function approach the alledged continuity of the rapidly varying u part of the true wavefunction is an approximation.

Table 1 All effective masses refer to the center of the Brillouin zone. The unprimed ones are taken along [001], the primed one along [111].

	E_{gap} (eV)	Δ (eV)	m_{EL}	m_{HH}	m_{LH}	m_{SO}	m'_{HH}
GaAs	1.430	.343	.0667	.3800	.0870	.1735	.9524
$Al_{.35}Ga_{.65}As$	1.898	.321	.0931	.4095	.1232	.2199	1.0131

Fig. 1 shows strong mixing and non-parabolic behavior of the hole bands for the GaAs/ $Al_{.35}Ga_{.65}As$ quantum well. Note that the designation HH,LH in the center portion of the figure makes no sense for the bands as a whole, i.e. as a function of $k_{||}$. We shall often label the bands in order of appearance starting at the bottom of the potential well; $i=1,2,\dots$ for the electrons and $j=1,2,\dots$ for the holes.

Fig. 2 shows that the so-called $n=1$ electron (EL1) to $n=2$ and $n=3$ heavy hole (HH2,HH3) transitions may occur in the excitation, gain or spontaneous emission

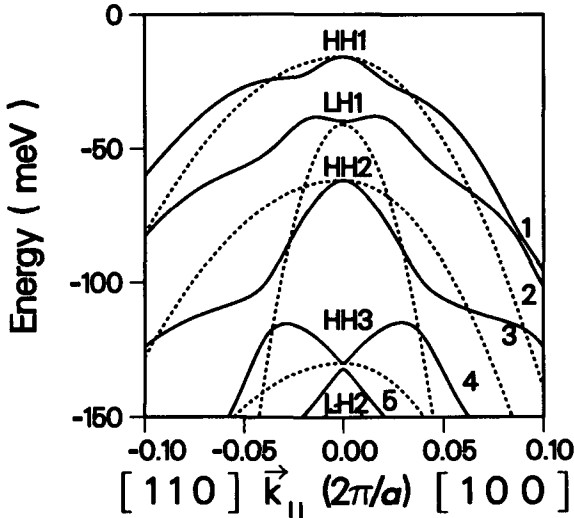


Figure 1 Hole confinement energy spectrum as calculated from our $k.p$ theory (drawn lines) and the conventional theory (dotted lines) for a GaAs/ $Al_{.35}Ga_{.65}As$ [001] quantum well of width 62.2 Å; a is the lattice constant. Note that the results for the conventional theory are based upon the different bulk effective masses along the different $k_{||}$ directions shown.

Effects of band mixing on the radiative properties of a quantum well

spectrum: for $k_{\parallel} \neq 0$ oscillator strength is borrowed from the $n=1$ electron to $n=1$ light hole (LH1) transition because of light hole-heavy hole admixture. Our $k.p$ model is able to explain the recently observed $n=1$ to $n=2$ and $n=3$ transitions /13/, when exciton effects are added .

Figs. 3,4 and 5 show the density of states (DOS) for electrons and holes and the joint density of states (JDOS). The strong deviations from the results of the conventional model, i.e. steplike behavior, are obvious. Note that both step edge positions, corresponding to confinement energies, and step heights are different. The singularities appearing close to the edges are due to the upward curvature of hole bands (Fig. 1). The DOS spectra are relevant for the calculation of the quasi-Fermi levels in the lasing quantum well.

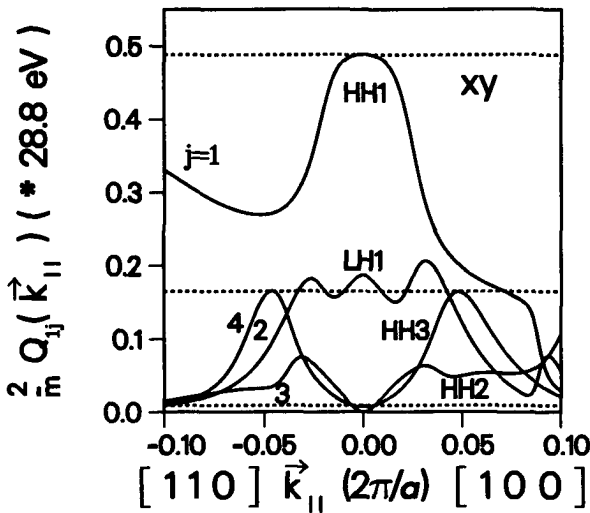


Figure 2 Optical matrix elements for light polarization (x or y) in the plane of the quantum well; $k.p$: drawn, conventional: dotted. The value for the optical matrix element of bulk GaAs for the x (or y or z) polarization is 28.8 eV. In the conventional theory only three allowed transitions appear in the picture; the EL1-HH3 transition is very weak.

Gain and spontaneous emission

The main difficulty in the calculation of the spectra of gain and spontaneous emission is to take proper account of the $k_{||}$ dependence of the optical matrix elements. This is also a major difference with earlier calculations/1-6/. The gain $g(\omega)$ for light at frequency ω and with polarization e is given by

$$g(\omega) = \frac{4\pi^2 e^2}{nm^2 c\omega} \sum_{ij} g_{ij}(\omega), \quad (2)$$

with n the effective refractive index of the quantum well. The partial gain $g_{ij}(\omega)$ on the transition between the electron confinement state $\psi_{ik_{||}}$ and the hole confinement state $\psi_{jk_{||}}$ is given by

$$g_{ij}(\omega) = \frac{2}{w} \int \frac{dk_{||}}{(2\pi)^2} Q_{ij}(k_{||}) \delta(E_i(k_{||}) - E_j(k_{||}) - \hbar\omega) [f_c(E_i(k_{||})) - f_v(E_j(k_{||}))], \quad (3)$$

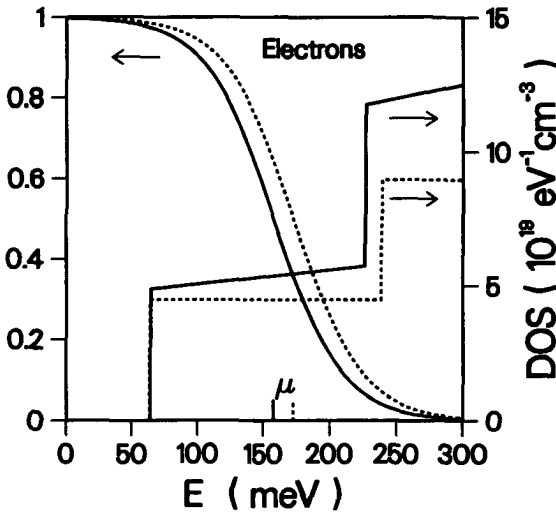


Figure 3 Electron DOS; $k.p.$: drawn, conventional: dotted. The Fermi-Dirac distribution functions for $n = p = 5 \cdot 10^{18} \text{cm}^{-3}$ and $T = 300 \text{ K}$, and the quasi-Fermi level positions μ , are also indicated.

Effects of band mixing on the radiative properties of a quantum well

where the prefactor 2 accounts for the spin degeneracy of the confinement states, w is the well width, the δ - function accounts for energy conservation, the optical matrix elements $Q_{ij}(k_{\parallel})$ are defined in eq.(1) and $f_c(E_i(k_{\parallel}))$ and $f_v(E_j(k_{\parallel}))$ are the Fermi-Dirac probabilities. The quasi-Fermi levels involved follow from charge neutrality, $n = p$, and the prescribed value of the injected electron density n .

For the spontaneous emission rate we can write down a formula similar to eq.(2), i.e.

$$r(\omega) = \frac{4\pi^2 e^2}{nm^2 c\omega} \sum_{ij} r_{ij}(\omega), \quad (4)$$

where the partial rates are given by

$$r_{ij}(\omega) = \frac{2n^2 \omega^2}{\pi \hbar c^2} \frac{2}{w} \int \frac{dk_{\parallel}}{(2\pi)^2} Q_{ij}(k_{\parallel}) \delta(E_i(k_{\parallel}) - E_j(k_{\parallel}) - \hbar\omega) \{ f_c(E_i(k_{\parallel})) [1 - f_v(E_j(k_{\parallel}))] \}. \quad (5)$$

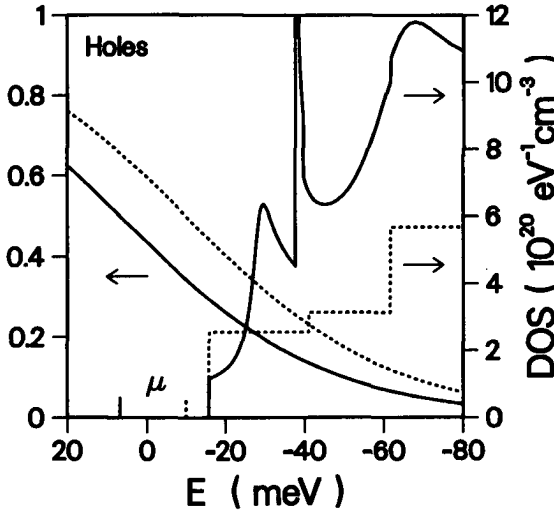


Figure 4 Hole DOS; k,p : drawn, conventional: dotted. The Fermi-Dirac distribution functions for $n = p = 5 \cdot 10^{18} \text{ cm}^{-3}$ and $T = 300 \text{ K}$, and the quasi-Fermi level positions μ , are also indicated.

The nominal current density follows from

$$j_{nom} = ew \int r_{av}(\omega) d\hbar\omega, \quad (6)$$

where r_{av} stands for the average of r with respect to light polarization. In the calculation of $g(\omega)$ and $r(\omega)$ the anisotropy of the integrands with respect to $k_{||}$ is ignored and the integration is cut off at $k_{||} = 0.1(2\pi/a)$; a is the lattice constant.

Figs. 6 and 7 show the gain and spontaneous emission spectra of the above described quantum well. The spectra exhibit the net effect of all such important aspects as the strongly non-parabolic behavior with $k_{||}$ of the hole confinement energies and the corresponding non-steplike behavior of the DOS, upward curvature of various hole bands leading to singularities in the DOS and JDOS and the $k_{||}$ dependence of the optical matrix elements. Note that the narrow peaks in Figs. 6 and 7 result from these singularities and should not be confused with exciton peaks. Two-particle interactions have not been added to the calculations.

Fig. 8 shows a gain/nominal current relation for a quantum-well laser.

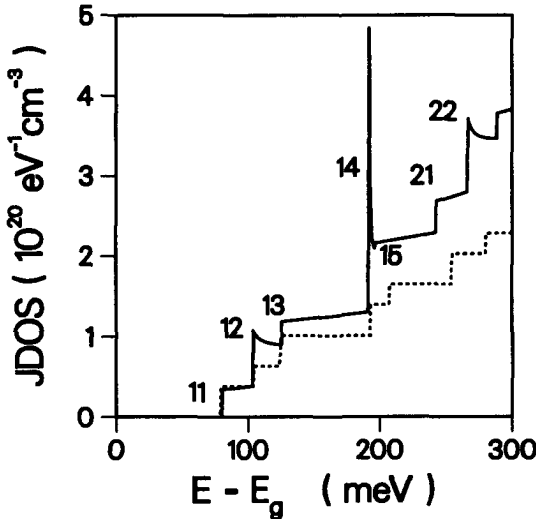


Figure 5 JDOS; $k.p.$: drawn, conventional: dotted.

Discussion

Although both the energy spectrum and the optical matrix elements vary strongly with $k_{||}$, the gain and the spontaneous emission spectrum show more or less the "step"-like structure as expected from the conventional model. However, the step edges corresponding to the confinement energies are somewhat different and the step heights are rather different. The step edges signalize the EL1-HH1 and EL1-LH1 transitions. All other transitions (Fig. 2) are invisible. As is clear from Figs. 1,3 and 4 the confinement energies of the EL1, HH1 and LH1 states at $k_{||} = 0$ do not, or only marginally, differ in the $k.p$ and the conventional approach. This is understandable since at $k_{||} = 0$ the HH1 band is decoupled from all other bands and the LH1 band is only weakly coupled to the SO bands. The forbidden or almost forbidden transitions at $k_{||} = 0$, which become allowed for $k_{||} \neq 0$, do not appear as visible structures in the spectra since the sum of the strengths for transitions from the various strongly admixed hole confinement states to an electron confinement state is more or less constant. Structure due to band mixing or non-parabolicity is visible in absorption spectra in between the steps /7,8/. Such structure is almost invisible in the gain and spontaneous

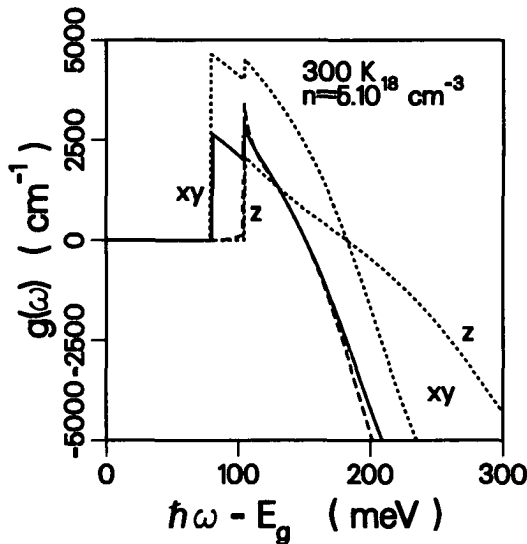


Figure 6 Gain spectrum for different light polarizations and $n = 5 \cdot 10^{18} \text{ cm}^{-3}$; $k.p$: drawn + dashed, conventional: dotted.

emission spectra since it is dominated by the rapidly decreasing Fermi-Dirac functions. The dependence on light polarization in Figs. 6 and 7 is rather different as predicted by $k.p$ and conventional theory. Whereas $k.p$ predicts hardly any difference in gain for the two polarizations (x or y versus z) a factor of 2 difference appears in the prediction from the conventional theory at the high energy tail. This can be understood in terms of the different ratios of occupation numbers of the HH1 and the LH1 states in the $k.p$ and the conventional theory. It is related to the different hole quasi-Fermi levels in the two theories (Figs. 3 and 4) which is due to the different hole DOS. Another consequence of the different quasi-Fermi levels is the different spectral width over which gain occurs: 151 meV, $k.p$, and 183 meV, conventional.

The maximum gain/nominal current density relation as calculated from the $k.p$ and the conventional approach are rather similar. However, one should realize that in order to achieve equal nominal current densities in the two cases one needs a higher injected density in the $k.p$ than in the conventional theory; compare the end-points of the curves for 300 K which both correspond to $n = 10^{19} \text{ cm}^{-3}$.

In conclusion, modelling of gain and spontaneous emission spectra requires the use of a rather extensive $k.p$ model. The conventional model discussed is inadequate but,

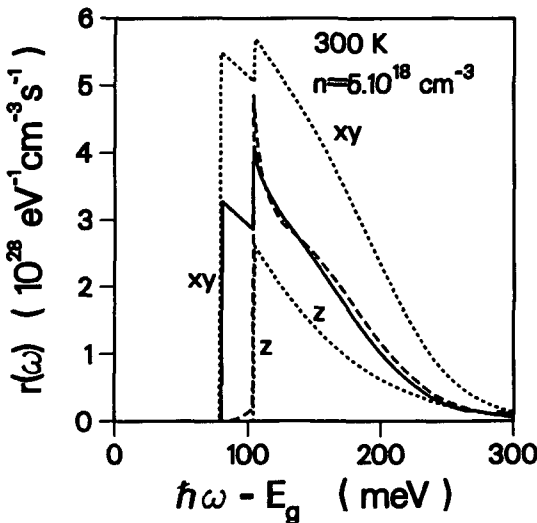


Figure 7 Spontaneous emission spectrum for different light polarizations and $n = 5 \cdot 10^{18} \text{ cm}^{-3}$; $k.p$: drawn + dashed, conventional: dotted.

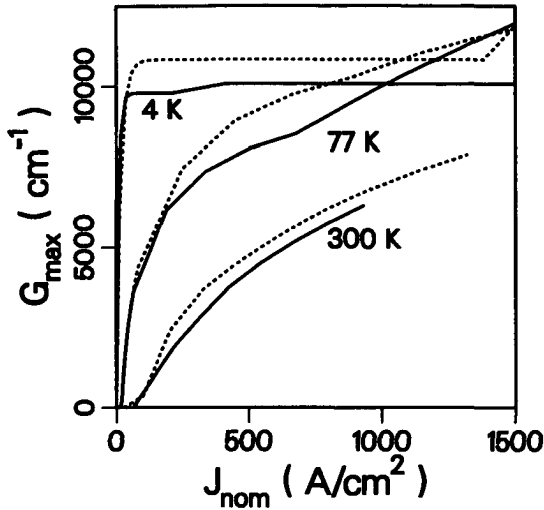


Figure 8 Maximum gain for in plane light polarization (x or y) as a function of nominal current density for various temperatures; $k.p.$: drawn, conventional: dotted. Injected densities have been varied from $n = 10^{17} \text{ cm}^{-3}$ to $n = 10^{19} \text{ cm}^{-3}$.

as a matter of course, the conventional model can be formally adjusted choosing masses different from the bulk masses. Moreover, one should realize that intra-band relaxation, well width fluctuation, current spreading and band-gap renormalization occurring at high injection densities will further modify these results. This is subject to present study in relation to experimental work.

References

1. N.K.Dutta, J.Appl.Phys.53, 7211 (1982)
2. D.Kasemset, C.Hong, N.B.Patel and P.D.Dapkus, IEEE J.Quant. Electron. 19,1025 (1983)
3. A.Sugimura, IEEE J.Quant.Electron. 20, 336 (1984)
4. M.Asada, A.Kameyama and Y.Suematsu, IEEE J.Quant.Electron. 20, 745 (1984)

Chapter 2

5. M.Yamada, S.Ogita, M.Yamagichi and K.Tabata, IEEE J.Quant.Electron. 21, 640 (1985)
6. Y.Arakawa and A.Yariv, IEEE J.Quant.Electron. 21, 1666 (1985)
7. Y.C.Chang and J.N.Schulman, Phys. Rev. B31, 2069 (1985).
8. M.F.H.Schuurmans and G.W.'t Hooft, Phys. Rev. B31, 8041 (1985); R.Eppenga, M.F.H.Schuurmans and S.Colak, Phys. Rev. B36, 1554 (1987); R.Eppenga, M.F.H.Schuurmans and S.Colak, Accurate calculation of (001) quantum-well confinement states and the corresponding gain/absorption spectrum, Proceedings of the 18th ICPS conference, p. 445, Stockholm, 1986.
9. M.Altarelli, Physica 117B/118B, 747 (1983) and J. Lumin. 30, 472 (1985)
10. R.Dingle, Festkorperprobleme XV,21 (1975)
11. G.Duggan, J.Vac.Sci.Techn.B3(4), 1224 (1985)
12. R.C.Miller, A.C.Gossard and D.A.Kleinman, Phys.Rev.B32,5443 (1985); J.Menendez, A.Pinczuk, D.J.Werner, A.C.Gossard and J.H.English, Phys.Rev.B33, 8863 (1985); H.Kroemer in "Molecular beam epitaxy and heterostructures", ed. L.L.Chang and K.Ploog, Nijhof, Dordrecht (1985)
13. R.C.Miller, A.C.Gossard, G.D.Sanders, Y.C.Chang and J.N.Schulman, Phys. Rev. B32, 8452 (1985)

Chapter 3

Band Mixing Effects on Quantum Well Gain

Gain in a quantum well is studied by using the optical matrix elements and the bandstructure computed by the $k.p$ method within the envelope function approximation. Due to band mixing, the $k.p$ method gives nonparabolic bands which affect both the minimum confinement energies and the density of states functions. The density of states functions are found to differ considerably from the simple step-like shape computed from the band edge effective masses. The band mixing also results in large differences in the momentum vector dependence of the matrix elements, and moreover, some of the transitions which were previously assumed to be forbidden become partially allowed. The quantum-well gain spectra calculated by the $k.p$ method and the k -selection rules clearly show the effects of band mixing both in shape and in peak magnitude. These results are considerably different than those obtained from the conventional methods which consider an effective mass electron (or hole) in a finite one-dimensional potential well with parabolic bands and with matrix elements which have constant total magnitude. A practical conclusion which is reached from these comparisons is that the threshold excitation in a quantum-well laser is found to be strongly underestimated if band-mixing effects are ignored.

Introduction

In recent years there have been several studies [1-6] to find out about the gain and its optimization in quantum-well (QW) lasers where the carriers are confined in an one-dimensional (1-D) finite potential well. Without exception, all of these studies have based their models on the energy levels calculated for an effective mass electron (or

hole) in this potential well /7/. The energy versus momentum vector $E - k$ dispersion curves for the electron in the QW plane were assumed to be defined by parabolic bands with bulk material effective mass values. In addition, the magnitudes of the optical matrix elements were assumed to be constant for the transitions anywhere in the bands (no k or E dependence). Other recent, more basic studies /8-11/ however, have shown that with more detailed analysis, the bandstructure and the optical matrix elements of the QW can be quite different from the ones calculated with the simple model described above. These recent more detailed analyses of the QW are based on techniques such as the tight binding method /8/, the pseudopotential method /9/, and the $k.p$ perturbation method /10,11/. All of these three techniques show clear effects of the band mixing on the QW subband levels and on the matrix elements. The main purpose of the present work is to study the gain and other radiative properties of a QW calculated by the $k.p$ method in the envelop function approximation. It should be noted that, although the $k.p$ method discussed in this work is used in the envelope function approximation /10/, we will refer to it simply as the “ $k.p$ method”. It should also be realized that the conventional technique referred to here contains modifications (for matrix elements) which are based on a simplified $k.p$ concept /4/ which takes into account the orientational properties of the Bloch functions at the zone center $k = 0$ point only. However, the full $k.p$ usage with band mixing in studies for QW laser properties had not been considered previously.

All of the gain related parameters given in the present work are calculated by using strict k -selection rules. There have been a few studies /12,13/ using no k -selection rules in conjunction with the simpler conventional QW model /1-7/ mentioned above. These studies /12,13/ aimed mainly at explaining the rounded and symmetric shape of the experimental gain /14,15/ and emission /16-18/ spectra observed from the QW lasers. These no k -selection-based studies however, predict gain peaks shifted towards higher energy than the QW band-gap. This prediction does not agree with the experimentally observed gain peak shifts towards the lower energies in multi-QW lasers /18/. Both rounded and red-shifted gain curves on the other hand, can be explained within the framework of the k -selection rules when band-gap renormalization /19/ and spatial inhomogeneities /20/ together with intraband relaxation /4,21/ are taken into account.

In this paper we briefly describe the methods used to obtain the QW bandstructure and optical matrix elements. The emphasis is on the new aspects of the results due to band mixing obtained by $k.p$ method in the envelope function approximation /11/. The local gain at various excitation densities are then computed by using the results of both the $k.p$ method and the conventional method. These are compared with each other.

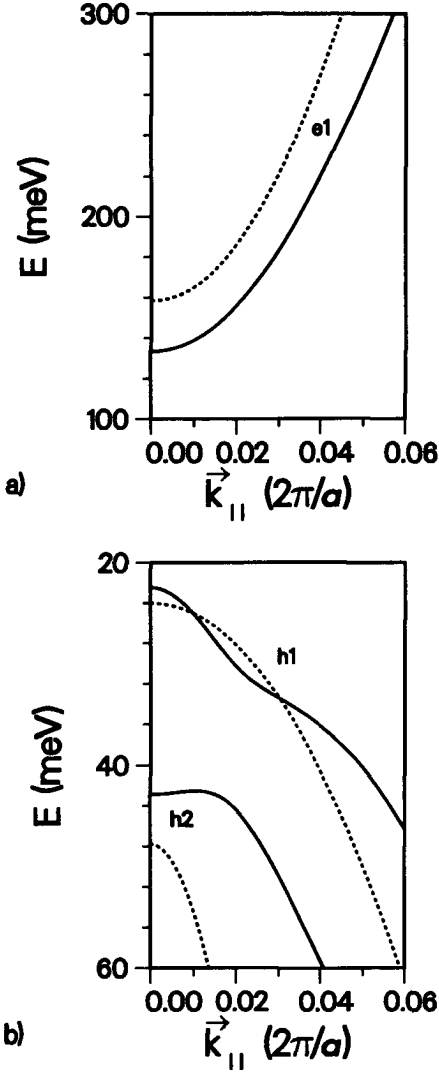


Figure 1 Energy bands in 34 Å QW computed by the $k.p$ method with envelope function approximation (solid curve), and by the conventional method assuming an effective mass electron in a 1-D potential well (dotted curve). a) Conduction subbands. b) Valence subbands. In each subband set E is measured from the bulk band edge away from the gap.

Band Mixing Effects on Quantum Well Gain

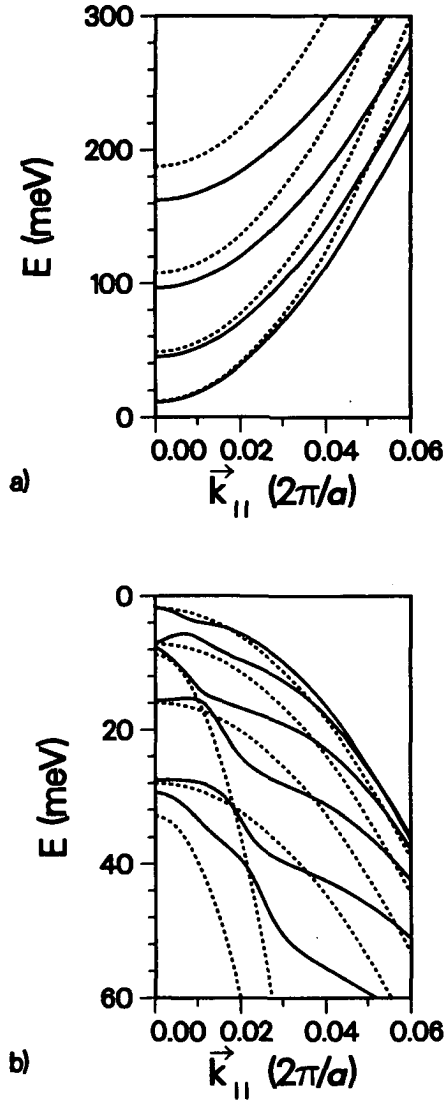


Figure 2 Same as Fig. 1 except that the QW thickness is 192 Å.

Intraband relaxation, many-body effects, and spatial inhomogeneities are then briefly discussed with respect to their role in explaining the main features of the experimental observations.

Energy Bands, Matrix Elements, and Density of States

The main features of the $k.p$ method as used for bulk semiconductor materials were reviewed by Kane /22/. The $k.p$ technique with the envelope function approximation /10/ has recently been used for obtaining the eigenstates and energies in both the compositional quantum wells /11/ and the space-charge-related potential wells at semiconductor heterojunctions /23/. In this method the wave functions of the QW are expanded in the wave functions of both constituent materials around the $k = 0$ point. The resulting Hamiltonian for the slowly varying part of the wave function, the envelope function, can be described by the corresponding $k.p$ matrix /22/ in each constituent material. For this paper the computations are done with an eight-band model /11/ which includes the electron, the light hole, the heavy hole, and the spin-orbit split-off bands and, perturbatively, the coupling to all other bands. This model takes into account nonparabolicity effects and valence-band mixing. After solving the eigenvalue problem with proper boundary conditions, the confinement energies E , and the wave functions for the electrons and holes are obtained. The bulk material parameters (effective masses, band energies) needed for the computations are obtained from the values given in /24/.

The $E - k$ dispersion curves for both the conduction and the valence subbands of a GaAs QW calculated by the $k.p$ technique (solid curves) are given in Figs. 1 and 2 for two different QW thicknesses, 34 and 192 Å. The barrier material is assumed to be $\text{Ga}_{1-x}\text{Al}_x\text{As}$ with $x = 0.25$. Although there is considerable uncertainty and debate concerning the band discontinuity ratios for this heterojunction /25,26/, we took the conventional value of 0.15 for the ratio $\Delta E_c/\Delta E_v$. The overall conclusions of this study do not depend on this sensitively. The QW layer plane is assumed to be parallel to the xy plane, and the z axis (the (001) crystal direction) is then perpendicular to the QW layer. The $E - k$ curves are given only for the x axis, (100), directed momentum vector k . Then $E - k$ curves are assumed to have rotational symmetry around the z axis. Although we found that this assumption will lead to an overestimation of the gain, the inclusion of anisotropies would not change the main conclusions.

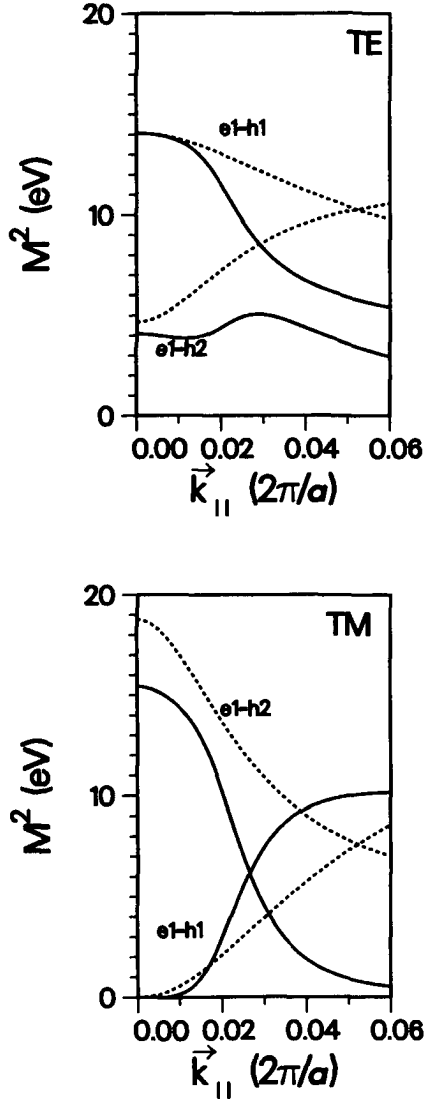


Figure 3 Squared momentum matrix elements for the transitions between the various subbands of the 34 Å thick QW. $h1$ and $h2$ correspond to the heavy hole and the light hole subbands, respectively.

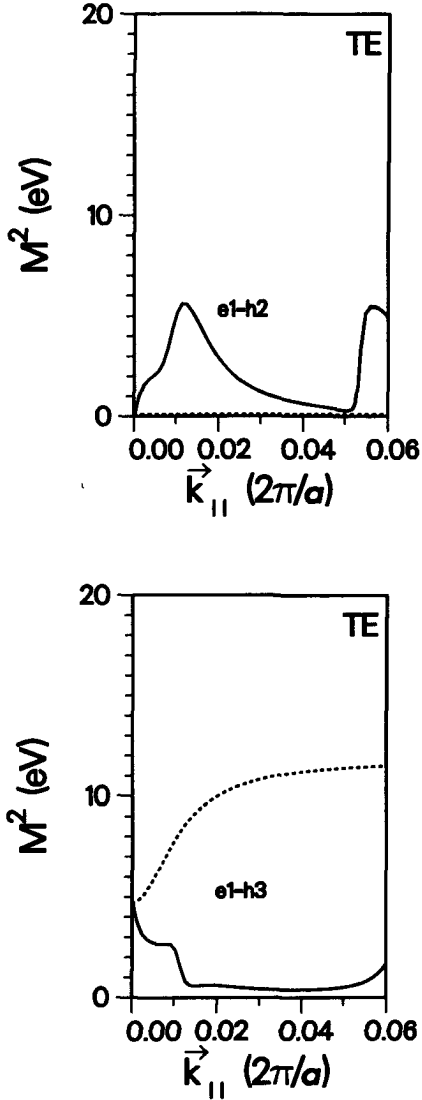


Figure 4 Examples of squared momentum matrix elements for two transitions in the 192 Å thick QW. $h2$ and $h3$ now correspond to the second heavy hole and the first light hole subbands, respectively.

The dotted $E - k$ dispersion curves given in Figs. 1 and 2 are the ones calculated by the conventional model /1-7/. Details of these calculations are summarized in Appendix A. The material parameters are the same /24/ as described above for the $k.p$ method.

From Figs. 1 and 2 it is seen that the valence subbands calculated by the $k.p$ method are totally nonparabolic due to the effects of the band mixing which is taken into account in this method. Such results for the valence bands have been observed in similar structures studied either by the $k.p$ method /10,11/, /23/ or by other detailed band-structure computation techniques /8,9/. The effects of the nonparabolicity of the bulk conduction bands which are taken into account by the $k.p$ method are also evident in the QW conduction subband results. For example, the minimum confinement energies at $k_{\parallel} = 0$ found by the $k.p$ method are lower than the ones computed by the conventional methods. There is consequently a large discrepancy in the transition energies predicted by the two methods for QW's with smaller thicknesses. This is mainly due to the small and strongly energy dependent effective masses of the electrons in the conduction bands.

Figs. 3 and 4 gives the optical matrix elements for the transitions between the different conduction and valence subbands of the QW's described above. The values of these optical matrix elements are defined by

$$M^2 = \left(\frac{2m_0 P^2}{\hbar^2} \right) \beta(k) = M_0^2 \beta(k) \quad (1)$$

where m_0 is the free-electron mass, P is the momentum matrix element between a s -like and a p -like Bloch state /10,11/, and $\beta(k)$ is the constant resulting from the coefficients of wave functions used in momentum matrix element integrations. The numerical value of M_0^2 is taken as 28.2 eV /24/. The solid curves in Figs. 3 and 4 are the ones computed with the $k.p$ approach for either the TE (in QW plane) or the TM (z axis direction) polarization modes for the transitions between the conduction subband ($e1$) and the two valence subbands ($h1$ and $h2$ for 34 Å QW, $h2$ and $h3$ for 192 Å QW). The dependence of $\beta(k)$ on k in the results of the $k.p$ calculations is due both to the mixing of wave functions /11/, and to the angular dependence of the projections of the transition matrix elements on the different axes (TM or TE). The matrix elements for a 192 Å QW are given for only two of the many possible transitions just to demonstrate the lifting of the strict selection rules ($e1$ to $h2$ is forbidden in the simple model) and the large effects of the band mixing in the $h3$ subband. Such effects are not strong in

the 34 Å QW due to the lower number of subbands and the larger energy separation between them.

The dotted curves in Figs. 3 and 4 give corresponding optical matrix elements calculated for the QW's with assumptions as used in the conventional QW gain models. The k_{\parallel} dependence of the matrix elements, or $\beta(k)$, is solely due in this case to the angular dependence of their projections on the respective axes as described in Appendix A. It should be noted that the matrix elements given in Figs. 3 and 4 are not yet averaged for the angle ϕ which the xy plane projection of a general k -vector may make with the x -axis. It is seen from these figures that the matrix element values calculated for a QW by the $k.p$ method are quite different from the ones obtained by the conventional methods.

The density of states functions calculated from the $E - k$ diagrams of Figs. 1 and 2 are given in Figs. 5 and 6. The values of the density of states (DOS) are defined by

$$\text{DOS}_b(E) = \left(\frac{1}{\pi L_w} \right) k_{\parallel} \frac{dk_{\parallel}}{dE_b} \quad (2)$$

where L_w is the QW thickness and the subscript (b) indicates the subband under consideration.

The continuous and the dotted curves give the density of states calculated by the $k.p$ method and the conventional method, respectively. As expected, the bands calculated by the conventional method result in a step function density of states. The conduction-band density of states generated by the $k.p$ method is also rather close in appearance to a step function. However the values of DOS for higher energy conduction subbands are predicted to be larger in the $k.p$ method due to nonparabolicity. The valence-band density of states computed by the $k.p$ method does not show any resemblance to the step-like density of states predicted by the conventional approach. In addition, the magnitudes of the density of the states at the valence-band edge are about a factor of 3 different for the two methods. Since the QW gain probes the band edges, the gain peak is expected to be less in the $k.p$ method than the gain peak predicted by the simpler conventional model.

Local Gain

The results given in Figs. 1-6 are basically sufficient for the gain, emission, and lifetime computations. However, the extent of the original density of states functions

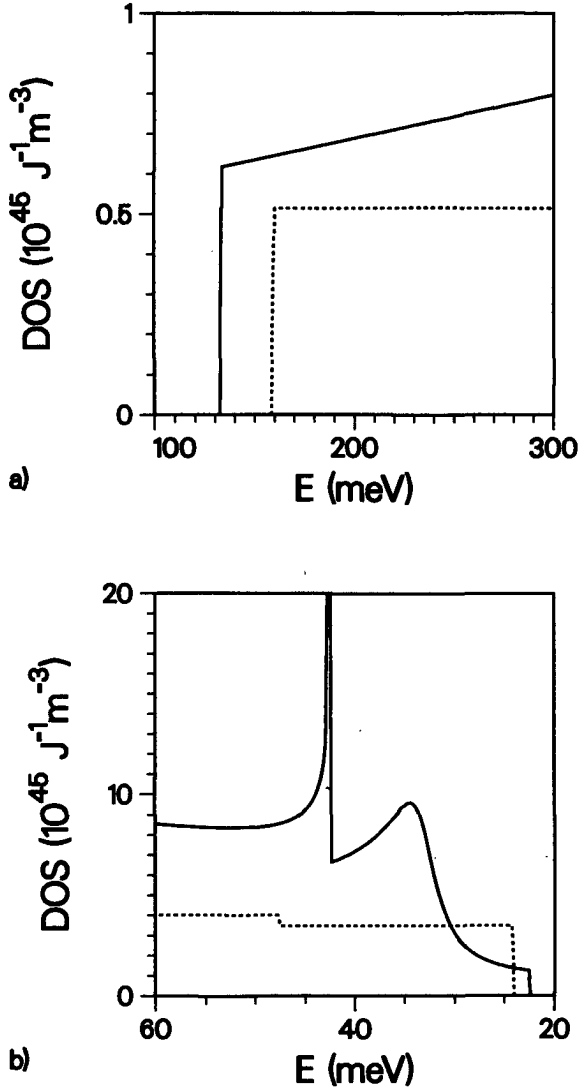


Figure 5 Density of states in the well region computed by the *k.p* method (solid curves), and the conventional method (dotted curve) for the 34 Å QW. a) Conduction bands. b) Valence bands. *E* is defined the same as in Fig. 1.

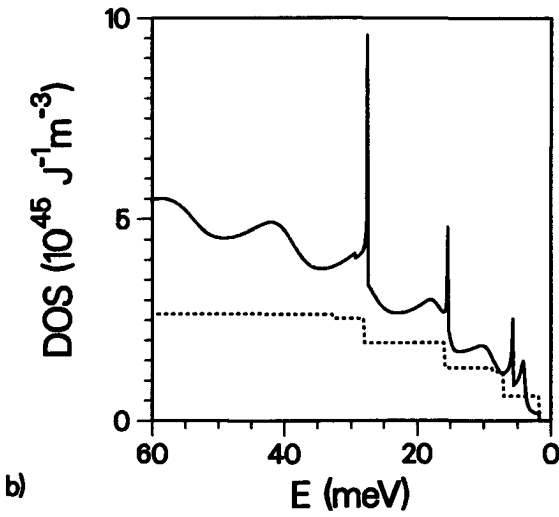
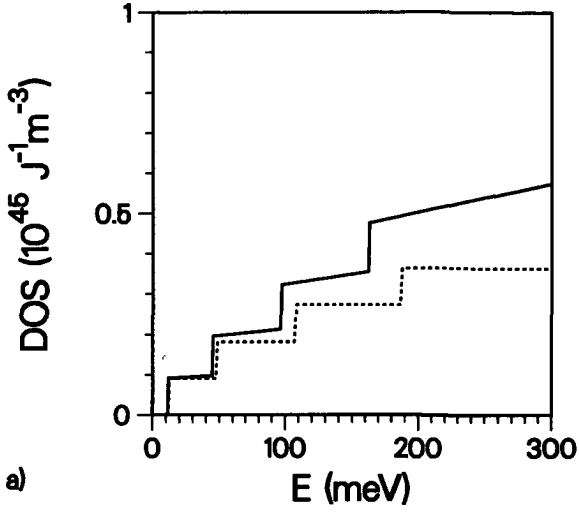


Figure 6 Same as Fig. 5 except that the QW thickness is 192 Å.

computed from Figs. 1 and 2 is rather small to determine the quasi-Fermi levels accurately for different carrier densities in the bands. Therefore, we have extended the density of states functions into the band in a continuous way by using the bulk values of the effective masses. We have also added the effects of the *L*-band minimum (no quantization). The Fermi levels are found for a given charge density, *n* or *p*, by assuming charge neutrality, $n = p$, and by integrating the charges within the conduction and valence bands numerically. The Fermi levels for the electrons E_n and for the holes E_p are defined to be positive towards the bands /1/ with the origin chosen at the bulk-band edges. The results show that there are differences of 5 - 10 meV in the values of both Fermi levels found by the two methods. This is, of course, the result of the differing density of states functions predicted by the two methods. Although the net total differences are small (≤ 10 meV), they result in observable variations in the values of the peak gain calculated by using the two methods.

Local gain for the QW is calculated from the data given in Figs. 1-4 and the Fermi levels found from Figs. 5 and 6 for different excited densities *n*. Since some of the subbands are double valued in energy, the gain computations are done in the *k* space. Therefore, the gain is first found for different area increments, $2\pi k_{||} dk_{||}$, in the *k* space within the QW plane, and then summed for the transitions having the same energy by using

$$g(E) = \int_0^\infty g'(k)\delta(E' - E)dE' \quad (3)$$

where $g'(k)$ is the gain for each *k*-space increment which is given in the Appendix B. $\delta(E' - E)$ is the delta function. $g(E)$ is then the summed gain spectra for each pair of electron and hole subbands. The total gain is then found by simply adding such gain spectra for each pair of subbands. Fig. 7 shows the QW gain spectra for two thicknesses and for the TE optical mode. The excitation densities are chosen to correspond roughly to the necessary pumping needed to reach threshold in a normal laser with 100/cm total losses. It is seen that at such excitation densities, due to the near threshold gain values, the percentage difference in the results of the two methods is large (roughly a factor of 2). The gain results for the TM optical mode show similar features and differences.

Fig. 8 gives the peak local values as a function of the excited-carrier density for the TE optical mode at two different QW thicknesses. The results are again compared with those of the conventional method. The large differences in the peak gain values found by the *k.p* and the conventional method for the 34 Å QW are mainly due to the dif-

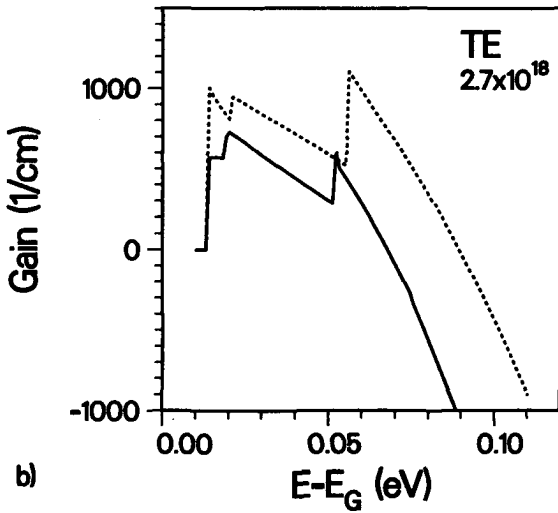
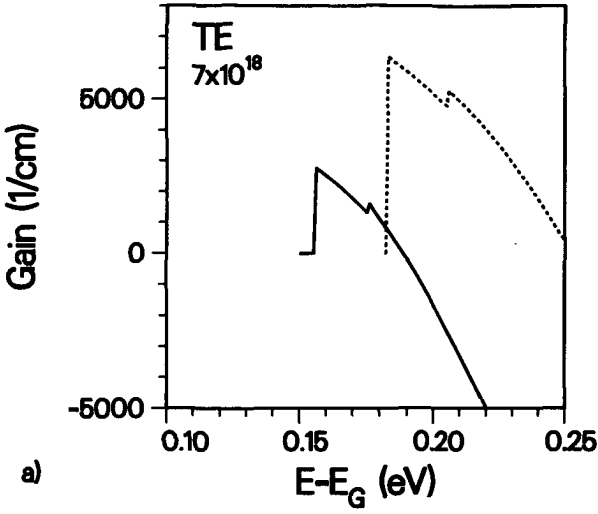


Figure 7 TE gain spectra for the a) 34 Å, and b) 192 Å thick QW computed by the *k.p* method (solid curves) and the conventional method (dotted curves) for excitation conditions close to threshold.

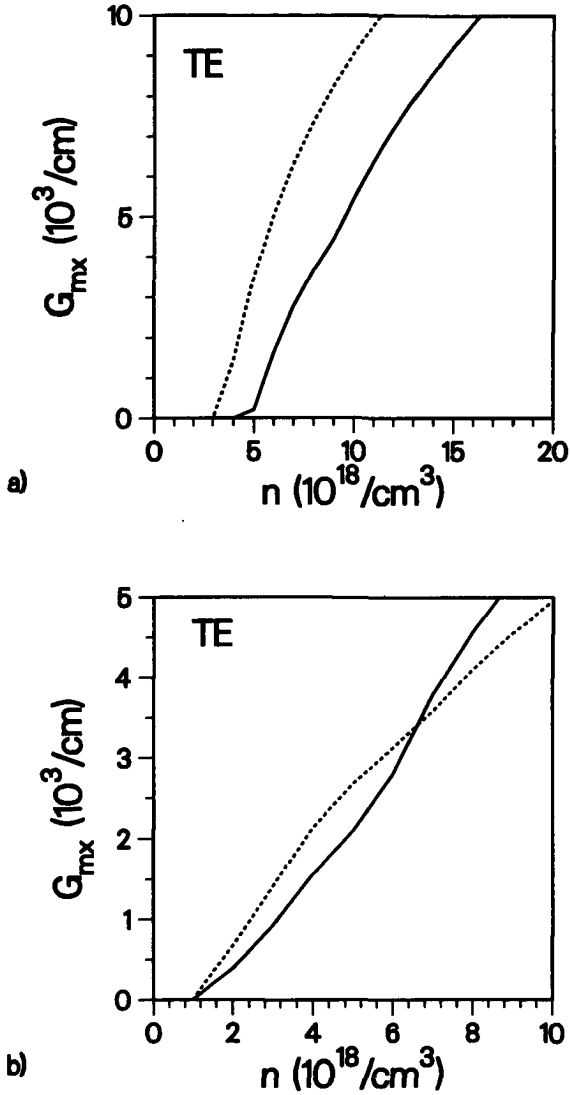


Figure 8 Peak TE gain values calculated by the two methods for different excited carrier densities in the (a) 34 Å, and (b) 192 Å thick QW.

ferences in the density of states functions computed with each method. For the 192 Å QW the overall differences in the DOS from the two methods are not as large as for the 34 Å QW. Therefore, peak values of the gain for 192 Å QW do not show large differences. Although the optical matrix elements seen in Figs. 3 and 4 calculated by the two methods also show differences, these are not expected to be the reason for the variations in peak gain values found by each method. This is also understood from the fact that at low excitation densities ($\lesssim 10^{17}/\text{cm}^3$), the peak absorption values calculated by each method show only small percentage differences.

We have also computed the radiative lifetime of the carriers in the QW for the band to band recombination by using the results of the k,p method or the conventional method. The results of 34 Å QW are given in Fig. 9. The computations were done with procedures similar to those described above by using the spontaneous emission rate expressions given in Appendix B. It should be emphasized, however, that the results in Fig. 9 were obtained by numerical integrations limited to the available ranges of the optical matrix elements and $E - k$ dispersion curves discussed earlier. For the lifetime computations the matrix elements given in Fig. 3 are averaged for all possible polari-

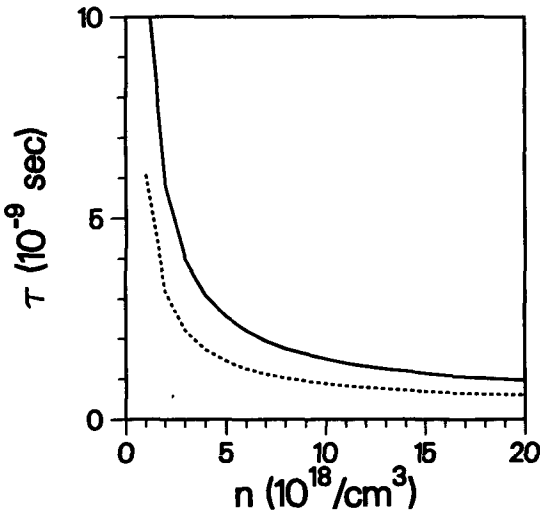


Figure 9 Radiative carrier lifetimes for the 34 Å QW computed by the k,p method (solid line) and the conventional method (dotted line) by taking into account transitions up to the range of the matrix elements given in Fig. 3.

zation directions of the optical field as discussed in /32/. The lifetimes calculated by the $k.p$ method are longer than those found by the conventional method. This means that the gain-current relationships for the 34 Å QW will differ less than the gain-carrier density curves shown in Fig. 8. The results of the lifetime data for the 192 Å QW are similar, except that for this QW thickness, the differences between the results of the two methods are less.

Experimental QW Gain Spectra

To be able to estimate the importance of the differences mentioned above (see Figs. 7 and 8), one should find out how far these one-electron models are from explaining the experimental results. For this purpose, in this section, we briefly review the published experimental work in this field. We find that the main features of the experimental QW gain spectra /14-18/ are a shift of the gain peak towards lower energies and a symmetric gain envelope function. The sharp gain cutoff predicted by either of the one-electron models has not been observed in experiments. As we mentioned earlier, the no- k -selection based computations /12,13/ result in rounded gain curves. But, the gain peak in this approach shifts towards blue contrary to experimental observations. In our opinion, the magnitude of this shift is too large to be compensated by band-gap narrowing discussed below. The gain envelope could also be made somewhat smoother by introducing the intraband relaxation concept /21/, but asymmetry and some spectral features still remain /4/. Besides, this concept alone may not explain the gain peak shift to lower energies observed for multi-QW lasers /18/. In order to explain the spectral shift and the symmetry, the effects due to the high-excitation /17,19/ and spatial inhomogeneities /20,27/ have to be considered. These effects cause different amounts of carrier-induced and electric-field-induced /28/ band-gap changes and broadening.

It would be rather difficult to calculate the broadening effects mentioned above by fundamental theories. Instead, one may introduce these effects in the results based on the one-electron model in a phenomenological fashion to estimate their influence on both to the shape and the magnitude of the gain. To do this one may consider an inhomogeneous QW laser, and add the contributions from each segment of such a laser with proper weights and sum them with proper band-gap energies /17,19,28/. The gain spectra then take on a much more symmetric appearance with reduced peak gain. Following these type of exercises with realistic assumptions we have found that the

reductions in the peak gain value due to broadening caused by inhomogeneities and many-body effects are about a factor of two [29] near the threshold-excitation range mentioned before. This is comparable with the peak gain value differences observed between the results of computations done either by the $k.p$ method or by the conventional method (see Figs. 7 and 8) for the 34 Å QW. Therefore, the methods in which the gain is studied by ignoring the differences due either to band mixing (the $k.p$ method) or to the high excitation and inhomogeneities overestimate the gain of thin QW's by about the same amount as compared to the results of the conventional method.

Conclusion

The bandstructure and the optical matrix elements of a QW have been studied by the $k.p$ perturbation method within the envelope function approximation. The $k.p$ method gives differences in the band structure (especially for the valence subbands) and in the matrix elements for large k values, and also for 'forbidden' transitions when compared with the results of the conventional approaches which have been used to model QW gain previously. These conventional approaches assume an effective mass electron in a finite potential well with parabolic electron $E - k$ dispersion curves and with constant matrix element amplitudes.

The shape of the density of states function calculated by the $k.p$ method differs from the simple step function shape which has been assumed previously. This gives different quasi-Fermi levels for holes as computed with the two methods. These differences in turn result in about a factor of 2 reduction in the peak gain values (near the threshold excitation density) calculated by the $k.p$ method as compared with the conventional method. However, in the case of gain-current relations, this difference is partially compensated by the fact that the lifetimes computed by the $k.p$ method are longer than found with the conventional method. The spectral shape of the gain found by these two methods shows observable differences. The main discrepancies in the spectra are in the confinement energies for the conduction subbands lying at higher energies in the well.

It has been discussed that the main experimental features of the gain in the QW, namely the smooth symmetric gain spectra which are shifted to lower energies, can be reproduced by the results of either of the methods by adding band-gap renormalization and spatial inhomogeneities together with intraband relaxation. When such additions

Band Mixing Effects on Quantum Well Gain

are made, the peak gain values of the smoothed symmetric spectra are also reduced by roughly the same amount as the peak gain value differences between the results of the $k.p$ and the conventional methods themselves.

The main differences between the two methods discussed here can in principle be compensated by 1) changing the effective valence-band density of states (or its shape) and 2) introducing energy-dependent effective masses /33/ in computations done by the conventional approaches. These two modifications would make the results of the conventional method more accurate while keeping the desirable feature of this method, namely its simplicity. A different type, but equally important, modification to either method would relate to the combined effects of inhomogeneities, high excitation, and electric fields near the junction. These latter types of effects introduce broadening in transitions in accord with the experimental shapes of gain spectra.

Appendix A

Conventional Model for the QW

In this appendix we review the assumptions and the relationships used in previous studies to model QW lasers. The information given below represents an up-to-date version of the published approaches with the exception of a very recent correction used in /33/ for the energy-dependent effective masses. The confinement energy levels E_n of the QW are calculated assuming an effective mass electron (hole) in a 1-D potential well of barrier height V which equals the band discontinuity. The resultant relationships are /4, (A3)/

$$\{(m_2^*/m_1^*) (V - E_n)/E_n\}^{1/2} = \begin{cases} \tan \\ -\cot \end{cases} \left(\frac{L_w(2m_1^*E_n)^{1/2}}{2\hbar} \right) \begin{cases} \text{for even } n \\ \text{for odd } n \end{cases}$$

where m_1^* and m_2^* are the effective masses of the electrons (holes) at the band edges in the quantum well and barrier, respectively. The $E - k$ dispersion curves for the confined electron (hole) within the QW plane are assumed to be parabolic, with a parabolicity defined by the band-edge effective mass of the electron (hole). These assumptions result in the dotted curves shown in Figs. 1 and 2.

Within the conventional QW model, it is also assumed that the Bloch part of the electron (hole) wave function is given everywhere in the confinement subband by the

Chapter 3

bulk Bloch function at the $k = 0$ point. Then the polarization properties of a transition between the bands for a given k -vector can be deduced by using the momentum matrix elements between the various $k = 0$ point Bloch functions [22,10] of the semiconductor. From such information one can obtain the projections of these matrix elements on different axes by knowing the angle between the k -vector and the axis. As mentioned in the text, if the momentum matrix element is defined as $M^2 = M_0^2 \beta(k)$ then the factors $\beta(k)$ for each transition can be defined by their x axis (TE) and z axis (TM) projections. Assuming $k_y = 0$ (no ϕ -angle averaging), the values of $\beta(k)$ for the TE and TM modes are given by

$$\begin{aligned} \text{TE, } x\text{-component} & \begin{cases} (1/2)(1 + \cos^2\theta) & \text{for } c - hh \\ (1/6)(1 + \cos^2\theta) + (2/3) \sin^2\theta & \text{for } c - lh \end{cases} \\ \text{TM, } z\text{-component} & \begin{cases} (1/2) \sin^2\theta & \text{for } c - hh \\ (1/6) \sin^2\theta + (2/3) \cos^2\theta & \text{for } c - lh \end{cases} \end{aligned}$$

where angle θ is between the z -axis (perpendicular to QW plane) and the $\vec{k} = k_x\hat{x} + k_y\hat{y}$ -vector of the states. This angle can be approximated by the relationship $\cos^2\theta \cong E_{cn}/\epsilon_{cn}$ [4] where E_{cn} is the confinement energy of a subband at $k = 0$, and ϵ_{cn} is the energy of the state given by $\epsilon_{cn} = E_{cn} + \hbar^2 k_x^2 / 2m_c^*$. This approximation assumes the equality of virtual k -values for the confinement functions of the electrons and holes in the potential well. This assumption is a good one for low lying levels of the well. Although the notation is different, the set given above is in agreement with the set given in [30]. The set of the assumptions and the expressions given above basically constitute the “conventional” model which has been widely used to obtain the gain and luminescence properties of QW lasers.

Appendix B

Gain and Spontaneous Emission Expressions in QW

Derivation of the gain expressions in the k space follows from the treatment given by Yariv [31] by simply adding the 2-D nature of the confined-carrier properties. The squared optical transition probability is defined by

$$H = \left(\frac{E_0^2}{2} \right) \left(\frac{e^2 \hbar^2}{2m_0(\hbar w)^2} \right) M_0^2 \beta(k)$$

where E_0 is the magnitude of the optical electric field vector, e and m_0 are the electron charge and mass, respectively, $(\hbar w)$ is the transition energy, and M_0^2 and $\beta(k)$ are defined in /1/. The absorption (gain) is then given by

$$\alpha = \left(\frac{4(\hbar w)}{\epsilon_0 \tilde{n} E_0^2 c L_w \hbar} \right) H (1 - f_n - f_p) k_{||} \frac{dk_{||}}{dE_T}$$

where ϵ_0 is the free-space dielectric permittivity, c is the speed of light in vacuum, \tilde{n} is the effective refractive index of the material. f_n and f_p are the values of the Fermi functions at the quasi-Fermi energies for the carriers. dE_T represents the differentiation with respect to the total energy interval for both electron and hole subbands. Assuming $(\hbar w) = (E_G + \Delta E)$ where E_G is the semiconductor band-gap energy, the gain $g'(k)$ expression becomes

$$g'(k) = \left(\frac{-1}{\epsilon_0 \tilde{n} c L_w \hbar E_G} \right) \left(\frac{1}{1 + (\Delta E/E_G)} \right) \left(\frac{e^2 \hbar^2}{2m_0} \right) M_0^2 \beta(k) (1 - f_n - f_p) k_{||} \frac{dk_{||}}{dE_T}$$

ΔE is the excess transition energy above the band gap as used in the figures. As mentioned earlier, the gain is first found for each small area increment, $2\pi k_{||} dk_{||}$, in the two-dimensional k space (in QW plane). The gain as a function of energy is then found by summing over the transitions having the same energy by using /3/. Although this approach is different from that used in the previous gain studies /1-5/, it simplifies the computations for the cases where the energy bands are double valued like the ones found by the $k.p$ method. The spontaneous emission is also computed in the k space and given by

$$r_{sp}(k) = \left(\frac{2\tilde{n} e^2 E_G (1 + (\Delta E/E_G))}{m_0 \epsilon_0 \hbar^2 c^3 L_w} \right) M_0^2 \frac{\beta(k)}{3} (f_n f_p) k_{||} \frac{dk_{||}}{dE_T}$$

where the factor of three in the denominator comes from averaging the matrix elements for all polarization directions of the spontaneous emission /32/. The spontaneous emission spectra in energy space for each subband pair and also the summed spectra for all pairs are found similarly as described in the text for gain (see 3). The radiative

Chapter 3

lifetime is then given by the carrier density divided by the total (integrated in energy) spontaneous emission rate.

Acknowledgement

The authors wish to thank Dr. P. Blood, Dr. S. Hagen, Dr. L. Molenkamp, Dr. G 't Hooft, Dr. A. Vink, and Dr. G. Acket for helpful discussions.

References

1. N.K. Dutta, "Calculated threshold current of GaAs quantum-well lasers", *J. Appl. Phys.*, vol. 53, pp. 7211-7214, 1982.
2. D. Kasemset, C. Hong, N.B. Patel, and P.D. Dapkus, "Graded barrier single quantum-well lasers - Theory and experiment", *IEEE J. Quantum Electron.*, vol. QE-19, pp. 1025-1030, June 1983.
3. A. Sugimura, "Threshold currents for AlGaAs quantum-well lasers", *IEEE J. Quantum Electron.*, vol. QE-20, pp. 336-343, Apr. 1984.
4. M. Asada, A. Kameyama, and Y. Suematsu, "Gain and intervalence-band absorption in quantum-well lasers", *IEEE J. Quantum Electron.*, vol. QE-20, pp. 745-753, July 1984.
5. M. Yamada, S. Ogita, M. Yamagishi, and K. Tabata, "Anisotropy and broadening of optical gain in a GaAs/AlGaAs multi-quantum-well laser," *IEEE J. Quantum Electron.*, vol. QE-21, pp. 640-645, June 1985.
6. Y. Arakawa and A. Yariv, "Theory of gain, modulation response, and spectral linewidth in AlGaAs quantum-well lasers", *IEEE J. Quantum Electron.*, vol. QE-21, pp. 1666-1674, Oct. 1985
7. R. Dingle, "Confined carrier quantum states in ultrathin semiconductor heterostructures", *Festkorperprobleme XV*, pp. 21-48, 1975.
8. J.N. Schulman and Y.-C. Chang, "Band mixing in semiconductor superlattices", *Phys. Rev.*, vol. B31, pp. 2056-2068, 1985.
9. D. Ninno, M.A. Gell, and M. Jaros, "Electronic structure and optical transitions in GaAs-GaAlAs (001) superlattices", *J. Phys. C*, 1986.
10. G. Bastard, "Envelope function approach to the superlattices band structure", in *Molecular Beam Epitaxy and Heterostructures*, L.L. Chang and K. Ploog, Eds. Dordrecht, The Netherlands and Boston, MA: Martinus Nijhoff 1985, pp. 381-423.
11. R. Eppenga, M.F.H. Schuurmans, and S. Colak, "Accurate calculation of (100) quantum-well confinement states and the corresponding gain/absorption

Band Mixing Effects on Quantum Well Gain

- spectrum", in Proc. Int. Conf. Phys. Semicond., Stockholm, Sweden, Aug. 1986, pp. 453-456.
12. P.T.L. Landsberg, M.S. Abrahams, and M. Osinski. "Evidence of no k-selection in gain spectra of quantum-well AlGaAs laser diodes" IEEE J. Quantum Electron., vol. QE-21, pp. 24-28, Jan. 1985.
 13. B. Saint-Cricco, F. Lozes-Dupuy, and G. Vassilieff, "Well width dependence of gain and threshold current in GaAlAs single quantum-well lasers", IEEE J. Quantum Electron., vol. QE-22, pp. 625-630, May 1986.
 14. N.K. Dutta, R.L. Hartman, and W.T. Tsang, "Gain and carrier lifetime measurements in AlGaAs single quantum-well lasers", IEEE J. Quantum Electron., vol. QE-19, pp. 1243-1246, Aug. 1983.
 15. M. Yamada, S. Ogita, M. Yuamagashi, K. Tabata, N. Nakaya, M. Asada, and Y. Suematsu, "Polarization dependent gain in GaAs/AlGaAs multi-quantum-well lasers: Theory and experiment", Appl. Phys. Lett., vol. 45, pp. 342-325, 1984.
 16. H. Iwamura, T. Saku, H. Kobayashi, and Y. Horikoshi, "Spectrum studies on a GaAs-AlGaAs multi-quantum-well laser diode grown by molecular beam epitaxy", J. Appl. Phys., vol. 54, pp. 2692-2695, 1983.
 17. S. Tarucha, H. Kobayashi, Y. Horikoshi, and H. Okamoto, "Carrier-induced energy-gap shrinkage in current-injection GaAs/AlGaAs MQW heterostructures", Japan J. Appl. Phys., vol. 23, pp. 874-878, 1984.
 18. P. Blood, E.D. Fletcher, P.J. Hulyer, and P.M. Snowton, "The emission wavelength of AlGaAs-GaAs multiple quantum-well lasers", Appl. Phys. Lett., vol. 48, pp. 1111-1113, 1986.
 19. D.A. Kleinman and R.C. Miller, "Band-gap renormalization in semiconductor quantum wells containing carriers", Phys. Rev., vol. B32, pp. 2266-2272, 1985.
 20. G.H.B. Thompson, "Physics of Semiconductor Laser Devices", New York: Wiley, 1980, sect. 6.3.
 21. B. Zee, "Broadening mechanism in semiconductor (GaAs) lasers: Limitations to single mode power emission", IEEE J. Quantum Electron., vol QE-14, pp. 727-736, 1978.
 22. E.O. Kane, "Energy band theory", in Handbook on Semiconductors. Amsterdam, The Netherlands: North Holland, 1982, vol. I, ch. 4A, pp. 193-217.
 23. U. Ekenberg and M. Altarelli, "Calculation of hole subbands at the GaAs-AlGaAs interface," Phys. Rev., vol. B30, pp. 3569-3572, 1984.
 24. M.F.H. Schuurmans and G.W. 't Hooft, "Simple calculation of confinement states in a quantum well", Phys. Rev., vol. B31, pp. 8041-8048, 1985.
 25. G. Duggan, "A critical review of heterojunction band offsets", J. Vac. Sci. Technol., vol. B3, pp. 1224-1230, 1985.

Chapter 3

26. G.W. 't Hooft and S. Colak, "Influence of the donor depth on the determination of the discontinuity of isotype heterojunctions by the capacitance-voltage technique", *Appl. Phys. Lett.*, vol. 48, pp. 1525-1527, 1986.
27. N.K. Dutta, "Current injection in multi-quantum-well lasers", *IEEE J. Quantum Electron.*, vol. QE-19, pp. 794-797, 1983.
28. D.A.B. Miller, D.S. Chemla, T.C. Damen, A.C. Gossard, W. Wiegman, T.H. Wood, and C.A. Burrus, "Electric field dependence of optical absorption near the band gap of quantum-well structures", *Phys. Rev.*, vol. B34, pp. 1043-1060, 1985.
29. S. Colak and R. Eppenga, unpublished results.
30. M. Yamanishi and I. Suemune, "Comment on polarization dependent momentum matrix elements in quantum-well lasers", *Japan J. Appl. Phys.*, vol. 23, pp. L35-L36, 1984.
31. A. Yariv, "Quantum Electronics", New York: Wiley, 1974, sect. 10.7.
32. G. Lasher and F. Stern, "Spontaneous and stimulated recombination radiation in semiconductors", *Phys. Rev.*, vol. 133, pp. A553-A563, 1964.
33. T. Hiroshima and R. Lang, "Effect of conduction band nonparabolicity on quantized energy levels of a quantum well", *Appl. Phys. Lett.*, vol. 49, pp. 456-457, 1986.

The Art of Semiconductor Laser Modeling

Efficient and powerful semiconductor lasers form an essential component of advanced information and communication systems. The best lasers today require less than 1 mA to start lasing, they produce up to 100 mW light output and they have overall efficiencies up to 40% /1/. Future designs should result in even better operating characteristics and longer lifetimes. Since the manufacturing of a single semiconductor laser takes at least several weeks and is expensive, modeling can be an important design tool.

On the simplest level a semiconductor laser may be viewed as a *pin* junction, consisting of a *p*-doped, an intrinsic and a *n*-doped region. Driven in forward bias, conduction-band electrons and valence-band holes, the so-called carriers, are injected into the intrinsic part of the structure from the *n*-doped and the *p*-doped region, respectively. In this so-called active region the injected electrons and holes recombine under the emission of light. Laser action occurs when the active region is embedded in an optical cavity and the junction is driven at sufficiently high currents /1-2/.

The basic design of the laser, in combination with the desired application, imposes several constraints upon the possible choices for the semiconductors constituting the laser. Efficient injection of electrons and holes into the active region only occurs if the bandgap of the doped semiconductors is larger than that of the intrinsic semiconductor. Efficient recombination can only be obtained if at least part of the active region consists of direct semiconductor material. The refractive index of the semiconductor imbedding the active region has to be larger than that of the active region in order to confine the light to that region. These and other demands can be fulfilled simultaneously by semiconductor combinations such as e.g. GaAs/AlGaAs and InGaAsP/InP, where GaAs and InGaAsP are the smaller bandgap semiconductors of each combination with wavelengths corresponding to the near-infrared (600-800 nm) and the infrared (1.3-1.5 μm), respectively. GaAs/AlGaAs lasers prove to be a good choice for information systems.

The GaAs/AlGaAs quantum-well laser has prospects for low-threshold and high-power applications /3/. In such a laser the quantum well and its undoped surroundings constitute the active region. The quantum well can be made to act as an efficient trap for the injected electrons and holes, causing the recombination to take place mainly in the quantum well. The frequency of the emitted light is determined by the properties of the quantum well, i.e. the width of the quantum well, the well composition and the

barrier composition. The well-width dependence of the laser frequency makes it possible to use GaAs as well material and still obtain light frequencies corresponding to AlGaAs emission. This is advantageous from the point of view of manufacturing the laser since it is much easier to grow high-quality GaAs than high-quality AlGaAs.

The confinement of the light within the active region and the current flow through the *pin* junction are two aspects of a semiconductor laser which can be accurately described from concepts of classical physics /1/. The third aspect, the recombination of electrons and holes in the active region, must be accounted for on the level of quantum mechanics. This cannot be done completely on the same elemental level. The art of laser modeling lies in recognizing the principal physical processes involved and implementing sensible approximate descriptions for them into the laser model.

In this chapter a model describing the recombination of electrons and holes in a single or multiple GaAs/AlGaAs quantum-well laser is presented; a multiple quantum-well laser contains a number of uncoupled identical quantum wells. Fundamental to it, is a quantum mechanical description of Γ -point eigenstates and energy levels of the quantum well, in which conduction-band non-parabolicity and valence-band mixing are incorporated. Effects associated with the influence of the X and L minima on the quasi-Fermi level of the electrons, the influence of the barrier on the quasi-Fermi levels of the electrons and holes, well-width fluctuations and current spreading are included in an approximate manner. Effects associated with carrier-carrier, carrier-phonon and $\Gamma-L$ scattering and bandgap renormalization are treated phenomenologically. Gain and spontaneous emission spectra are calculated with this model at several levels of sophistication.

Basic Model

The absorption and emission spectra of a quantum well can be calculated from the knowledge of the electron-confinement energies $E_e(k_{\parallel})$, the hole-confinement energies $E_h(k_{\parallel})$ and the optical matrix elements $Q_{ij}(k_{\parallel})$ connecting them; k_{\parallel} is the two-dimensional wavenumber associated with the translational invariance in the plane of the quantum well. The squared optical matrix element of a transition between an electron-confinement state $\psi_{ik_{\parallel}}$ and a hole-confinement state $\psi_{jk_{\parallel}}$ for light of polarization e is defined as

$$Q_{ij}(k_{\parallel}) = \left| \langle \psi_{ik_{\parallel}} | e \cdot \frac{\hbar}{i} \nabla | \psi_{jk_{\parallel}} \rangle \right|^2. \quad (1)$$

Chapter 4

We describe the electron ($\psi_{i\mathbf{k}_\parallel}$) and hole ($\psi_{j\mathbf{k}_\parallel}$) confinement states of the quantum well by an advanced eight-band $\mathbf{k}\cdot\mathbf{p}$ theory /4/. It produces all required quantities i.e. the electron-confinement energies $E_i(\mathbf{k}_\parallel)$, the hole-confinement energies $E_j(\mathbf{k}_\parallel)$ and the optical matrix elements $Q_{ij}(\mathbf{k}_\parallel)$. The essentials of this $\mathbf{k}\cdot\mathbf{p}$ theory are briefly summarized in the following. Each material constituting the quantum well is described by eight Γ -point basis states. The electron (EL), light-hole (LH), heavy-hole (HH) and spin-orbit split-off (SO) bands are treated exactly and all other bands perturbatively. Apart from the gap and the spin-orbit splitting, the model contains 6 parameters for each material. They may be taken to be the EL, LH, HH and SO effective mass m_{EL} , m_{LH} , m_{HH} and m_{SO} at the center Γ of the Brillouin zone along $[001]$, the HH effective mass m'_{HH} at Γ along $[111]$ and a parameter B which describes the inversion asymmetry of each material; B is set equal to zero.

The recombination process is assumed to be quasi-static i.e. the dynamics of the electron and hole-injection process are disregarded. This is warranted since the injected electrons and holes equilibrate with each other and the lattice on a (sub)picosecond ($\lesssim 10^{-12}$ s) /5/ time scale. The recombination of electrons and holes takes place on a nanosecond (10^{-9} s) time scale /6,7/. The resulting equilibrium distributions of the injected conduction-band electrons and valence-band holes over the available energy levels can be described by the Fermi-Dirac distribution function for the electrons $f_{in}(\mathbf{k}_\parallel) = 1/\{\exp((E_i(\mathbf{k}_\parallel) - E_n)/k_B T) + 1\}$ and the holes $f_{jp}(\mathbf{k}_\parallel) = 1/\{\exp((E_j(\mathbf{k}_\parallel) - E_p)/k_B T) + 1\}$, respectively, with corresponding electron (E_n) and hole (E_p) quasi-Fermi energies. k_B is Boltzman's constant and T is the temperature of the lattice. Charge neutrality, i.e. the injected electron density n is equal to the injected hole density p , determines the quasi-Fermi levels E_n and E_p via the implicit relations

$$n = \frac{2}{w} \sum_i \int \frac{dk_{\parallel}}{(2\pi)^2} f_{in}(\mathbf{k}_{\parallel}) \quad (2a)$$

and

$$p = \frac{2}{w} \sum_j \int \frac{dk_{\parallel}}{(2\pi)^2} f_{jp}(\mathbf{k}_{\parallel}) . \quad (2b)$$

Here w is the quantum-well width and the prefactor 2 accounts for the spindegeneracy. The summations run over all electron (i) and hole (j) bands and the integrals are over the 2-dimensional Brillouin zone.

Momentum and energy conservation must be fulfilled in light absorption and emission. Momentum conservation results in k_{\parallel} -conservation since the wavenumber of the photons ($\sim 10^{-3} \text{ \AA}^{-1}$) is small compared with the wavenumber of the electrons and holes ($\sim 0.1 \text{ \AA}^{-1}$). Energy conservation is expressed by the relation $E_{ij}(k_{\parallel}) - \hbar\omega = 0$, where $E_{ij}(k_{\parallel})$ is the energy difference $E_i(k_{\parallel}) - E_j(k_{\parallel})$.

The gain $g(\omega)$ for light of frequency ω is given by

$$g(\omega) = \frac{g_0}{\omega} \sum_{ij} \frac{2}{w} \int \frac{dk_{\parallel}}{(2\pi)^2} Q_{ij}(k_{\parallel}) [f_{in}(k_{\parallel}) - f_{jp}(k_{\parallel})] \delta(E_{ij}(k_{\parallel}) - \hbar\omega), \quad (3)$$

where the constant g_0 equals $4\pi^2 e^2 / (nm^2 c)$ in cgs units and n is the effective refractive index of the quantum well. The δ function takes care of the energy conservation.

Similarly, the spontaneous emission rate per unit energy $r(\omega)$ can be obtained from

$$r(\omega) = g_0 r_0 \omega \sum_{ij} \frac{2}{w} \int \frac{dk_{\parallel}}{(2\pi)^2} Q_{ij}(k_{\parallel}) f_{in}(k_{\parallel}) [1 - f_{jp}(k_{\parallel})] \delta(E_{ij}(k_{\parallel}) - \hbar\omega), \quad (4)$$

where r_0 equals $2n^2 / (\pi \hbar c^2)$.

The nominal current density j_{nom} is defined as the current density required to maintain the actual spontaneous emission rate. It is evaluated from $j_{nom} = ew \int r_{av}(\omega) d\hbar\omega$, where $r_{av}(\omega)$ stands for the average of $r(\omega)$ with respect to light polarization. The integration over the light frequency can be performed analytically resulting in

$$j_{nom} = 2e\hbar g_0 r_0 \omega \sum_{ij} \int \frac{dk_{\parallel}}{(2\pi)^2} E_{ij}(k_{\parallel}) Q_{ij}^{av}(k_{\parallel}) f_{in}(k_{\parallel}) [1 - f_{jp}(k_{\parallel})], \quad (5)$$

where $Q_{ij}^{av}(k_{\parallel})$ is the average of $Q_{ij}(k_{\parallel})$ with respect to the light polarization.

Note that the expressions (2)-(5) contain no integrations with respect to energy over the usually strongly peaked densities of states functions. Instead, all integrations are with respect to k_{\parallel} and involve smooth and well-behaved integrands (the integrations over the δ functions are of course trivial).

Modeling

In this section other physical aspects of the quantum well are incorporated into the basic model. Many can be approximated by a phenomenological description.

Chapter 4

The energies of the confinement states are calculated from a k,p -theory which is based on Γ -point states. Energy bands corresponding to non-confined Γ -point derived well quantum-well states, resonant or non-resonant in the quantum well, are not calculated. The X and L -point-related quantum-well states in the well and the barrier, confined or non-confined, are disregarded altogether. This leads to an overestimation of the conduction-band quasi-Fermi energy and an underestimation of the valence-band quasi-Fermi energy at high injection levels. We include several omitted quantum-well states in an approximate way. The effect of the confining potential on these states is disregarded. In this spirit, the non-confined non-resonant Γ -point-derived quantum-well states are then bulk barrier states and the X and L -derived, confined and non-confined, quantum-well states are bulk well and barrier states. Non-confined resonant Γ -point-derived quantum-well states are not included in these approximations. The effect of the extra states on the quasi-Fermi levels is approximated by adding the expressions

$$2 \sum_l \int \frac{dk}{(2\pi)^3} f_{in}^W(k) + \frac{b-w}{Nw} 2 \sum_l \int \frac{dk}{(2\pi)^3} f_{in}^B(k) \quad (6a)$$

and

$$\frac{b-w}{Nw} 2 \sum_m \int \frac{dk}{(2\pi)^3} f_{pn}^B(k) \quad (6b)$$

to the right-hand sides of Eqs. 2a and 2b, respectively. The summation over l runs over $\{X,L\}$ for the well contribution and over $\{\Gamma,X,L\}$ for the barrier contribution, the summation over m runs over $\{HH,LH,SO\}$ and the integration is over the three-dimensional Brillouin zone. The prefactor $(b-w)/Nw$ measures the relative volume of the barrier compared with that of the well; b is the total width of the active region ($\sim 1000-2000$ Å) and N is the number of quantum wells in the active region. The Fermi-Dirac distribution functions $f_{in}^W(k)$, $f_{in}^B(k)$ and $f_{pn}^B(k)$ equal $1/\{\exp((E_l^W(k) - E_n)/k_B T) + 1\}$, $1/\{\exp((E_m^B(k) - E_p)/k_B T) + 1\}$ and $1/\{\exp((E_m^B(k) - E_p)/k_B T) + 1\}$, respectively. The bulk conduction bands of the well $E_l^W(k)$ and the barrier $E_l^B(k)$ and the bulk valence bands of the barrier $E_m^B(k)$ are suitably approximated. Recombination in the well and barriers, associated with the population of the states added, will be ignored.

An electron and a hole scatter $\approx 10^{-9}/10^{-12} = 1000$ times before recombination. The effects of scattering on the transitions can be incorporated phenomenologically by re-

laxing the condition of energy conservation or the condition of momentum conservation or both. We retain the momentum conservation and relax the energy conservation constraint. This is accomplished by the replacing the $\delta(\varepsilon)$ -function ($\varepsilon \equiv E_q(\mathbf{k}_q) - \hbar\omega$) in the expressions for the gain spectrum (Eq. 3) and the spontaneous emission (Eq. 4) spectrum by a Lorentzian $L_\varepsilon(\varepsilon) = \frac{\tau}{\pi} (1 + (\varepsilon\tau/\hbar)^2)^{-1}$ of equal integral strength /8-9/. Other approaches can be found elsewhere /10-16/. The effective carrier-carrier scattering time τ will be $\approx 10^{-12} - 10^{-13}$ sec. Generally, τ will depend both on the carrier density n and on the photon energy $E = \hbar\omega$ /10-16/. However, the carrier density and energy dependence of τ are subject to debate /10-16/. For simplicity, we take τ to be constant. The expression for the nominal current density j_{nom} (Eq. 5) remains unchanged for constant τ since $\delta(\varepsilon)$ and $L_\varepsilon(\varepsilon)$ have equal integral strength.

The attractive Coulomb interaction between electrons and holes leads, at high carrier injection levels corresponding to $n = p > 10^{15}$ cm⁻³, to a narrowing of the bandgap. This effect is often referred to as bandgap renormalization. It can be accounted for by adding an energy $\Delta E_g(n)$ to all electron confinement energies. Bandgap renormalization is well understood in 3 dimensions. However, in 2 dimensions there is a controversy about both its magnitude and its functional dependence on the carrier density n exists /16-20/. We use the following approximation

$$\Delta E_g(n) = -\alpha n^{1/3}, \quad (7)$$

where the positive constant α equals 1.10⁻⁸ eVcm /16/.

Large-scale (> 100 Å in lateral size) monolayer steps are always present in actually grown GaAs/AlGaAs quantum-well lasers. The effect of these well-width "fluctuations" on calculated spectra can be calculated by appropriate averaging of Eqs. 2-5 over discrete well widths w_α . This leads e.g. to the following relation for the electron quasi-Fermi level

$$n = \sum_\alpha f_\alpha n_{w_\alpha}, \quad (8)$$

where f_α is the fraction of quantum wells ($\sum_\alpha f_\alpha = 1$) with well width $w_\alpha = w + \alpha b$; w is the average well width, b the monolayer thickness and $\alpha = 0, \pm 1, \pm 2$, etc. . The electron $\{n_{w_\alpha}\}$ (or hole $\{p_{w_\alpha}\}$) densities are calculated from Eqs. 2a and 2b (with or without the inclusion of Eqs. 6a and b) for the corresponding well widths $\{w_\alpha\}$. It is important to note that (i) the same quasi-Fermi levels E_n and E_p are used for every well width and (ii) that the charge neutrality condition $n = p$ is only fulfilled for the system

as a whole and not for each individual well ($n_{w_a} \neq p_{w_a}$) (although only minor deviations occur).

The current and thereby the injected carrier densities are not evenly distributed over the plane of the well. This current spreading is mainly due to the potential distribution in the laser structure. Its effect will be modeled by averaging the gain and the spontaneous emission spectra over an appropriately chosen normalized distribution $c(n)$ of electron densities ($\int c(n) dn = 1$). This results in, for example, the following expression for the average gain $\bar{g}(\omega)$:

$$\bar{g}(\omega) = \int c(n) g_n(\omega) dn, \quad (9)$$

where $g_n(\omega)$ is the gain as calculated from Eq. 3 for carrier density n . Since the quasi-Fermi levels E_n and E_p depend on the carrier density n , different quasi-Fermi levels exist along the well.

Results

The model is applied to a single GaAs/Al_{0.35}Ga_{0.65}As quantum well of 62.2 Å. The parameters used in the $k \cdot p$ calculation of the electron and hole-confinement energies are chosen to accurately reproduce the bulk bandstructures of GaAs and Al_{0.35}Ga_{0.65}As and are listed in Table I. The ratio of conduction to valence-band discontinuity is taken to be 67/33. Figures containing the conduction-band and valence-band confinement energies and the optical matrix elements between them as a function of $k_{||}$ can be found elsewhere [21]. In all calculations of quasi-Fermi levels, gain spectra, spontaneous emission spectra and nominal current densities, the anisotropy of the integrands with respect to $k_{||}$ is ignored and the integrations are cut off at $k_{||} = 0.1 \frac{2\pi}{a}$; a is the lattice constant.

Figure 1 shows the calculated conduction-band and valence-band quasi-Fermi levels as a function of the injected carrier density. The dashed line represents the results of a calculation using the Γ -point-derived confinement states (notation Γ^n). The inclusion of bulk like X and L -point-derived states in the well (dotted line) lowers the conduction-band quasi-Fermi level. It is lowered even further by the inclusion of the bulk-like Γ -point-derived non-confined states and the X and L -point-derived states of the barrier (upper solid line). The valence-band quasi-Fermi level is accordingly increased by inclusion of the bulk like Γ -point-derived non-confined states of the barrier

Table I All effective masses refer to the Γ center of the Brillouin zone. The unprimed ones are taken along [001], the primed one along [111]; m_e is the electron mass.

	E_g (eV)	Δ (eV)	m_{EL}/m_e	m_{HH}/m_e	m_{LH}/m_e	m_{SO}/m_e	m'_{HH}/m_e
GaAs	1.430	.343	.0667	.3800	.0870	.1735	.9524
$Al_{0.35}Ga_{0.65}As$	1.898	.321	.0931	.4095	.1232	.2199	1.0131

(lower solid line). Each extra band l around k_i is approximated by parabolic dispersion relation of the form $E_l(k) = E_i + \hbar^2|k - k_i|^2/2m_l$. The values of E_i and m_l are given in Table II. Since the density of states of the confinement conduction bands ($\propto m_{EL} \approx 0.067 m_e$) is much smaller than that of the confinement heavy-hole valence bands ($\propto m_{HH} \approx 0.38-0.95 m_e$), the X and L -point-derived conduction-band states become populated at a lower electron density than the non-confined Γ -point-derived

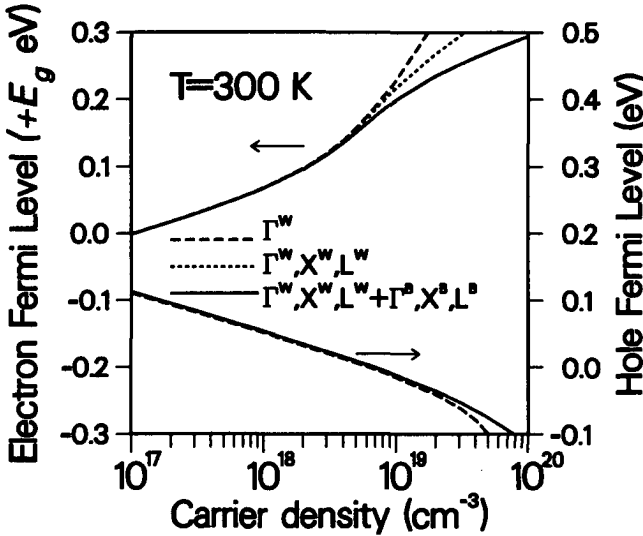


Figure 1 Calculated quasi-Fermi levels at $T=300$ K as a function of the injected carrier density for a 62.2 \AA GaAs/ $Al_{0.35}Ga_{0.65}As$ quantum well with a barrier width b of 2000 \AA . The following bands are included for the three cases: Γ confinement states (dashed, Γ^w), + X and L -point-derived states of the well (dotted, Γ^w, X^w, L^w), + non-confined Γ -point-derived states and X and L -point-derived states of the barrier (drawn, $\Gamma^w, X^w, L^w + \Gamma^b, X^b, L^b$).

Table II All energies are relative to the top of the valence band of the corresponding material.

k_i :	GaAs		$\text{Al}_{0.35}\text{Ga}_{0.65}\text{As}$		
	X	L	Γ	X	L
E_i (eV)	1.900	1.708	1.898	1.961	1.933
m_i/m_e	0.850	0.550	0.0931	0.826	0.592

valence-band states. For example, at a carrier density of $n = 2.10^{19} \text{ cm}^{-3}$, 45 % of the electrons occupy X and L and non-confined Γ -point-derived conduction-band states and only 12 % of the holes occupy non-confined Γ -point-derived valence-band states. The effect of the extra states is therefore most pronounced for the conduction-band quasi-Fermi level. In the following the effect of the X and L -point-derived states and the non-confined Γ -point-derived states of the barrier on the quasi-Fermi levels is ignored.

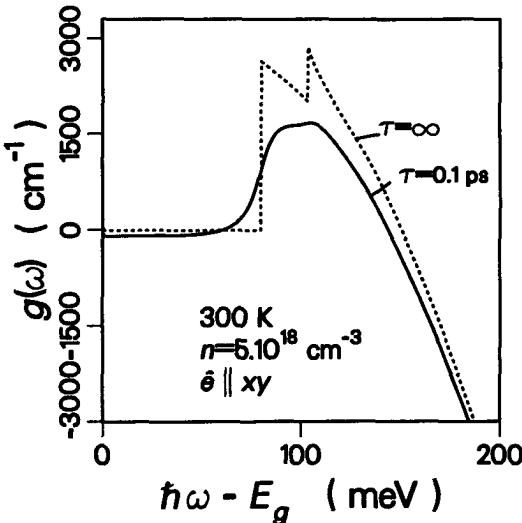


Figure 2 Calculated gain spectra for light polarization in the plane of the quantum well ($\hat{e} \parallel xy$) in a 62.2 Å GaAs/ $\text{Al}_{0.35}\text{Ga}_{0.65}\text{As}$ quantum well. A value of ∞ for the parameter τ corresponds to strict energy conservation.

In Figures 2 and 3, gain and spontaneous emission spectra are depicted. The dotted line represents a calculation that takes into account energy conservation, and the drawn line represents a calculation that includes Lorentzian broadening. The value of 0.1 ps (=6.6 meV) for the parameter τ was deduced from the observed broadening of the low energy side of measured spontaneous emission spectra /22/. The value is in agreement with the values for the measured time scales of various scattering mechanisms such as e.g. electron-electron scattering, electron-phonon scattering and $\Gamma - X$ scattering /23/. The most pronounced effect of broadening is the reduction of the maximum gain from 2950 cm^{-1} ($\tau = \infty$) to 1600 cm^{-1} . From here on all spectra are calculated using a Lorentzian broadening with $\tau = 0.1$ ps.

Figures 4 and 5 display calculated gain and spontaneous emission spectra taking well-width fluctuations into account. The calculation is done for a structure with weights $f_0 = 0.6$, $f_1 = 0.2$ and $f_{-1} = 0.2$, i.e. 60% has the average well width, 20% is one monolayer (2.827 Å) thicker and 20% is one monolayer thinner. The solid line represents a calculation with the average well width, ignoring the well-width fluctuations. The dashed line in each Figure (hardly discernible from the solid line) re-

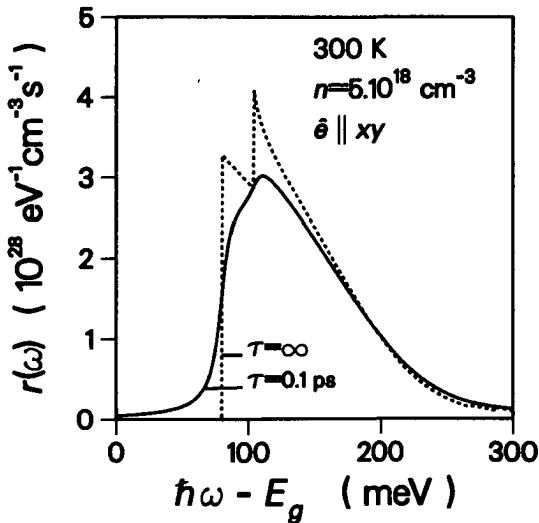


Figure 3 Calculated spontaneous emission spectra for light polarization in the plane of the quantum well ($\hat{e} \parallel xy$) in a 62.2 Å GaAs/ $\text{Al}_{0.35}\text{Ga}_{0.65}\text{As}$ quantum well. A value of ∞ for the parameter τ corresponds to strict energy conservation.

presents a calculation which includes the effects of well-width fluctuations. It consist of the weighted sum of the spectra for the respective well widths as represented by the dotted lines (note that the multiplication with the weight factors f_k has already been performed). Figures 4 and 5 clearly show that the effects of well-width fluctuations are extremely small and are masked by the $1/\tau$ broadening effects of scattering.

Figures 6 and 7 show calculated gain and spontaneous emission spectra in which current spreading is taken into account. The injected electron densities were taken to be $n = 5.10^{18} \text{ cm}^{-3}$ for 60% of the quantum well and $n_- = 4.10^{18} \text{ cm}^{-3}$ and $n_+ = 6.10^{18} \text{ cm}^{-3}$ for the two remaining 20% fractions of the quantum well, respectively ($c(n) = 0.6$ and $c(n_-) = c(n_+) = 0.2$ in Eq. 9). The corresponding nominal current densities are calculated to be 217, 316 and 426 A cm^{-2} for injected electron densities of $n = 4.10^{18}$, 5.10^{18} and $6.10^{18} \text{ cm}^{-3}$, respectively. The dashed lines in Figures 6 and 7 represent the averaged spectra and are calculated from the weighted sum of the spectra

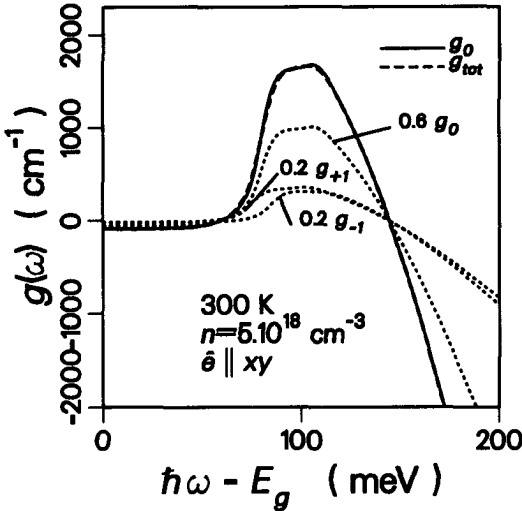


Figure 4 Well width fluctuation effect on calculated gain spectra as illustrated for light polarization in the plane of the quantum well ($\hat{\epsilon}||xy$) in $62.2 \text{ \AA} \pm 1$ monolayer ($= \pm 2.827 \text{ \AA}$) GaAs/ $\text{Al}_{0.35}\text{Ga}_{0.65}\text{As}$ quantum wells (g_0 and $g_{\pm 1}$, respectively). The gain spectra are multiplied with the weight factors 0.6, 0.2 and 0.2. The total gain g_{tot} is the sum of the three dotted curves and describes the effect of well width fluctuation of 1 monolayer with given weight factors. The solid line represents the gain at the average width.

for the respective electron densities (dotted lines). The drawn lines represent a calculation for the average injected carrier density. The effect of current spreading on calculated spectra is , as that of well-width fluctuations, very small and is negligible as compared to the effect of scattering.

Figure 8 displays the calculated maximum gain as a function of the nominal current density for several values of the scattering time τ . The effect of well-width fluctuations and current spreading on the maximum gain and nominal current density is small and was therefore not included in the calculations. As is obvious from Figure 8 the maximum gain depends strongly on the value of τ .

In Figure 9 both measured (circles) and calculated (drawn line) results for the maximum gain and the nominal current density are presented /22/. The experiment was performed on a 20 Å single quantum well in a GRINSCH laser structure. The

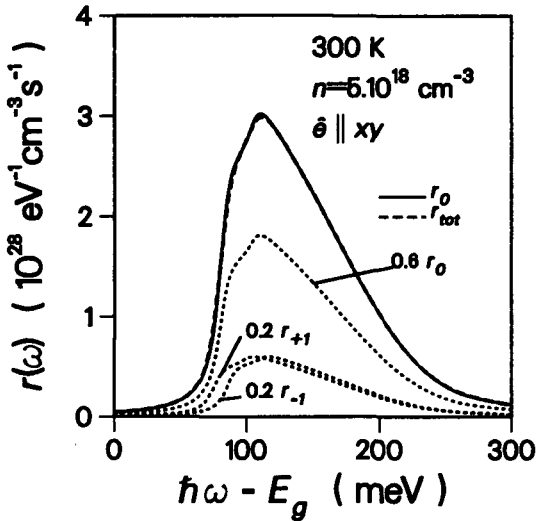


Figure 5 Well width fluctuation effect on calculated spontaneous emission spectra as illustrated for light polarization in the plane of the quantum well ($\hat{e} \parallel xy$) in 62.2 Å ± 1 monolayer ($= \pm 2.827$ Å) GaAs/Al_{0.35}Ga_{0.65}As quantum wells (r_0 and $r_{\pm 1}$, respectively). The spontaneous emission spectra are multiplied with the weight factors 0.6, 0.2 and 0.2. The total spontaneous emission r_{tot} is the sum of the three dotted curves and describes the effect of well width fluctuation of 1 monolayer with given weight factors. The solid line represents the spontaneous emission at the average width.

calculations were done for a 20 Å GaAs/Al_{0.30}Ga_{0.70}As quantum well with the parameter τ set equal to 0.1 ps; all other parameters used in the calculation can be found in Table III. During the measurements the temperature was kept at 153 K in order to avoid a substantial population of the barriers. For the highest injected electron densities ($J_{nom} \sim 900$ A cm⁻² corresponding to $n \sim 1.8 \cdot 10^{19}$ cm⁻³) the calculation suggests that at most 10-20% of the injected electrons and holes populate the barriers. The excellent agreement between the calculated and measured results may be somewhat fortuitous in view of the uncertainties in the experimental determination of the current density.

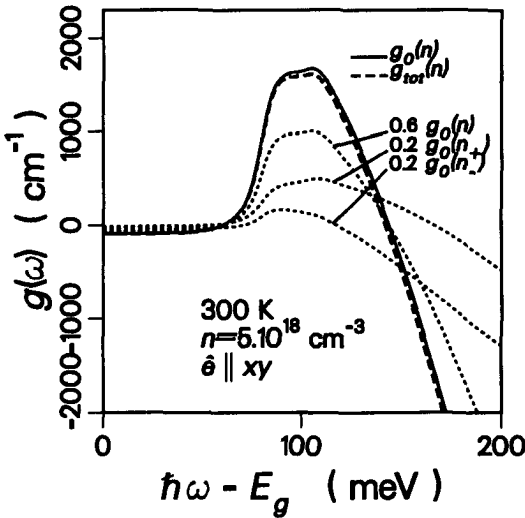


Figure 6 Current spreading effect on calculated gain spectra as illustrated for light polarization in the plane of the quantum well ($\hat{e}||xy$) in 62.2 Å GaAs/Al_{0.35}Ga_{0.65}As quantum well for three injected carrier densities ($n = 5.10^{18}$ cm⁻³, $n_- = 4.10^{18}$ cm⁻³ and $n_+ = 6.10^{18}$ cm⁻³) and multiplied with the weight factors 0.6, 0.2 and 0.2. The total gain g_{tot} is the sum of the three dotted curves and describes the effect of current spreading by the introduction of carrier density fluctuations of 1.10^{18} cm⁻³ with the given weight factors. The solid line represents the gain at the average carrier density $n = 5.10^{18}$ cm⁻³.

Discussion

In Figure 1 the effect of population of non- Γ -derived confinement states on the quasi-Fermi levels is presented. It was shown that for injected carrier densities $n > 1.10^{19} \text{ cm}^{-3}$ a substantial population of X and L -point-derived states of the well and non-confined Γ -point-derived and X and L -point derived states of the barrier results. The resulting reduction in the electron and the hole quasi-Fermi level separation is completely disregarded in most other work [8,12,9,15]. Still, for these high electron densities the present analysis is far from complete since the population of these states would result in e.g. radiative recombination in the barriers. This effect is not incorporated in the model. Moreover, non-radiative processes are disregarded altogether.

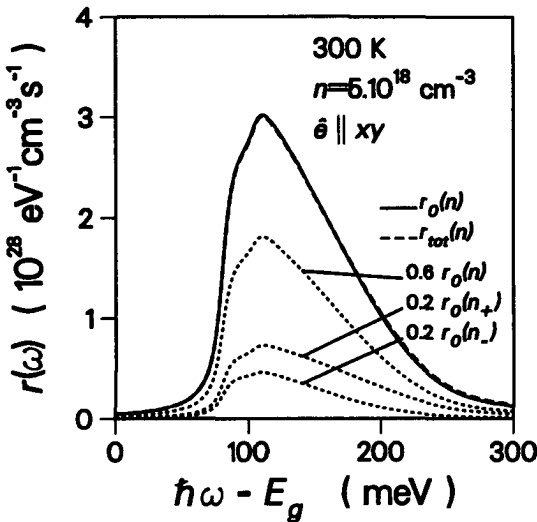


Figure 7 Current spreading effect on calculated spontaneous emission spectra as illustrated for light polarization in the plane of the quantum well ($\hat{e}||xy$) in 62.2 \AA GaAs/ $\text{Al}_{0.35}\text{Ga}_{0.65}\text{As}$ quantum well for three injected carrier densities ($n = 5.10^{18} \text{ cm}^{-3}$, $n_- = 4.10^{18} \text{ cm}^{-3}$ and $n_+ = 6.10^{18} \text{ cm}^{-3}$) and multiplied with the weight factors 0.6, 0.2 and 0.2. The total spontaneous emission r_{tot} is the sum of the three dotted curves and describes the effect of current spreading by the introduction of carrier density fluctuations of $1.10^{18} \text{ cm}^{-3}$ with the given weight factors. The solid line represents the spontaneous emission at the average carrier density $n = 5.10^{18} \text{ cm}^{-3}$.

The relative importance of several broadening mechanisms can be obtained from Figures 2-8. It is clear that for the chosen value 0.1 ps of the parameter τ , the broadening caused by carrier-carrier scattering masks the broadening caused by well-width fluctuations and current spreading. The reason for this is that these broadening effects are to a reasonable approximation linear in the well-width difference and the current spreading, respectively. Moreover, the energy associated with scattering (0.1 ps \sim 6.6 meV) is in the same energy range as the differences in confinement energies (\sim 5 meV) for monolayer well-width fluctuations and the difference of the quasi-Fermi level separation (\sim 21 meV) caused by spreading in injected electron densities.

An interesting improvement of the model as compared to other work is the formulation of all important quantities in terms of integrals over the parallel wavenumber $k_{||}$, thus circumventing the necessity to evaluate integrals involving density of states functions. This has practical implications as mentioned before, but more important, it has implications for the description of a quantum well if more than one confinement valence or conduction band is incorporated. A single integration with respect to energy over a density of states function implies the use of only one electron Fermi-Dirac

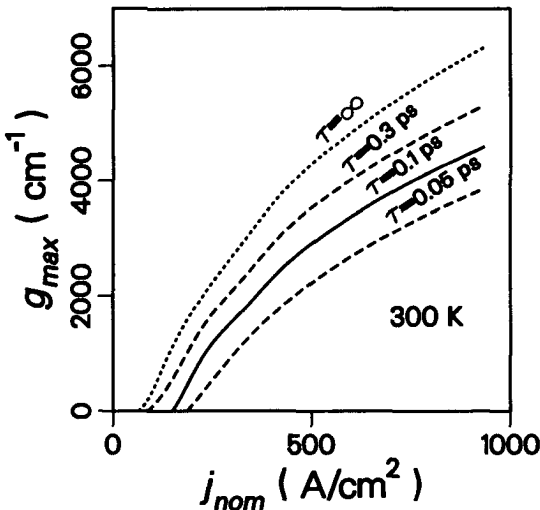


Figure 8 Calculated maximum gain for light polarization in the plane of the quantum well ($\hat{e}_{||xy}$) as a function of the current density in 62.2 Å GaAs/ $\text{Al}_{0.35}\text{Ga}_{0.65}\text{As}$ quantum well for several values of the parameter τ .

Table III All effective masses refer to the Γ center of the Brillouin zone. The unprimed ones are taken along [001], the primed one along [111]; m_e is the electron mass.

	E_g (eV)	Δ (eV)	m_{EL}/m_e	m_{HH}/m_e	m_{LH}/m_e	m_{SO}/m_e	m'_{HH}/m_e
GaAs	1.484	.343	.0665	.3400	.0940	.1794	.7000
$Al_{0.30}Ga_{0.70}As$	1.857	.323	.0891	.4150	.1194	.2161	0.7769

function and one hole Fermi-Dirac function; such an approach cannot thus describe more than two confinement bands. As is clear from Eqs. 2 and 3 each band must have a separate Fermi function.

Finally, it should be noted that the present model contains inconsistencies if applied to a single quantum well i.e. to a separate entity without the surrounding laser structure. For example, well-width fluctuations result in small differences in the injected electron and hole densities for each well width, given a single electron and hole quasi-Fermi level in the calculation. As a result the current through these wells is cal-

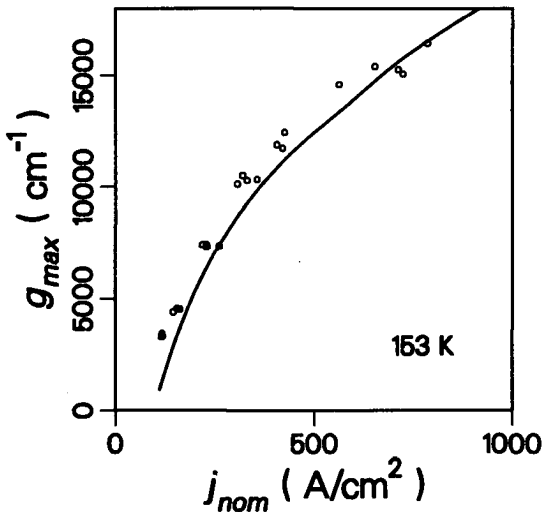


Figure 9 Calculated (drawn line) and measured (circles) maximum gain for light polarization in the plane of the quantum well ($\hat{e}||xy$) as a function of the current density in 20 Å GaAs/ $Al_{0.30}Ga_{0.70}As$ quantum well.

Chapter 4

culated to be different. Well-width fluctuations thus result in (small) current spreading. Another example is current spreading which by itself leads to large differences in quasi-Fermi level separation. This would result in electric currents along the well. However, in the actual laser structure, electric fields sustain the differences in the quasi-Fermi level separation. They are the basic reason for the current spreading. It is clear from these examples that for a really consistent description of a quantum-well laser the surrounding laser structure with its accompanying electric fields should also be considered in the modeling.

The model presented for a quantum-well laser is very advanced when compared to other ones. It fully accounts for the effects of valence-band mixing and conduction-band non-parabolicity in a consistent manner. Other models employ parabolic bands and disregard valence-band mixing altogether. The k_{\parallel} dependence of the optical matrix elements is either completely neglected /2,12-16/ or treated in a very approximate manner /8/. Most other work focuses on the effects of broadening caused by carrier-carrier scattering /2-15/. In this model also the effects of X and L -derived states and non-confined Γ -derived quantum-well states of the barrier on the quasi-Fermi levels and the effects of well-width fluctuations and current spreading on gain and spontaneous emission spectra has been considered. Blood et al. /16/ have shown that probably all these effects have to be included in the model simultaneously if an accurate description of a quantum-well laser is sought.

In conclusion, it has been shown that for injected electron densities greater than $1.10^{19} \text{ cm}^{-3}$ X and L well and Γ , X and L barrier states become substantially populated and must be considered in the description of a quantum-well laser. Furthermore, the broadening effect caused by scattering dominates over all other broadening effects. An accurate and more fundamental description of the effects of scattering processes on recombination is called for.

References

1. see e.g. H.C. Casey and M.B. Panish, "Heterostructure Lasers" Part A and B, Academic Press (New York, 1978);
G.H.B. Thompson, "Physics of Semiconductor Laser Devices", New York: Wiley, 1980
H. Kressel and J.K. Butler, "Semiconductor Lasers and Heterojunction LED's", Academic Press (New York, 1977)
2. A. Yariv, "Theory and applications of quantum mechanics", New York: Wiley, 1982, Ch. 21.

The Art of Semiconductor Laser Modeling

3. W.T. Tsang, "Heterostructure Semiconductor Lasers Prepared by Molecular Beam Epitaxy", *IEEE J. Quantum Electron.*, Vol. QE-20, pp. 1119-1132, Oct. 1984.
N. Holonyak, Jr, R.M. Kolbas, R.D. Dupuis and P.D. Dapkus, "Quantum Well Heterostructure Lasers", *IEEE J. Quantum Electron.*, Vol. QE-16, pp. 170-186, Feb. 1980.
4. R. Eppenga, M.F.H. Schuurmans and S. Colak, "New k.p theory for GaAs/GaAlAs-type quantum wells", *Phys. Rev.*, Vol. B36, pp. 1554-1564, 1987;
M.F.H. Schuurmans and G.W. 't Hooft, "Simple calculation of confinement states in a quantum well", *Phys. Rev.*, Vol. B31, pp. 8041-8048, 1985.
5. D.J. Erskine, A.J. Taylor and C.L. Tang, "Femtosecond studies of intraband relaxation in GaAs, AlGaAs and GaAs/AlGaAs multiple-quantum-well structures", *Appl. Phys. Lett.*, Vol. 45, pp. 54-56, 1984.
6. N.K. Dutta, R.L. Hartman, and W.T. Tsang, "Gain and carrier lifetime measurements in AlGaAs single quantum-well lasers", *IEEE J. Quantum Electron.*, Vol. QE-19, pp. 1243-1246, Aug. 1983.
7. S. Colak, R. Eppenga and M.F.H. Schuurmans, "Band Mixing Effects on Quantum Well Gain", *IEEE J. Quantum Electron.*, Vol. QE-23, pp. 960-968, June 1987.
Y. Arakawa, H. Sakaki, M. Nishioka, J. Yoshino and T. Kamiya, "Recombination lifetime of carriers in GaAs-GaAlAs quantum wells near room temperature", *Appl. Phys. Lett.*, Vol. 46, pp. 519-521, March 1985.
8. M. Asada, A. Kameyama, and Y. Suematsu, "Gain and intervalence-band absorption in quantum-well lasers", *IEEE J. Quantum Electron.*, Vol. QE-20, pp. 745-753, July 1984.
9. Y. Arakawa and A. Yariv, "Theory of gain, modulation response, and spectral linewidth in AlGaAs quantum-well lasers", *IEEE J. Quantum Electron.*, Vol. QE-21, pp. 1666-1674, Oct. 1985
Y. Arakawa and A. Yariv, "Quantum Well Lasers: Gain, Spectra, Dynamics" *IEEE J. Quantum Electron.*, Vol. QE-22, pp. 1887-1899, Sept. 1986.
10. A.G. Aleksanian, I.A. Poluektov and YU.M. Popov, "Theory of Optical Gain and Threshold Properties of Semiconductor Lasers", *IEEE J. Quantum Electron.*, Vol. QE-10, pp. 297-305, March 1974.
11. B. Zee, "Broadening mechanism in semiconductor (GaAs) lasers: Limitations to single mode power emission", *IEEE J. Quantum Electron.*, vol QE-14, pp. 727-736, 1978.
12. P.T. Landsberg, M.S. Abrahams, and M. Osinski. "Evidence of no k-selection in gain spectra of quantum-well AlGaAs laser diodes", *IEEE J. Quantum Electron.*, Vol. QE-21, pp. 24-28, Jan. 1985;
P.T. Landsberg and D.J. Robbins, "Lifetime Broadening of a parabolic band edge of a pure semiconductor at various temperatures", *Solid-State Elec.*, Vol. 28, pp. 137-141, 1985.

Chapter 4

13. M. Yamada, S. Ogita, M. Yamagishi, and K. Tabata, "Anisotropy and broadening of optical gain in a GaAs/AlGaAs multi-quantum-well laser", *IEEE J. Quantum Electron.*, Vol. QE-21, pp. 640-645, June 1985.
14. B. Saint-Cricq, F. Lozes-Dupuy, and G. Vassilieff, "Well-width dependence of gain and threshold current in GaAlAs single quantum-well lasers", *IEEE J. Quantum Electron.*, Vol. QE-22, pp. 625-630, May 1986.
15. E. Zielinski, H. Schweizer, S. Hausser, R. Stuber, M.H. Pilkuhn and G. Weimann, "Systematics of Laser Operation in GaAs/AlGaAs Multi-quantum-well Heterostructures", *IEEE J. Quantum Electron.*, Vol. QE-23, pp. 969-976, June 1987.
16. P. Blood, S. Colak and A.I. Kucharska, "Influence of broadening and high injection effects on GaAs-AlGaAs quantum well lasers", in print *IEEE J. Quantum Electron.*
17. S. Tarucha, H. Kobayashi, Y. Horikoshi, and H. Okamoto, "Carrier-induced energy-gap shrinkage in current-injection GaAs/AlGaAs MQW heterostructures", *Japan J. Appl. Phys.*, Vol. 23, pp. 874-878, 1984.
18. D.A. Kleinman and R.C. Miller, "Band-gap renormalization in semiconductor quantum wells containing carriers", *Phys. Rev.*, Vol. B32, pp. 2266-2272, 1985.
19. G. Tränkle, H. Leier, A. Forchel, H. Haug, C. Ell and G. Weimann, "Dimensionality dependence of the band-gap renormalisation in two and three dimensional electron-hole plasmas in GaAs", *Phys. Rev. Lett.*, Vol. 58, pp. 419-422, Jan. 1987.
20. A. Tomita and A. Suzuki, "Carrier-Induced Lasing Wavelength Shift for Quantum Well Diodes", *IEEE J. Quantum Electron.*, Vol. QE-23, pp. 1155-1159, July 1987.
21. R. Eppenga, S. Colak and M.F.H. Schuurmans, "Effects of band mixing on the radiative properties of a quantum well", in *Proc. SPIE Novel Optoelectronic Devices*, Vol. 800, pp. 38-42, 1987.
22. S.H. Hagen, H.F.J. van 't Blik, M.J.B. Boermans, R. Eppenga, "Experimental determination of the relation between modal gain and current density for AlGaAs single quantum-well lasers grown by metalorganic vapour phase epitaxy", in print *Appl. Phys. Lett.*
23. see e.g. "Hot Carriers in Semiconductors", *Proc. of the Fifth Int. Conf.*, eds. J. Shah and G.J. Iafrate, *Solid State Elec.*, Vol. 31 (1988)

The effect of bulk inversion asymmetry on [001], [110] and [111] GaAs/AlAs quantum wells

The spinsplitting of the conduction band due to the inversion asymmetry of the microscopic crystal potential is predicted to depend linearly on the components of the parallel wavenumber k_{\parallel} for small k_{\parallel} in undoped GaAs/AlAs quantum wells. The linear dependence is due to the quantization of the confinement levels; the bulk spinsplitting depends cubically on k . We have calculated the splitting both numerically and analytically for GaAs/AlAs quantum wells grown along the [001], [110] and [111] direction. In the linear regime the average spinsplitting is shown to be about a factor of two smaller for [110] quantum wells than for [001] and [111] grown quantum wells. The splitting is calculated to be $\Delta E = 4$ meV at $k_{\parallel} = 0.072\pi/a$ for a 25 Å [001] grown GaAs/AlAs quantum well.

Spinsplittings of energy bands of zinc-blende semiconductor modulation-doped heterostructures and quantum wells have been extensively studied both experimentally /1/ and theoretically /2/. The splittings are then caused by the inversion asymmetry of the macroscopic, i.e. slowly varying on the scale of the lattice parameter a , interface, or confinement potential. Homogeneous zinc-blende semiconductors exhibit an intrinsic spinsplitting due to the inversion asymmetry of the microscopic crystal potential /3/. As a result terms linear in $k \equiv |k|$ may appear in the valence-band structure, but calculations of Cardona et al./4/ show that the corresponding splittings are extremely small, < 1 meV, for zinc-blende semiconductors. In addition terms cubic in k may occur both in the conduction band and the valence bands. They are associated with Kane's /3/ B parameter and are not all that small. Christensen and Cardona /5/ obtain a theoretical estimate of 75 meV for the maximum splitting in GaAs occurring for k along [110]. Effects of this splitting have been observed in spin-polarized photoemission /6/, the Hanle effect /7/ and infrared spin-resonance /8/.

This communication addresses the effects of the inversion asymmetry of the microscopic crystal potential in undoped GaAs/AlAs quantum wells grown along the

[001], [110] and [111] direction i.e. in systems having a macroscopic inversion-symmetric confinement potential. We show that the spinsplitting depends linearly on the components of the parallel wavenumber k_{\parallel} for small k_{\parallel} ($\equiv |k_{\parallel}|$) and calculate its magnitude both numerically and analytically as a function of k_{\parallel} ; the crystal-momentum-like quantum number k_{\parallel} describes the translational symmetry in the parallel plane of the quantum well.

We derive a $k.p$ Hamiltonian for the conduction bands of bulk zinc-blende semiconductors, which reproduces their spinsplittings, and develop the corresponding envelope function formalism for the quantum well consisting of these semiconductors. Perturbation theory is used to obtain analytical expressions for the spinsplitting occurring in the energy spectrum of the quantum wells as a function of k_{\parallel} . In these expressions contributions both linear and cubic in k_{\parallel} appear. Their origin is discussed.

We first derive an envelope function formalism for the conduction bands of [001] grown GaAs/AlAs and alike (type I) quantum wells which includes the spinsplitting due to the inversion asymmetry of the microscopic potential. We proceed along the lines of our earlier work and omit details /9/. For each bulk constituent l ($l = W$ for the well and $l = B$ for the barrier) we expand the conduction-band wavefunction $\psi_{k_{\parallel}}^l(\mathbf{r})$ into s -like spin-up ($u_{\uparrow}^l = |s_{\uparrow}\rangle$) and spin-down ($u_{\downarrow}^l = -|s_{\downarrow}\rangle$) conduction-band Γ -point states as

$$\psi_{k_{\parallel}}^l(\mathbf{r}) = e^{ik_{\parallel}r_{\parallel}} (F_{\uparrow k_{\parallel}}^l(z) u_{\uparrow}^l(\mathbf{r}) + F_{\downarrow k_{\parallel}}^l(z) u_{\downarrow}^l(\mathbf{r})), \quad (1)$$

where the envelope vectorfunction $F_{k_{\parallel}}^l \equiv (F_{\uparrow k_{\parallel}}^l(z), F_{\downarrow k_{\parallel}}^l(z))$ satisfies the Schrödinger-equation $(\underline{H}_{k_{\parallel}}^l - E_{k_{\parallel}}^l I) F_{k_{\parallel}}^l = \mathbf{0}$; z is along the growth direction of the quantum well. The Hamiltonian matrix $\underline{H}_{k_{\parallel}}^l$ can be obtained from the eight-band Kane-type $k.p$ -Hamiltonian /9/ by Löwdin renormalization /10/ and the omission of $O(k^4)$ terms and is given by

$$\underline{H}_{k_{\parallel}}^l = \begin{vmatrix} E_c + \tilde{e} + \frac{\gamma}{2} \tilde{k}_z(k_x^2 - k_y^2) & \frac{\gamma}{2} [\tilde{k}_z^2(k_x + ik_y) - ik_x k_y(k_x - ik_y)] \\ \frac{\gamma}{2} [\tilde{k}_z^2(k_x - ik_y) + ik_x k_y(k_x + ik_y)] & E_c + \tilde{e} - \frac{\gamma}{2} \tilde{k}_z(k_x^2 - k_y^2) \end{vmatrix}. \quad (2)$$

Here, and in the following when confusion is unlikely, we have omitted the superscript l . The energy E_c is the energy at the bottom of the conduction band, the "energy operator" $\tilde{e} = \frac{\hbar^2}{2m^*} (k_x^2 + k_y^2 + \tilde{k}_z^2)$, m^* is the Γ -point conduction-band effective electron mass, γ is the spinsplitting parameter as defined by Christensen and Cardona /5/ and \tilde{k}_z is the operator id/dz . Setting $F_{k_{\parallel}} \propto e^{ik_x z}$ the two energy eigenvalues of the

Schrödinger-equation clearly exhibit the bulk spinsplitting and are given by $E_{k_{\pm}} = \hbar^2 k^2 / 2m^* \pm \gamma / 2 \sqrt{k^2(k_x^2 k_y^2 + k_y^2 k_z^2 + k_z^2 k_x^2) - 9k_x^2 k_y^2 k_z^2}$. The spinsplitting is cubic in the components of k and attains a maximum value $\frac{\gamma}{2} k^3$ for k along the [110] direction; it is zero for k along [001] and [111].

The envelope function formalism developed for bulk zinc-blende semiconductors can now be suitably modified to describe type-I quantum wells. We must join the envelope functions $F_{k_{||}}^W$ of the well W and $F_{k_{||}}^B$ of the barrier B across the interfaces. We take the usual boundary conditions /9,11/ i.e. continuity, $F_{k_{||}}^W = F_{k_{||}}^B$, and "differentiability", $(A^W \frac{\partial}{\partial z} + \frac{1}{2} B^W) F_{k_{||}}^W = (A^B \frac{\partial}{\partial z} + \frac{1}{2} B^B) F_{k_{||}}^B$, at each interface. The matrices A^l and B^l depend on $k_{||}$ and are defined by the following decomposition of Hamiltonian: $H^l = A^l \frac{\partial^2}{\partial z^2} + B^l \frac{\partial}{\partial z} + C^l$. Confined states are obtained by specifying the boundary conditions for $z \rightarrow \pm \infty$: $\lim_{z \rightarrow \pm \infty} F_{k_{||}}(z) = 0$.

We solve the Schrödinger equation plus boundary conditions for a quantum well of width w numerically. At a sought confinement energy $E_{k_{||}}$ we determine the four $k_z^l(E_{k_{||}})$ -values and the corresponding eigenvectorfunctions $F_{k_{||}}^l(z)$ which satisfy the Schrödinger equation in each constituent l of the quantum well. Note that for $\gamma^B \neq 0$ the four $k_z^B(E_{k_{||}})$ -values in the barrier are not just imaginary, but complex numbers. The quantum well envelope vectorfunction is then written as a linear combination of these eigenvectorfunctions. Application of the boundary conditions yields the confinement energy.

Our formalism can also be applied to type-I quantum wells grown along the [110] and [111] direction. If the rotation from $z = [001]$ to $z' = [110]$ or [111] is governed by the orthogonal transformation $r' = Or$, all we have to do is apply the same rotation to $k = (k_{||}, k_z)$. We obtain $\underline{H}(k') = \underline{H}(k = O^T k')$; k_z' is along the quantum well growth direction and $k_{||}'$ in the quantum well plane /12/. The determination of the boundary conditions is now carried through for the primed variables. In solving the envelope function problem for non-[001] grown quantum wells a problem arises since \underline{H} now depends on $(k_z')^3$. We omit the corresponding spurious solutions /9/ and the effect of the $(k_z')^3$ term on the boundary conditions /13/. In the following the primes are omitted.

We can also derive analytical results for the spinsplitting in a quantum well. For $k_{||} = 0$ the eigenstates are doubly degenerate as a result of time-reversal symmetry: no spinsplitting exists. For $k_{||} \neq 0$ analytical expressions for the spinsplitting can be obtained by the application of degenerate perturbation theory. The Hamiltonian is decomposed as $\underline{H} = \underline{H}_0 + \underline{H}_p$ where $\underline{H}_0 = (E_c + \tilde{e})I$ and \underline{H}_p contains the remaining i.e. the γ -dependent terms. In \underline{H}_0 the two spin bands are decoupled and the standard single-

band spin-degenerate quantum well model is obtained /9/. The two degenerate envelope functions $F_{k_{\parallel}}^{(1)} \equiv (F_{k_{\parallel}}(z), 0)$ and $F_{k_{\parallel}}^{(2)} \equiv (0, F_{k_{\parallel}}(z))$ at a degenerate energy $E_{k_{\parallel}}$ obviously both satisfy $(H_0 - E_{k_{\parallel}})F_{k_{\parallel}}^{(j)} = 0$. The perturbation H_p results in the spinsplitting $\Delta E_{k_{\parallel}} = 2\sqrt{V_{11}^2 + |V_{12}|^2}$, where $V_{ij} = \langle F_{k_{\parallel}}^{(i)} | H_p | F_{k_{\parallel}}^{(j)} \rangle$. For [001] and [110] grown quantum wells V_{11} is zero and the spinsplitting $\Delta E_{k_{\parallel}} = 2|V_{12}|$ can be written as

$$\Delta E_{k_{\parallel}} = \left| \overline{\gamma k_z^2} (k_x + i k_y) - \bar{\gamma} i k_x k_y (k_x - i k_y) \right| \quad (3)$$

for [001] grown quantum wells where k_x and k_y are along the [100] and [010] direction, respectively, and

$$\Delta E_{k_{\parallel}} = \frac{1}{2} \left| -\overline{\gamma k_z^2} \frac{(1-i)}{\sqrt{2}} k_y + \bar{\gamma} \frac{(1-i)}{\sqrt{2}} k_y (k_y^2 - 2k_x^2) \right|, \quad (4)$$

for [110] grown quantum wells where k_x and k_y are along the [00 $\bar{1}$] and [$\bar{1}$ 10] direction, respectively. For a [111] grown quantum well the resulting expression for the spinsplitting is

$$\Delta E_{k_{\parallel}} = \frac{1}{2\sqrt{3}} \left[16 \overline{(\gamma k_z^2)^2} (k_x^2 + k_y^2) - 8 \bar{\gamma} \overline{\gamma k_z^2} (k_x^2 + k_y^2)^2 + \bar{\gamma}^2 (k_x^6 + 21k_x^4 k_y^2 - 9k_x^2 k_y^4 + 3k_y^6) \right]^{1/2} \quad (5)$$

where k_x and k_y are along the [11 $\bar{2}$] and [$\bar{1}$ 10] direction, respectively. The barred quantities in these expressions are defined as averages of the spinsplitting parameter γ and the confinement wavenumber k_z over the probability density of the confinement state i.e. $\overline{\gamma k_z^2} = \int_{-\infty}^{+\infty} F_{k_{\parallel}}^*(z) \tilde{k}_z \gamma(z) \tilde{k}_z F_{k_{\parallel}}(z) dz$ and $\bar{\gamma} = \int_{-\infty}^{+\infty} F_{k_{\parallel}}^*(z) \gamma(z) F_{k_{\parallel}}(z) dz$, where the single-band envelope function $F_{k_{\parallel}}(z)$ satisfies the normalization condition $\int_{-\infty}^{+\infty} F_{k_{\parallel}}^*(z) F_{k_{\parallel}}(z) dz = 1$.

The integrals consist of a well contribution, a barrier contribution and, for $\overline{\gamma k_z^2}$, of interface contributions resulting from δ -singularities of $d^2 F_{k_{\parallel}}/dz^2$ and $d\gamma(z)/dz$ at the interfaces. The barred quantities depend weakly on k_{\parallel} ($< 2\%$ difference for $k_{\parallel} \in [0, 0.062\pi/a]$) through the weak k_{\parallel} -dependence of $F_{k_{\parallel}}(z)$. For wide wells, $w > 200\text{\AA}$, $\bar{\gamma}$ and $\overline{\gamma k_z^2}$ are to within a few percent equal to γ^w and $\gamma^w (k_z^w)^2$, respectively, where k_z^w is the quantized wavenumber in the well.

Our model contains five parameters: the effective electron masses m_w^* and m_b^* , the spinsplitting parameters γ^w and γ^b and the conduction-band discontinuity ΔE_c . We apply the model to GaAs/AlAs quantum wells. We thus take $m_w^* = 0.067$, $m_b^* = 0.150$

and put ΔE_c equal to 0.99 eV. The spinsplitting parameter was calculated for GaAs by Christensen and Cardona /5/ using the LMTO method. We take their value i.e. $\gamma^W = 17 \text{ eV}\text{\AA}^3$. For AlAs no value exists. We have therefore performed an Augmented Spherical Wave (ASW) /14/ bandstructure calculation for GaAs and AlAs including the spin-orbit interaction operator in the Hamiltonian /15/. Figure 1 contains our calculated results for the spinsplitting of the conduction bands of GaAs and AlAs. Our results for GaAs agree with those of Christensen and Cardona to within 5% percent. For AlAs the spinsplitting is found to have the same sign as for GaAs and it is $\approx 30\%$ smaller than that of GaAs. We consequently take $\gamma^B = 12 \text{ eV}\text{\AA}^3$.

The Figures 2-3 display our analytical results for the spinsplitting of the conduction bands of 50 Å wide [001], [110] and [111] grown GaAs/AlAs quantum wells. We have verified that our analytical results agree with our numerical results to within 0.1%. Obviously, the spinsplitting depends strongly on the growth direction of the quantum well. Unlike the bulk spinsplitting which is cubic in k , it is not cubic in k_{\parallel} . Moreover, it is strongly anisotropic. The k_{\parallel} -dependence as shown in Fig. 2 can be interpreted in detail from Eqs. (3)-(5). For small k_{\parallel} , $k_{\parallel} \ll k_z^W$, the term containing $\overline{\gamma k_z^2}$ is dominating and the spinsplitting is linear in k_{\parallel} ; it is approximately equal to $\overline{\gamma k_z^2} k_{\parallel}$, $1/2 \overline{\gamma k_z^2} k_y$, and $2/\sqrt{3} \overline{\gamma k_z^2} k_{\parallel}$ for [001], [110] and [111] grown quantum wells, respectively. The origin of the linear contribution in k_{\parallel} is obvious from these formulas: it is due to the quantum well induced quantization of k_z in the third order $k_z^2 k_x$ and

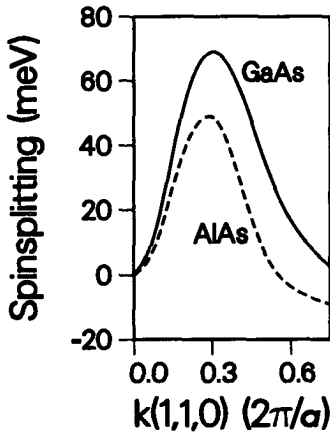


Figure 1 Calculated ASW results for the spinsplitting of the conduction bands in GaAs (drawn) and AlAs (dotted) along $\Gamma - K$.

$k_z^2 k_y$ bulk contributions. Note that terms even in k_{\parallel} do not exist because of time reversal symmetry.

For larger k_{\parallel} the term containing $\bar{\gamma}$ in Eqs. (3)-(5) is dominating and the spinsplitting is cubic in k_{\parallel} . For $k_{\parallel} \gg k_z^W$, the maximum value of the spinsplitting occurs for k_{\parallel} along [110] for [001] grown quantum wells and for k_{\parallel} along $[\bar{1}10]$ for both [110] and [111] grown quantum wells; it can be approximated by $\frac{\gamma}{2} k_{\parallel}^3$. The maximum spinsplitting does not depend on the growth direction and is comparable to the maximum spinsplitting in the bulk $\frac{\gamma}{2} k^3$ appearing for k along [110]. This is not surprising since for large k_{\parallel} the kinetic energy ($\sim \hbar^2 k_{\parallel}^2 / (2m_w^*)$) is much larger than the confinement energy ($\sim \hbar^2 (k_z^W)^2 / (2m_w^*)$). For certain k_{\parallel} directions the spinsplitting for the [001] and [110] grown quantum wells changes sign (see Fig. 2) due to a competition between the linear and the cubic terms in Eqs. (3)-(4). For $k_{\parallel} = (0, k_{\parallel})$, i.e. along [010], only the linear term is present for a [001] grown quantum well and the departure from a straight line is only caused by the k_{\parallel} dependence of $\overline{\gamma k_z^2}$. In Fig. 3 the spinsplitting is

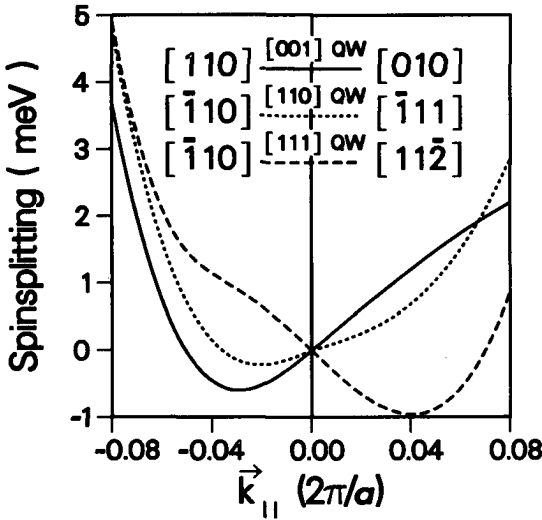


Figure 2 Calculated (from Eqs. (3)-(5)) spinsplitting of the first conduction-band confinement level for 50 Å [001] (drawn), [110] (dotted) and [111] (dashed) grown GaAs/AlAs quantum wells. The parameters have the following values: $\bar{\gamma} = 16.84 \text{ eV}\text{\AA}^3$ and $\overline{\gamma k_z^2} = 0.028 \text{ eV}\text{\AA}$ at $k_{\parallel} = 0$, $\bar{\gamma} = 16.80 \text{ eV}\text{\AA}^3$ and $\overline{\gamma k_z^2} = 0.025 \text{ eV}\text{\AA}$ at $k_{\parallel} = 0.082\pi/a$; cf. $\gamma = 17.00 \text{ eV}\text{\AA}^3$ and $\gamma^W (k_z^W)^2 = 0.032 \text{ eV}\text{\AA}$.

shown as a function of the direction of k_{\parallel} while k_{\perp} is kept constant. The anisotropy of the spinsplitting exhibits the symmetry of a square, a rectangle and a regular hexagon for the $[001]$, $[110]$ and $[111]$ grown quantum wells, respectively, as is demanded from the symmetry of the corresponding 2-D unit cells. For $[110]$ grown quantum wells an extreme anisotropy is found since the spinsplitting is always zero for $k_{\parallel} = (k_{\parallel}, 0)$ i.e. $[00\bar{1}]$.

In conclusion, we have numerically and analytically calculated the spinsplitting of the conduction bands of GaAs/AlAs quantum wells grown along the $[001]$, $[110]$ and $[111]$ direction. For large k_{\parallel} , $k_{\parallel} \gg k_z^w$, the bulk result is essentially retrieved; the maximum spinsplitting is cubic in k_{\parallel} and approaches the maximum bulk value. However, for small k_{\parallel} , $k_{\parallel} \ll k_z^w$, different behavior is found: the spinsplitting is linear in k_{\parallel} . This dependence does not originate from the well-known bulk linear k -terms which are known to be very small $/4/$. It is caused by the confinement of the quantum

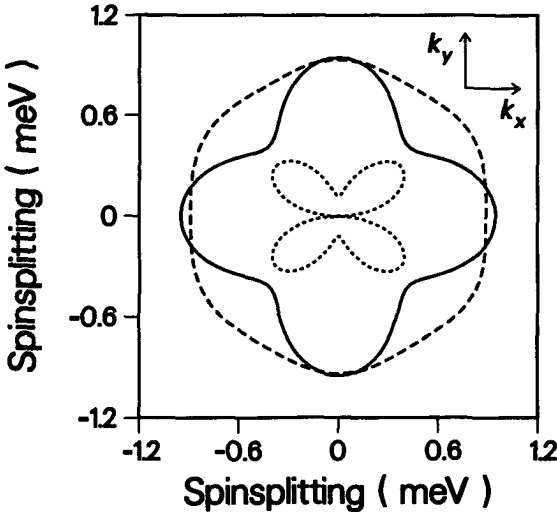


Figure 2 Calculated (from Eqs. (3)-(5)) spinsplitting of the first conduction-band confinement level for 50 Å $[001]$ (drawn), $[110]$ (dotted) and $[111]$ (dashed) grown GaAs/AlAs quantum wells for different $k_{\parallel} = (k_x, k_y)$ directions where $k_{\parallel} = 0.032\pi/a$; k_x is along $[100]$, $[00\bar{1}]$ and $[11\bar{2}]$ and k_y is along $[010]$, $[\bar{1}10]$ and $[\bar{1}\bar{1}0]$ for $[001]$, $[110]$ and $[111]$ grown quantum wells, respectively. The parameters have the following values: $\bar{\gamma} = 16.83 \text{ eV\AA}^3$, $\bar{\gamma}k_z^2 = 0.027 \text{ eV\AA}$ and $k_z^w = 0.0382\pi/a$.

well states whereby k_z^w becomes quantized. We also note that in the linear regime the spinsplitting averaged over all directions of k_{\parallel} is about a factor of two smaller for [110] grown quantum wells than for [001] and [111] grown quantum wells. The magnitude of the spinsplitting in the linear regime is 4 meV at $k_{\parallel} = 0.072\pi/a$ for k_{\parallel} along [100] in a [001] grown 25 Å GaAs/AlAs quantum well. The corresponding confinement energy $E_{k_{\parallel}}$ is 580 meV. Larger values of the spinsplitting, i.e. up to the bulk values ~ 50 meV, are obtained further out in the 2D Brillouin zone where cubic and bulk like behavior prevail. We note that the present theory does not accurately predict the spinsplitting in this case since the bulk bandstructures of the constituents of the quantum well are not properly accounted for in the corresponding part of the 3D Brillouin zone.

It would be interesting to perform infrared spin-resonance or spin-polarized photo-emission experiments on these systems to measure in particular the linear k_{\parallel} dependence of the spinsplitting for small k_{\parallel} . Thin quantum wells (~ 25 Å) should be used to obtain a maximum effect.

References

1. J.P. Eisenstein, H.L. Störmer, V. Narayanamurti, A.C Gossard and W. Wiegman, Phys. Rev. Lett. 53, 2579 (1984); M.H. Meynadier, J. Orgonasi, D. Delalande, J.A. Brum, G. Bastard and M. Voos, Phys. Rev. B34, 2482 (1986)
2. G. Lommer, F. Malcher and U. Rössler, Phys. Rev. Lett. 60, 728 (1988); U. Ekenberg and M. Altarelli, Phys. Rev. B30,3569 (1984); E. Bangert and G. Landwehr, Superlattices and Microstructures 1, 363 (1985); D.A. Broido and L.J. Sham, Phys. Rev. B31, 888 (1985)
3. E.O. Kane, in Handbook on Semiconductors (North-Holland, New York, 1982), Vol. I, p. 193.
4. M. Cardona, N.E. Christensen and G. Fasol, Phys.Rev. Lett. 56, 2831 (1986)
5. N.E. Christensen and M. Cardona, Solid State Comm. 51, 491 (1984)
6. S.F. Alvarado, H. Riechert and N.E. Christensen, Phys.Rev. Lett. 55, 2716 (1985).
7. A.T. Gorelenok, V.A. Marushchak and A.N. Titkov, Izv. Akad. Nauk, SSSR Ser. Fiz. 50, 290 (1986)
8. D. Stein, K. v. Klitzing and G. Weiman, Phys.Rev. Lett. 51, 130 (1983)
9. M.F.H. Schuurmans and G.W.'t Hooft, Phys. Rev. B31, 8041 (1985); R. Eppenga, M.F.H. Schuurmans and S. Colak, Phys. Rev. B36, 1554 (1987)
10. P.O. Löwdin, J. Chem. Phys. 19, 1396 (1951).

Chapter 5

11. M. Altarelli, *Physica* 117B/118B, 747 (1983) and *J. Lumin.* 30, 472 (1985); M. Altarelli, U. Ekenberg and A. Fasolino, *Phys.Rev.* B32, 5138 (1985).
12. The orthogonal transformation results in replacing (k_x, k_y, k_z) by $((k_z' - k_y')/\sqrt{2}, (k_z' + k_y')/\sqrt{2}, -k_x')$ and $(k_x'/\sqrt{3} - k_y'/\sqrt{2} + k_z'/\sqrt{6}, k_x'/\sqrt{3} + k_y'/\sqrt{2} + k_z'/\sqrt{6}, k_x'/\sqrt{3} - k_z'/\sqrt{2/3})$ for quantum wells grown along [110] and [111], respectively.
13. The net effect of the $(k_x')^3$ terms in the boundary conditions turns out to be zero in our perturbative analysis.
14. A.R. Williams, J. Kübler and C.D. Gelatt, *Phys. Rev. B* 19, 6094 (1979).
15. R. Eppenga, M.F.H. Schuurmans and H.W.A.M. Rompa, in print *J. of Phys. and Chem. of Solids*.

Thin [001] and [110] GaAs/AlAs superlattices: direct or indirect?

We have calculated oscillator strengths of across-gap transitions in $n \times n$ GaAs/AlAs superlattices ($n=1,2$) grown along the [001] and [110] directions using the Augmented Spherical Wave (ASW) *ab-initio* bandstructure method. We find that the rate for radiative emission across the direct gap in the very thin [001] superlattices is at least two orders of magnitude smaller than the corresponding quantity in GaAs. The radiative transition rates across the direct and indirect gaps turn out to be comparable in these superlattices. The 2×2 [110] superlattice is direct and has a direct-gap oscillator strength which is 78% of that of GaAs.

Recently, Ishibashi et al. have been able to grow high quality, very thin $n \times n$ GaAs/AlAs [001] superlattices with $n=1,2,\dots$ /1/. The question has been raised whether such $n \times n$ superlattices are direct or indirect; the corresponding alloy $\text{Al}_{0.5}\text{Ga}_{0.5}\text{As}$ is indirect /2/. The work of Ishibashi et al./1/ provides evidence for the superlattices to be *energywise* direct from $n=2$ onwards. The $n=1$ superlattice appears to be *energywise* indirect. The lowest Γ -point conduction-band state of the thin ($n=1,2$) superlattices is a band-folded X -state. Obviously the optical matrix element from this state to the top of the valence-band state will be small.

In this paper we perform *ab-initio* calculations of the rate for radiative emission across the direct gap in the very thin 1×1 and 2×2 [001] superlattices and show that it is at least two orders of magnitude smaller than the corresponding quantity in GaAs and that the radiative transition rates across the direct and indirect gap are comparable in these superlattices. We note that such calculations cannot be done using semi-empirical (for example envelope-function-type /3/) approaches since for the thin superlattices considered here the superlattice crystal potential must be determined selfconsistently.

For a spectroscopist the distinction between a direct and an indirect semiconductor is related to the typically much larger transition rate for emission of radiation across the direct gap than across the indirect gap. From the point of view of spectroscopy

the very thin [001] superlattices are thus neither direct nor indirect. Moreover, the radiative transitions are very weak, corresponding to lifetimes of $0.1\mu\text{s} - 1\mu\text{s}$. These superlattices therefore may not be very useful for applications involving light emission.

Earlier theoretical calculations of Christensen et al. /4/, Nakayama et al. /5/, Bylander et al. /6/, Gilbert et al. /7/ and Nelson et al. /8/ have focused on the superlattice bandstructure. Their results are more or less inline with the findings of Ishibashi et al./1/: for $n=1$ the minimum of the conduction band is found to be at R /4-7/ making the 1×1 superlattice *energywise* indirect. For $n=2$ the minimum of the conduction band is found to be at Γ by Nakayama et al. /5/ and in between Γ and Z by Gilbert et al. /7/. Theoretically it is not clear whether the 2×2 [001] superlattice is *energywise* direct or indirect /8/.

This paper is focused on the transition rate aspect. We calculate oscillator strengths of Γ -point across-gap transitions in very thin ($n=1,2$) GaAs/AlAs superlattices grown along the [001] and [110] directions using the Augmented Spherical Wave (ASW) /9/ *ab-initio* bandstructure method. A self-consistent potential for the $n \times n$ [001] and [110] GaAs/AlAs superlattices was generated by solving the Kohn and Sham equation /10/ iteratively within the ASW basis set /9/, using the local density approximation (LDA) for the exchange and correlation functional /10/. Scalar-relativistic effects were ignored and "empty" spheres were placed at the interstitial sites /11/. The ASW basis set consisted of s , p and d orbitals centered at each atomic and "empty" sphere site. All muffin-tin sphere radii were taken to be equal. The lattice constant was set equal to 5.653 \AA . The number of special k -points in the irreducible wedge of the Brillouin zone was taken to be 18 (6) for the tetragonal structure and 27 (8) for the orthorhombic structure (the numbers in parentheses apply to the 2×2 SL). Self-consistency of the superlattice crystal potential was achieved at a level of 1 mRy.

The across-gap oscillator strength between a valence-band state ϕ_v and a conduction-band state ϕ_c induced by light of polarization e is equal to $\frac{2}{m} |\langle \phi_v | p \cdot e | \phi_c \rangle|^2 / \Delta E$; here m is the electron mass, p is the momentum operator and ΔE is the energy difference between the states ϕ_v and ϕ_c . We have shown before that calculated oscillator strengths are typically accurate to within 20% /12/ despite the fact that the gap is typically calculated to be 30-50% too small /12/. Details concerning the calculation of the oscillator strengths from the selfconsistently obtained wavefunctions can be found elsewhere /12/. We estimate the accuracy of the relative positions of the energy levels in the conduction band to be around 30-100 meV /13/.

Our results for the optical properties of the superlattices are as follows; results for ground state properties are summarized in footnote 14. For the 1×1 [001] $\equiv 1 \times 1$

[110] GaAs/AlAs superlattice we find Fig. 1. The bottom of the conduction band is at $R(L)$, which is the folded L point of the underlying fcc lattice. The lowest superlattice conduction-band Γ -state is X_2 -derived, i.e. $\Gamma(X_2)$, and is 71 meV higher in energy than $R(L)$. The Γ -derived state $\Gamma(\Gamma)$ is still 23 meV higher in energy. The heavy-hole (HH) and light-hole (LH) derived top of the valence-band states $\Gamma(HH)$ and $\Gamma(LH)$ are split by 23 meV, the $\Gamma(HH)$ state being higher in energy. In accordance with the experimental result /1/ and other bandstructure calculations /4-8/ the 1×1 GaAs/AlAs superlattice is thus found to be *energywise* indirect. We find that the direct-gap oscillator strength $\Gamma(X_2) - \Gamma(HH)$ of the 1×1 GaAs/AlAs superlattice is very small, 0.3% of that of bulk GaAs and 0.6% of the $\Gamma(\Gamma) - \Gamma(HH)$ superlattice oscillator strength.

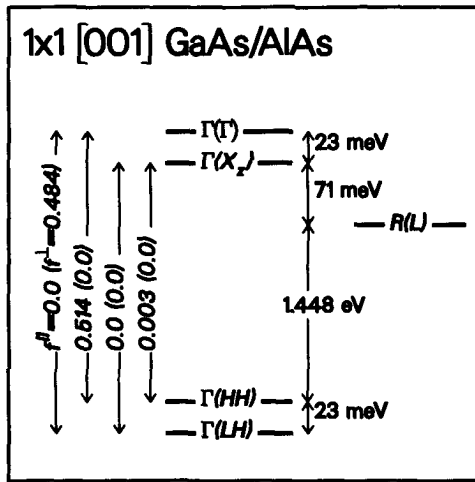


Figure 1 Schematic representation of the energy levels at high symmetry points of the 1×1 [001] GaAs/AlAs superlattice. $\Gamma(HH)$ and $\Gamma(LH)$ denote superlattice valence-band states and $\Gamma(X_2)$, $\Gamma(\Gamma)$ and $R(L)$ denote conduction band states. The fcc origin of the superlattice symmetry points is indicated in parenthesis. The calculated oscillator strengths f between a conduction band state Γ_c and a valence band state Γ_v for light polarization in plane ($f^{\parallel} \equiv f^{xx} + f^{yy}$) and along [001] ($f^{\perp} \equiv f^{zz}$) are in units of the calculated direct-gap oscillator strength $f^{GaAs} \equiv f^{xx} + f^{yy} + f^{zz}$ ($= 13.8/12$) of bulk GaAs. For comparison: the calculated result of f^{AlAs} is 7.0 for bulk AlAs /12/.

For the 2×2 [001] superlattice we arrive at a more complicated picture; see Fig. 2. The indirect gap $M(X_z) - \Gamma(HH)$ is barely smaller (1 meV) than the direct gap $\Gamma(X_z) - \Gamma(HH)$. We find the lowest Γ -derived superlattice-conduction-band state $\Gamma(\Gamma)$ to be 135 meV higher in energy than the state $\Gamma(X_z)$. The $\Gamma(X_z) - \Gamma(HH)$ oscillator strength in the 2×2 [001] GaAs/AlAs superlattice is found to be 6% of that of bulk GaAs and 13% of the $\Gamma(\Gamma) - \Gamma(HH)$ superlattice oscillator strength.

The results for the 2×2 [110] superlattice are depicted in Fig. 3. The superlattice has a direct gap $\Gamma(\Gamma) - \Gamma(HH)$ which is 143 meV smaller than the smallest indirect gap $Y(X_z) - \Gamma(HH)$. The direct-gap oscillator strength is 78% of that of bulk GaAs. Note also that for this growth direction the twofold degeneracy of the heavy-hole bands is lifted resulting in three separate valence bands at Γ instead of two folded heavy-hole and one folded light-hole Γ_{fcc} -derived bands.

The values for the calculated oscillator strengths are related to the origin of the corresponding conduction-band state; they are large for Γ -derived conduction-band

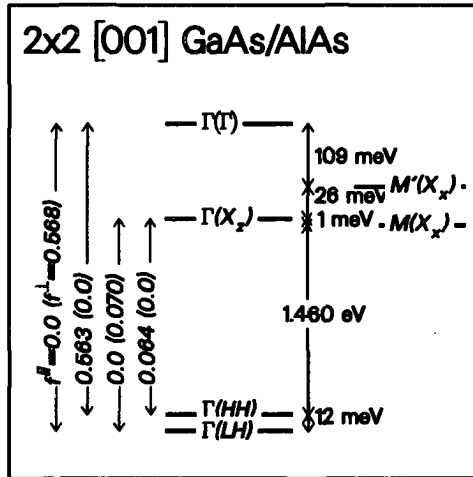


Figure 2 Schematic representation of the energy levels at high symmetry points of the 2×2 [001] GaAs/AlAs superlattice. $\Gamma(HH)$ and $\Gamma(LH)$ denote superlattice valence-band states and $\Gamma(X_z)$, $\Gamma(\Gamma)$, $M(X_z)$ and $M'(X_z)$ denote conduction band states. Notation and units for the calculated oscillator strengths f^\parallel and f^\perp are the same as in Fig. 1.

Table I Relative character of the superlattice states at the Γ bottom of the conduction band in terms of the bulk GaAs and AlAs Γ and X conduction band states.

	state	$\Gamma(\text{GaAs})$	$X(\text{GaAs})$	$\Gamma(\text{AlAs})$	$X(\text{AlAs})$
$1 \times 1 [001]$	$\Gamma(X_c)$	< 0.01	0.47	< 0.01	0.53
	$\Gamma(\Gamma)$	0.65	< 0.01	0.35	< 0.01
$2 \times 2 [001]$	$\Gamma(X_c)$	0.13	0.39	0.08	0.40
	$\Gamma(\Gamma)$	0.58	< 0.01	0.42	< 0.01
$2 \times 2 [110]$	$\Gamma(\Gamma)$	0.60	< 0.01	0.40	< 0.01
	$\Gamma(X_c)$	0.12	0.34	< 0.01	0.54

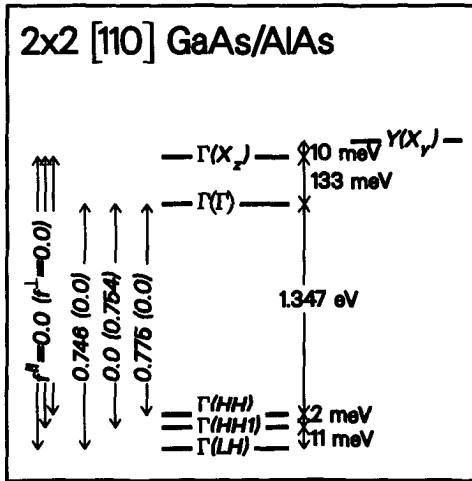


Figure 3 Schematic representation of the energy levels at high symmetry points of the $2 \times 2 [110]$ GaAs/AlAs superlattice. $\Gamma(HH)$, $\Gamma(HH1)$ and $\Gamma(LH)$ denote superlattice valence band states and $\Gamma(X_c)$, $\Gamma(\Gamma)$ and $Y(X_c)$ denote conduction band states. Notation and units for the calculated oscillator strengths f^{\parallel} and f^{\perp} are the same as in Fig. 1.

states and small for any other (e.g. X)-derived conduction-band state. In Table I we present the character of the superlattice states at the Γ bottom of the conduction band in terms of the bulk GaAs and AlAs Γ and X conduction-band states. This decomposition is only indicative since (i) it is based on the s and p percentage of the Ga and Al-based ASW basisfunctions of the relevant wavefunction and (ii) it ignores other mixed-in states.

We now discuss the issue of the superlattices being *energywise* and *spectroscopically* direct or indirect. The 2×2 [110] superlattice is direct in any sense, i.e. it is energywise direct and has a large direct-gap oscillator strength. The situation for the 2×2 [001] superlattice is complicated. We find energy differences $\Delta E(\Gamma(X_x) - M(X_x)) \approx 1$ meV and $\Delta E(\Gamma(\Gamma) - \Gamma(X_x)) \approx 130$ meV, i.e. energywise the superlattice is barely indirect. Elementary calculation shows that the ratio r of the radiative transition rates for the direct $\Gamma(X_x) - \Gamma(HH)$ and the indirect $M(X_x) - \Gamma(HH)$ transition is given by $r \approx 0.01 (S/\Delta E)^2 / 17/$. Here S is an energy measure of the strength of the electron-phonon coupling involved in the phonon-assisted indirect rate and ΔE is the difference in energy between the direct and the indirect transitions involved in the perturbative calculation of that rate or, if the relevant phonon energy is larger, ΔE is that phonon energy (10-30 meV /18/). We estimate $S \approx 10 - 100$ meV /19/ and therefore $r \approx 1$. The 2×2 [001] superlattice can therefore be qualified neither direct nor indirect from a spectroscopic point of view. The 1×1 [001] superlattice is energywise indirect. However, here again one should realize that the direct ($\Gamma(X_x) - \Gamma(HH)$) and the indirect transitions ($R(L) - \Gamma(HH)$) have comparable strength and are extremely weak. The oscillator strength of the direct transition ($\Gamma(X_x) - \Gamma(HH)$) is only 0.6% of that of the $\Gamma(\Gamma) - \Gamma(HH)$ transition.

Both for the 1×1 and the 2×2 [001] superlattices the radiative rates, both on the direct and the indirect transition, are so small, corresponding with $\approx 0.1 \mu s$ lifetimes at low temperatures, that non-radiative processes associated with impurities, may interfere with the radiative processes. Precisely this occurs in the experiments of Ishibashi et al. /1/. This is clear from their experimental results on the quantum efficiencies and their assumption that the indirect recombination is completely non-radiative. In view of our theoretical results this implies that the direct recombination would probably also have a substantial contribution due to non-radiative decay. We note that Nelson et al. /8/ have shown that the lowest conduction-band state becomes a Γ -point GaAs derived conduction-band state for the wider $n \times n$ superlattices ($n = 10-12$) implying a large across-gap oscillator strength.

We stress that the issue of a superlattice being energywise direct or indirect can not be fully settled by *ab-initio* bandstructure calculations since they are known to be able to produce relative positions of energy levels in conduction-band spectra only to an accuracy of 30-100 meV /13/. The 2×2 [001] superlattice is particularly difficult in this respect since the relevant energy difference $E(\Gamma(X_z)) - E(M(X_x))$ is so small (≈ 1 meV). This is unfortunate since the ordering of the X_y and X_z -derived states is subject to debate /20/. We note however that the accuracy of this calculated energy difference is on a considerably better level (a few meV) than the 30-100 meV mentioned before since both states originate from in the equivalent bulk X states. But even the ordering of $\Gamma(X_z)$ and $\Gamma(\Gamma)$ is subject to debate. We find $\Gamma(X_z)$ to be 135 meV lower in energy than $\Gamma(\Gamma)$. Nakayama and Kamimura /5/ find the opposite result: from Fig. 4 of their paper we estimate $\Gamma(\Gamma)$ to be ≈ 100 meV lower in energy. These authors have adjusted the α -parameter of the exchange-correlation potential in order to obtain calculated bandstructures of bulk GaAs and AlAs which agree better with the experimental bandstructures. Nevertheless differences between experimental and theoretical conduction bandstructures are still on the level of 100-200 meV. This is close to the level of inaccuracy of the relative positions of conduction-band energy levels expected anyway for true *ab-initio* bandstructure calculations /13/.

In conclusion, we have calculated the radiative rates on direct transitions and estimated the phonon-assisted radiative rates on indirect transitions in 1×1 and 2×2 [001] and [110] GaAs/AlAs superlattices. The rates in [001] superlattices are at least two orders of magnitude smaller than the across-gap direct transitions in GaAs. These superlattices therefore do not hold many prospects for light emission applications. Our calculations show that the interpretation of spectroscopic experiments on the "energywise direct/indirect" issue will be hindered by the fact that radiative rates on direct and indirect transitions, and possibly also non-radiative rates, are of comparable magnitude. We therefore suggest to settle the direct/indirect issue by the use of pressure or magnetic fields to discriminate between the different anisotropy in k -space of the various "direct" (Γ) and "indirect" valleys. We have also shown that from a spectroscopic point of view the 2×2 [001] superlattice can neither be called direct nor indirect since the corresponding transitions are equally strong. The 2×2 [110] superlattice is energywise and spectroscopically direct since bandfolding and mixing yields a Γ -derived lowest conduction band state.

References

1. A. Ishibashi, Y. Mori, M. Itabashi and N. Watanabe, J. Appl. Phys. 58, 2691 (1985)
2. see e.g. H.C. Casey and M.B. Panish, Heterostructure Lasers Part A, Academic Press (New York, 1978)
3. see e.g. G. Bastard and J.A. Brum, IEEE Journ. of Quant. Elec. QE-22, 1625 (1986) and references therein.
4. N.E. Christensen, E. Molinari and G.B Bachelet, Solid State Comm. 56, 125 (1985)
5. T. Nakayama and H. Kamimura, J. Phys. Soc. Japan 54, 4726 (1985)
6. D.M. Bylander and L. Kleinman, Phys. Rev. B 34, 5280 (1986)
7. T.G. Gilbert and S.J. Gurman, Superl. and Microstr. 3, 17 (1987)
8. J.S. Nelson, C.Y. Fong and I.P. Batra, Appl. Phys. Lett. 50, 1595 (1987)
9. A.R. Williams, J. Kubler, C.D. Gelatt, Phys.Rev. B19, 6094 (1979)
10. P. Hohenberg and W. Kohn, Phys. Rev. 136B, 864 (1964); W. Kohn and L.J. Sham, Phys. Rev. 140A, 1133 (1965)
11. T. Jarlborg and A.J. Freeman, Phys. Lett. 74A, 349 (1979)
12. H.W.A.M. Rompa, R. Eppenga and M.F.H. Schuurmans, Physica 145B, 5 (1987)
13. G.W. Godby, M. Schluter and L.J. Sham, Phys. Rev. B35, 4170 (1987); These authors have shown that the experimental conduction bands of GaAs and AlAs can, to within 100 meV, be obtained from their *ab-initio* density functional calculations using a rigid shift of 0.8 eV for GaAs and 0.9 eV for AlAs. Using a similar approach we find the calculated relative energy positions in the conduction bands of GaAs and AlAs to be accurate on the level of 30 meV.
14. Our calculated results for the ground state properties of these superlattices are in accordance with the results from other *ab-initio* calculations. We define the GaAs/AlAs interface heat of formation as $\Delta H(n \times n) = [E(n \times n \text{ GaAs/AlAs}) - (E(\text{GaAs}) + E(\text{AlAs}))/2]/n$; we have calculated the total energies $E(\text{GaAs})$ and $E(\text{AlAs})$ under the same conditions as the SL calculation i.e. using the same unit cell, the same number of k-points in the BZ, etc. We find $\Delta H(1 \times 1[001]) \equiv \Delta H(1 \times 1[110]) \approx 30$ meV (cf. Bylander and Kleinman (15 meV) using relativistic pseudopotentials /15/ and Wood et al. (25 meV) using both semirelativistic pseudopotentials and the LAPW method /16/). We find $\Delta H(2 \times 2[001]) \approx 19$ meV and $\Delta H(2 \times 2[110]) \approx 30$ meV. By shifting the bulk GaAs and AlAs potential rigidly to fit the potential of the corresponding monolayers of the GaAs/AlAs SL optimally, we find a value of 0.6 meV for the valence band offset $\Gamma(HH)^{\text{GaAs}} - \Gamma(HH)^{\text{AlAs}}$ in both [001] and [110] GaAs/AlAs superlattices (cf. 446 meV for [001] and 447 meV for [110] in Ref. 15).
15. D.M. Bylander and L. Kleinman, Phys. Rev. B 36, 3229 (1987); D.M. Bylander and L. Kleinman, Phys. Rev. Lett. 59, 2091 (1987)
16. D.M. Wood, S.H. Wei and A. Zunger, Phys. Rev. Lett. 58, 1123 (1987)

Chapter 6

17. Note that we need not consider the virtual process involving the valence band states since the corresponding energy denominator is much larger.
18. A.S. Barker, J.L. Merz and A.C. Gossard, *Phys. Rev.* B17, 3181 (1978); C. Colvard, R. Merlin, M.V. Klein and A.C. Gossard, *Phys. Rev. Lett.* 45, 298 (1980); C. Colvard, R. Merlin, M.V. Klein and A.C. Gossard, *J. de Physique C6*, 631 (1981)
19. O.J. Glembocky and F.H. Pollak, *Phys. Rev. Lett.* 48, 413 (1982); O.J. Glembocky and F.H. Pollak, *Phys. Rev.* B25, 1193 (1982);
20. E. Finkman, M.D. Sturge and M.C. Tamargo, *Appl. Phys. Lett.* 49, 1299 (1986); J. Ihm, *Appl. Phys. Lett.* 50, 1068 (1987)

Summary

The fabrication of layered crystalline semiconductor structures, the so-called semiconductor heterostructures, has resulted in a new class of devices which exhibit interesting physical effects and have important technological applications. The interfaces between the different semiconductor layers that can be obtained by using the molecular beam epitaxy (MBE) growth technique, are monolayer sharp and perfect, i.e. the atoms 'sit exactly on top of each other'. The free carriers in such structures, i.e. the conduction-band electrons and the valence-band holes, are confined to a few energetically favorable layers. Quantum size effects become important if the de Broglie wavelength of the carriers becomes equal to or smaller than the thickness of these layers. The motion of the free carriers may then become effectively two-dimensional.

The GaAs/Al_xGa_{1-x}As quantum well forms an example of such a layered semiconductor structure. It consists of a thin (10-100Å) layer of GaAs in between two thick layers of Al_xGa_{1-x}As. This structure finds an important application as the active region of a GaAs/Al_xGa_{1-x}As quantum-well laser. In that region conduction-band electrons and valence-band holes recombine under the emission of (laser) light.

This thesis deals with the electronic and optical properties of GaAs/Al_xGa_{1-x}As quantum wells. The one-electron conduction-band states and valence-band states, and the corresponding energy levels, are calculated using a semi-empirical model. On the basis of *k.p* theory a Schrödinger-like equation is derived which describes the slowly (on the scale of the lattice parameter) varying part of the wavefunction, the so-called envelope function.

In Chapter 1 a new *k.p* model for GaAs/Al_xGa_{1-x}As-type quantum wells is presented. It employs a unified description of the conduction and valence-bands and fully accounts for the conduction-band non-parabolicity and the valence-band mixing. The model is thus capable of explaining the principal features in state-of-the-art photoluminescence excitation spectra of GaAs/Al_xGa_{1-x}As quantum wells. Moreover, calculated electron and hole-confinement energies, and the strengths of the optical transitions between electron and hole-confinement states, are found to be in good agreement with those obtained from the more complicated tight-binding theory of Chang and Schulman. The inclusion of the spin-orbit split-off band is shown to be important for the description of GaAs/AlAs quantum wells.

In Chapter 2 and 3 the *k.p* model is applied to describe the optical properties of a GaAs/Al_xGa_{1-x}As quantum well which forms the active layer in a GaAs/Al_xGa_{1-x}As quantum-well laser. Calculated gain and spontaneous emission spectra are shown to differ considerably from those obtained from simpler models. The implications of the

Summary

theoretical results for the interpretation of measured gain and spontaneous emission spectra are discussed in Chapter 3. It is concluded that a one-electron k,p description of the quantum well without the introduction of broadening mechanisms cannot explain satisfactorily the experimental results.

A more realistic model of a GaAs/Al_xGa_{1-x}As quantum well laser is presented in Chapter 4. It incorporates the effects of broadening mechanisms such as e.g. carrier-carrier scattering, well width fluctuations and current spreading, on calculated gain and spontaneous emission spectra. Carrier-carrier scattering is shown to affect the maximum-gain-versus-current-density relation dramatically. Its inclusion in the calculations is found to be paramount to obtain good agreement with the experimentally determined maximum-gain-versus-current-density relation.

Chapter 5 deals with an interesting detail: the effect of the inversion asymmetry of the bulk constituents on quantum-well confinement states. Analytical expressions are presented that describe the resulting spinsplitting of the conduction-bands in GaAs/Al_xGa_{1-x}As quantum wells grown along the [001], [110] and [111] crystallographic direction. The spinsplitting of the bands is found to be linear in $k_{||}$, whereas the corresponding quantity in the bulk is cubic in k . Moreover, the spinsplitting is found to be strongly dependent on the crystallographic growth direction of the quantum-well layers.

Finally, the optical properties of very thin GaAs/AlAs superlattices are discussed in Chapter 6 on the basis of the *ab-initio* augmented spherical wave (ASW) bandstructure method (no recourse is made to experimentally determined parameters). The oscillator strengths of the direct across-gap transitions are found to be very small in these thin superlattices: $\lesssim 5\%$ of that of bulk GaAs. The rates for radiative emission across the direct and the indirect gap are shown to be comparable in magnitude. These superlattices therefore show little prospect for light emission applications.

Stellingen

behorende bij het proefschrift getiteld

“The Electronic and Optical Properties of GaAs/AlGaAs Quantum Wells”

R. Eppenga

I

Elektrische velden geven geen aanleiding tot spinsplitsing van excitontoestanden.

G.D. Sanders en K.K. Bajaj, Phys. Rev. B36, 4849 (1987)

II

De 'diamagnetische shift' in GaAs/AlGaAs-quantumputten, zoals die door Lefebvre et al. gemeten is, komt overeen met die, welke op grond van Landé-factoren voor elektronen en gaten in de bulkmaterialen GaAs en AlGaAs verwacht wordt, als in het excitonmodel dat op het omhullende-functie-formalisme gebaseerd is, de valentiebandmenging wordt meegenomen.

P. Lefebvre, B. Gil, J.P. Lascaray, H. Mathieu, D. Bimberg, T. Fukunaga and H. Nakashima, Phys. Rev. B37, 4171 (1988).

III

De reflectiecoëfficiënt in de formule van Landauer voor de conductantie kan voor de experimenten van Timp et al. op eenvoudige wijze met 'biljartbalmechanika' gevonden worden.

G. Timp, H.U. Baranger, P. deVegvar, J.E. Cunningham, R.E. Howard, R. Behringer and P.H. Mankiewich, Phys. Rev. Lett. 60, 2081 (1988).

IV

Dunne $(\text{GaP})_n/(\text{AlP})_n$ -superroosters ($n = 1-4$) zijn ongeschikt voor lichtemissietoepassingen.

M.F.H. Schuurmans, H.W.A.M. Rompa and R. Eppenga, Journal of Luminescence 37, 269 (1987).

V

Op grond van de resultaten van *ab-initio* bandstructuurberekeningen voor AlAs moet aan de indirecte L - Γ -bandafstand voor AlAs een waarde van 2,95 eV toegekend worden.

Vgl. met de algemeen gebruikte waarde 2,30 eV hiervoor, H.C. Casey and M.B. Panish, "Heterostructure Lasers" Part A, Academic Press (New York, 1978).

VI

Om de gemeten fotoluminescentie-excitatiespectra van GaAs/Al_xGa_{1-x}As-quantumputten ($x > 0.3$) op een 1 milli-elektronvoltschaal te kunnen verklaren is het noodzakelijk de spinbaanafgesplitste gatenband mee te nemen in k,p -modellen van deze structuren.

"Determination of valence-band effective-mass anisotropy in GaAs quantum wells by optical spectroscopy", L.W. Molenkamp, R. Eppenga, G.W. 't Hooft, P. Dawson, C.T. Foxon en K.J. Moore, geaccepteerd voor publikatie als Rapid Communication in Phys. Rev. B.

VII

De energieën van de toestanden in dunne (GaAs)_n/(AlGaAs)_n-superroosters ($n \gtrsim 3$) en dunne GaAs/AlGaAs-quantumputten ($w_{\text{GaAs}} \gtrsim 8.5 \text{ \AA}$), die met de Γ -punttoestanden van het bulkmateriaal samenhangen, kunnen met het omhullende-functieformalisme tot op enkele milli-elektronvolts nauwkeurig berekend worden.

VIII

Ladingdrager-ladingdragerverstrooiing is bij geïnjecteerde elektronichtheden van meer dan 10^{18} cm^{-3} het overheersende verbreidingsmechanisme in versterkingsspectra en spontane emissiespectra van GaAs/AlGaAs-quantumputlasers.

IX

De spinsplitsing in de geleidingsband is *minimaal* in GaAs/AlGaAs quantumputten die gegroeid zijn in de kristallografische richting waarin de spinsplitsing van de geleidingsband in het bulkmateriaal *maximaal* is.

Dit proefschrift, hoofdstuk 5.

X

De frequentie van de fileberichten op de radio is niet voldoende hoog.

XI

Het gebruik van knipperlichten door de politie en hulpverleners in ongevaarlijke situaties kan aanleiding geven tot gevaarlijk gedrag van weggebruikers.

Delft, 15 september 1988

Samenvatting

De fabricage van gelaagde, eenkristallijne halfgeleiderstructuren, de zogenaamde halfgeleider-heterostructuren, heeft geresulteerd in een nieuwe klasse van componenten die interessante fysische verschijnselen vertonen en belangrijke technologische toepassingen hebben. De verschillende halfgeleiderlagen, verkregen met de techniek van molekuulbundel-epitaxie (MBE), gaan op monolaagniveau abrupt in elkaar over en zijn perfect passend, d.w.z. de atomen 'zitten precies op elkaar'. De vrije ladingdragers in zulke structuren, de geleidingsbandelektronen en de valentiebandgaten, zijn opgesloten in energetisch-voordelige lagen. Quantumeffecten worden belangrijk als de De Broglie golflengte van de vrije ladingdragers gelijk aan of kleiner dan de dikte van deze lagen wordt. In dat geval kunnen de vrije ladingdragers effectief alleen in een tweedimensionaal vlak bewegen.

Een voorbeeld van een dergelijke structuur vormt de GaAs/Al_xGa_{1-x}As-quantumput. Deze bestaat uit een dunne (10-100 Å) GaAs-laag tussen twee dikke Al_xGa_{1-x}As-lagen. Een belangrijke toepassing is het gebruik van deze structuur in de GaAs/Al_xGa_{1-x}As-quantumputlaser. In de GaAs-laag recombineren geleidingsbandelektronen en valentiebandgaten onder de uitzending van licht.

In dit proefschrift worden de elektronische en optische eigenschappen van GaAs/Al_xGa_{1-x}As-quantumputten behandeld. Met een semi-empirisch model worden de één-elektrongeleidingsbandtoestanden en -valentiebandtoestanden en de daarbij behorende energieniveaus berekend. Er wordt een soort Schrödinger vergelijking gebaseerd op de *k,p*-theorie afgeleid die het langzaam (op de schaal van de roosterconstante) variërende deel van de golf functie, de zogenaamde omhullende functie, beschrijft.

In hoofdstuk 1 wordt een nieuw *k,p*-model voor GaAs/Al_xGa_{1-x}As-quantumputten ingevoerd. Het beschrijft zowel de geleidingsband als de valentiebanden. Er wordt rekening gehouden met het feit dat de geleidingsband afwijkt van een (zuivere) parabool en dat de valentiebanden met elkaar mengen. Met het model waarin deze effecten zijn meegenomen zijn alle belangrijke kenmerken in de recentelijk gemeten fotoluminescentie-excitatiespectra van GaAs/Al_xGa_{1-x}As-quantumputten te verklaren. Bovendien blijken de berekende opsluitenergieën voor elektronen en gaten, en de sterkte van de optische overgangen tussen deze opsluittoestanden van de elektronen en gaten, goed overeen te komen met die verkregen met behulp van de veel ingewikkelder zgn. 'ticht-binding'-theorie van Chang en Schulman. Het meenemen van de spin-baanafgesplitste band in de berekeningen blijkt van belang te zijn voor de beschrijving van GaAs/AlAs-quantumputten.

Samenvatting

In hoofdstuk 2 en 3 wordt het k,p -model gebruikt om de optische eigenschappen van een GaAs/Al_xGa_{1-x}As-quantumput, die de kern van een GaAs/Al_xGa_{1-x}As-quantumputlaser vormt, te beschrijven. De berekende versterkings- en spontane-emissiespectra wijken aanzienlijk af van die verkregen met eenvoudiger modellen. In hoofdstuk 3 worden de gevolgen van de theoretische resultaten voor de interpretatie van de gemeten versterkings- en spontane-emissiespectra besproken. Het is niet mogelijk de experimentele resultaten bevredigend met een één-elektron- k,p -beschrijving van een quantumput te verklaren zonder verbredingsmechanismen te introduceren.

In hoofdstuk 4 wordt een realistischer model van een GaAs/Al_xGa_{1-x}As-quantumputlaser geïntroduceerd. Er wordt nu wel rekening gehouden met de effecten van verbredingsmechanismen zoals bijvoorbeeld ladingdrager-ladingdrager-verstrooiing, putbreedtevariaties en de stroomverdeling op berekende versterkings- en spontane-emissiespectra. Het blijkt dat ladingdrager-ladingdragerverstrooiing de relatie tussen de maximale versterking en de stroomdichtheid ingrijpend beïnvloed. Het meenemen hiervan in de berekeningen is noodzakelijk om een goede overeenkomst met de experimenteel gemeten relatie tussen de maximale versterking en de stroomdichtheid te verkrijgen.

In hoofdstuk 5 wordt een interessant detail behandeld: het effect van de inversie asymmetrie van de bulkmaterialen waaruit de quantumput is opgebouwd op de quantumputopsluittoestanden. Er worden analytische uitdrukkingen afgeleid voor de resulterende spinsplitsing van de geleidingsbanden in GaAs/Al_xGa_{1-x}As-quantumputen gegroeid langs de kristallografische [001], [110] en de [111] richtingen. Deze spinsplitsing blijkt lineair in $k_{||}$ te zijn, terwijl deze grootte in het bulkmateriaal kubisch is in k . Bovendien hangt de spinsplitsing sterk af van de kristallografische groeirichting van de lagen waaruit de quantumput bestaat.

Tenslotte worden in hoofdstuk 6 de optische eigenschappen van superroosters bestaande uit enkele GaAs- en AlAs-monolagen bediscussieerd zoals deze verkregen zijn met de ASW-bandstructuurmethode ('Augmented Spherical Wave'-bandstructuurmethode). Dit is een 'ab-initio' methode, d.w.z. dat er geen gebruik gemaakt wordt van experimenteel bepaalde parameters. De oscillatorsterkten van de directe overgangen over de bandafstand blijken zeer klein te zijn in deze dunne superroosters: $\lesssim 5\%$ van die van bulk-GaAs. Bovendien zijn de overgangswaarschijnlijkheden voor stralende emissie langs de directe en de indirecte bandafstand van dezelfde orde van grootte. Deze superroosters lijken daarom minder geschikt als gedacht wordt aan toepassingen waarin lichtemissie belangrijk is.

Curriculum Vitae

Rob Eppenga

- 26 maart 1958 geboren te Weesp
- 1970 - 1972 VWO, Dalton Scholengemeenschap te 's-Gravenhage
1972 - 1976 VWO, Sint Oelbertgymnasium te Oosterhout,
eindexamen Gymnasium-B
- 1976 begin studie natuurkunde aan de
Rijksuniversiteit te Utrecht
- 29 januari 1979 kandidaatsexamen N1 (cum laude)
- 27 juni 1983 doktoraalexamen Theoretische Natuurkunde (cum laude);
afstudeeronderwerp: "Monte Carlo studie van een eenvoudig
model van een nematisch vloeibaar kristal in twee en in drie
dimensies", onder leiding van Dr. D. Frenkel.
- 1 oktober 1983 in dienst bij het Philips Natuurkundig Laboratorium;
groep Theoretische Natuurkunde,
onder leiding van Prof.Dr.Ir. M.F.H. Schuurmans.